Development of multicellular *in vitro* models of the meningeal blood-CSF barrier to study *Neisseria meningitidis* infection

Entwicklung multizellulärer *in vitro* Modelle der meningealen Blut-Liquor Schranke zur Untersuchung der *Neisseria meningitidis* Infektion

Doctoral thesis for a doctoral degree
at the Graduate School of Life Sciences,
Julius-Maximilians-Universität Würzburg,
Section Infection and Immunity

submitted by

Leo Maximilian Endres

from

Bamberg, Germany

Würzburg, 2023

Submitted on: ……..……..

Office stamp

Members of the Thesis Committee

Chairperson: Prof. Dr. Markus Sauer

Primary Supervisor: Prof. Dr. Alexandra Schubert-Unkmeir

Supervisor (Second): Prof. Dr. Roy Gross

Supervisor (Third): Jun. Prof. Dr. Alexander Westermann

TABLE OF CONTENTS

SUMMARY **6**

ZUSAMMENFASSUNG **7**

1 INTRODUCTION **9**

1.1 *NEISSERIA MENINGITIDIS*: EPIDEMIOLOGY 9

1.2 *NEISSERIA MENINGITIDIS*: PATHOGENESIS 10

1.2.1 Colonization of the nasopharyngeal niche *10*

1.2.2 Interaction with the nasopharyngeal epithelium *12*

1.2.3 Proliferation in the bloodstream *12*

1.3 THE BLOOD-CNS INTERFACE 13

1.3.1 The meningeal blood-CSF barrier *14*

1.3.2 Brain endothelial cells *16*

1.4 *N. MENINGITIDIS* INTERACTION WITH THE MBSCFB 17

1.4.1 N. meningitidis interaction with BECs *17*

1.4.2 N. meningitidis interaction with LMCs *20*

1.5 MODELING *N. MENINGITIDIS* INTERACTION WITH THE MBSCFB 21

1.6 AIM OF THE STUDY 23

2 MATERIALS **24**

2.1 LABORATORY EQUIPMENT 24

2.2 CHEMICALS AND REAGENTS 25

2.3 CELLS AND BACTERIAL STRAINS 27

2.4 MEDIA, BUFFERS, AND SOLUTIONS 27

2.5 ANTIBODIES AND PRIMERS 29

3 METHODS **30**

3.1 CELL CULTURE 30

3.1.1 hCMEC/D3 culture *30*

3.1.2 Meningioma cell culture *30*

3.1.3 Matrigel coating of tissue culture plastic for iPSC culture *30*

3.1.4 iPSC maintenance culture *31*

3.1.5 Cryopreservation of iPSCs *31*

3.1.6 Generation of brain endothelial-like cells from iPSCs *32*

3.1.7 Co-culture of iBECs and meningioma cells *32*

3.1.8 Co-culture of hCMEC/D3s and meningioma cells *33*

3.2 TRANSENDOTHELIAL ELECTRICAL RESISTANCE 33

3.3 SODIUM FLUORESCEIN PERMEABILITY 34

3.4 Immunofluorescence ... 34
3.5 Bacterial culture ... 35
3.6 Infection assays ... 35
3.7 Gentamicin protection assay ... 35
3.8 Transmigration assay ... 36
3.9 Structured illumination microscopy ... 36
3.10 Transmission electron microscopy ... 37
3.11 Quantitative RT-PCR ... 37
3.11.1 RNA extraction ... 37
3.11.2 cDNA synthesis ... 37
3.11.3 Quantitative PCR ... 38
3.12 *SNAI1* knockdown ... 39
3.13 IL-8 ELISA ... 39
3.14 Statistics ... 40

4 RESULTS ... 41

4.1 Development and characterization of BEC-LMC co-culture models ... 41
4.2 Influence of LMC co-culture on tightness and stability of the BEC barrier ... 44
4.3 *N. meningitidis* interaction with and traversal of the BEC-LMC models ... 46
4.4 Barrier deterioration upon prolonged *N. meningitidis* infection ... 49
4.5 *N. meningitidis* induced immune activation of BECs ... 55

5 DISCUSSION ... 58

5.1 Development and characterization of the BEC-LMC co-culture models ... 58
5.1.1 Model development ... 58
5.1.2 Characterization of the BEC-LMC co-culture models ... 59
5.1.3 Influence of LMC co-culture on tightness and stability of the BEC barrier ... 62
5.2 *N. meningitidis* interaction with the BEC-LMC co-culture models ... 64
5.2.1 Adherence and Invasion of the BEC layer ... 64
5.2.2 Barrier disruption upon infection ... 64
5.2.3 Meningococcal traversal of the mBCSFB ... 67
5.2.4 N. meningitidis-induced immune activation ... 69
5.3 Conclusion and future perspectives ... 70

REFERENCES ... 73

AFFIDAVIT ... 85

EIDESSTATTLICHE ERKLÄRUNG ... 85

APPENDIX ... 86

List of Figures ... 86

LIST OF TABLES 86
ABBREVIATION INDEX 87
LIST OF PUBLICATIONS 88
ACKNOWLEDGMENTS 89

SUMMARY

Neisseria meningitidis (the meningococcus) is one of the major causes of bacterial meningitis, a life-threatening inflammation of the meninges. Traversal of the meningeal blood-cerebrospinal fluid barrier (mBCSFB), which is composed of highly specialized brain endothelial cells (BECs), and subsequent interaction with leptomeningeal cells (LMCs) are critical for disease progression. Due to the human-exclusive tropism of *N. meningitidis,* research on this complex host-pathogen interaction is mostly limited to *in vitro* studies. Previous studies have primarily used peripheral or immortalized BECs alone, which do not retain relevant barrier phenotypes in culture. To study meningococcal interaction with the mBCSFB in a physiologically more accurate context, BEC-LMC co-culture models were developed in this project using BEC-like cells derived from induced pluripotent stem cells (iBECs) or hCMEC/D3 cells in combination with LMCs derived from tumor biopsies.

Distinct BEC and LMC layers as well as characteristic expression of cellular markers were observed using transmission electron microscopy (TEM) and immunofluorescence staining. Clear junctional expression of brain endothelial tight and adherens junction proteins was detected in the iBEC layer. LMC co-culture increased iBEC barrier tightness and stability over a period of seven days, as determined by sodium fluorescein (NaF) permeability and transendothelial electrical resistance (TEER). Infection experiments demonstrated comparable meningococcal adhesion and invasion of the BEC layer in all models tested, consistent with previously published data. While only few bacteria crossed the iBEC-LMC barrier initially, transmigration rates increased substantially over 24 hours, despite constant high TEER. After 24 hours of infection, deterioration of the barrier properties was observed including loss of TEER and altered expression of tight and adherens junction components. Reduced mRNA levels of ZO-1, claudin-5, and VE-cadherin were detected in BECs from all models. qPCR and siRNA knockdown data suggested that transcriptional downregulation of these genes was potentially but not solely mediated by Snail1. Immunofluorescence staining showed reduced junctional coverage of occludin, indicating *N. meningitidis*-induced post-transcriptional modulation of this protein, as previous studies have suggested. Together, these results suggest a potential combination of transcellular and paracellular meningococcal traversal of the mBCSFB, with the more accessible paracellular route becoming available upon barrier disruption after prolonged *N. meningitidis* infection. Finally, *N. meningitidis* induced cellular expression of pro-inflammatory cytokines and chemokines such as IL-8 in all mBCSFB models. Overall, the work described in this thesis highlights the usefulness of advanced *in vitro* models of the mBCSFB that mimic native physiology and exhibit relevant barrier properties to study infection with meningeal pathogens such as *N. meningitidis*.

ZUSAMMENFASSUNG

Neisseria meningitidis (der Meningokokkus) ist einer der Hauptursachen bakterieller Meningitis, einer lebensbedrohlichen Entzündung der Hirnhäute. Entscheidend für das für das Voranschreiten der Krankheit ist die Fähigkeit des Erregers, die meningeale Blut-Liquor-Schranke (mBCSFB), bestehend aus spezialisierten Hirnendothelzellen (BECs) und leptomeningealen Zellen (LMCs), zu überwinden und in den submeningealen Raum einzudringen. Da es sich bei *N. meningitidis* um ein rein humanes Pathogen handelt, beschränkt sich die Erforschung dieser speziellen Interaktion primär auf die Verwendung von *in vitro* Modellen. Bisher wurden hierfür hauptsächlich periphere oder immortalisierte BECs verwendet, welchen jedoch wichtige Barriere-Eigenschaften fehlen. Um die Interaktion von *N. meningitidis* mit der mBCSFB in einem physiologisch relevanteren Umfeld zu untersuchen, wurden in dieser Arbeit neuartige BEC-LMC Kokulturmodelle entwickelt.

Dabei wurden sowohl BEC-ähnliche Zellen, die aus induzierten pluripotenten Stammzellen generiert wurden (iBECs), als auch hCMEC/D3 Zellen verwendet und zusammen mit LMCs aus Tumorbiopsien kultiviert. Mittels Transmissions-Elektronenmikroskopie und Immunfluoreszenzfärbung konnten die unterschiedlichen Zellschichten und deren Expression charakteristischer zellulärer Marker dargestellt werden. Durchgängige Expression von wichtigen Bestandteilen Barriere-formender Zellverbindungen, sogenannter Tight und Adherens Junctions, wurde in der iBEC-Schicht beobachtet. Die Integrität der zellulären Barriere wurde mittels transendothelialer elektrischer Resistenz (TEER) und Permeabilität gegenüber Natrium-Fluorescein (NaF) bestimmt. Erhöhte TEER-Werte und verringerte NaF-Permeabilität, gemessen über einen Zeitraum von sieben Tagen, zeigten eine durch die Kokultur mit LMCs ausgelöste Steigerung der Dichtigkeit und Stabilität der iBEC-Barriere.

Infektionsexperimente mit *N. meningitidis* zeigten in allen Modellen vergleichbare bakterielle Adhäsion und Invasion der BEC-Schicht. Bakterielle Transmigration durch die gesamten Zellbarriere war im iBEC-LMC Modell kurz nach Infektion nur in geringem Maße detektierbar, nahm jedoch innerhalb von 24 Stunden deutlich zu. Interessanterweise wurde bis zu 24 Stunden nach Infektion noch eine hohe Integrität der Barriere gemessen, welche allerdings im weiteren Verlauf verloren ging. Neben signifikantem TEER-Verlust wurde eine verringerte Expression der Tight und Adherens Junction Proteine ZO-1, claudin-5, und VE-cadherin mittels qPCR festgestellt. qPCR und siRNA Knockdown Experimente deuteten darauf hin, dass dies möglicherweise, aber nicht ausschließlich, auf den Transkriptionsfaktor Snail1 zurückzuführen war. Zusätzlich zu den beobachteten Effekten auf die zelluläre Transkription von Tight Junction Genen, zeigten Immunfluoreszenzfärbungen eine verringerte Expression von Occludin an den Zell-Zell-Verbindungen, was auf eine post-translationale Modulation schließen lässt. Zusammen deuten die Ergebnisse dieser Infektionsstudien auf eine mögliche Kombination aus trans- und parazellulärer bakterieller Transmigration der mBCSFB hin.

Zuletzt wurden in dieser Arbeit noch die Immunaktivierung von BECs nach *N. meningitidis* Infektion in den neuen BEC-LMC Kokulturmodellen untersucht. Hierbei wurde eine erhöhte Expression von Zytokinen, insbesondere Interleukin-8, beobachtet.

Insgesamt konnten in dieser Arbeit neue, fortschrittlicher *in vitro* Modelle der mBCSFB entwickelt werden, welche die humane Physiologie besser widerspiegeln und daher für Infektionsstudien mit Meningitis-verursachenden Erregern wie *N. meningitidis* von besonderem Nutzen sind.

1 INTRODUCTION

1.1 *Neisseria meningitidis*: Epidemiology

Neisseria meningitidis (*Nm*, meningococcus) is an obligate human, Gram-negative, diplococcal bacterium that can cause invasive meningococcal disease (IMD). The most prominent clinical manifestations of IMD are septicemia and meningitis that can occur separately or together, with meningitis accounting for up to 60% of cases [1]. Meningococcemia presents most commonly as petechial or purpuric rash. Typical symptoms of meningococcal meningitis include fever, vomiting, headache, photophobia, and stiffness of the neck. Although treatable with modern antibiotic therapy, survivors of IMD often experience long-term sequelae including chronic pain, scarring, and amputation after septicemia, and neurological, hearing, and visual impairment following meningitis [1]. Furthermore, mortality of IMD remains high, with case fatality rates of up to 20%, despite intensive treatment with first and third generation β-lactam antibiotics such as penicillin and ceftriaxone [2]. This may also be attributed to antimicrobial resistances due to chromosomally encoded penicillin-binding proteins or plasmid-encoded β-lactamase, which is the less common [3-5].

N. meningitidis asymptomatically colonizes the nasopharynx of healthy individuals, a phenomenon commonly referred to as carriage, and is transmitted via respiratory droplets. Carriage rates vary greatly depending on age and other risk factors [6]. Highest carriage prevalence is observed in young adults under the age of 30 [6, 7], with extended, close person-to-person contact being the greatest risk factor, as observed in military or university environments [8]. Diverse risk of meningococcal carriage and prevalence of IMD is also observed between populations of different geographic regions. Arid environmental conditions were correlated with increased carriage risk in the meningitis belt of sub-Saharan Africa [9], a region that includes the majority of countries with the highest endemic rates [10]. Finally, co-infection with other respiratory pathogens such as Influenza virus A has been correlated with increased risk of IMD [11].

Epidemics and larger outbreaks are typically associated with distinct *N. meningitidis* strains. Meningococcal strains are classified into serogroups according to composition and serologic differences of the polysaccharide capsule, which encases the bacterium and can be found in all invasive isolates. Strains from six (A, B, C, W, X, Y) of the thirteen known serogroups are responsible for the majority of IMD cases [12]. In addition to capsule serotyping, sequence types (ST) of *N. meningitidis* isolates are determined using multi-locus sequence typing of seven housekeeping genes (abcZ, adk, aroE, fumC, gdh, pdhC and pgm) [13]. Different STs with homology in at least four of the seven loci are grouped into a clonal complex (cc), some of which are known as hyperinvasive lineages that are associated with epidemics and global outbreaks. For example, primarily cc5 isolates of serogroup A

were responsible for disease in the African meningitis belt and cc11 strains of serogroups C, W, and B caused worldwide IMD outbreaks [14]. Recently, whole-genome sequencing (WGS) has become increasingly available and has been used to evaluate species diversity in relation to epidemiology in even greater detail [14].

Various vaccines have been developed to combat meningococcal disease. Polysaccharide-protein conjugate vaccines are available for immunization against serogroups A, C, Y and W-135 based on the specific capsule polysaccharides [15]. Due to poor immunogenicity and auto-immunity concerns, this approach was not used for the development of a vaccine against serogroup B isolates [16]. Instead, reverse vaccinology enabled by WGS led to the formulation of the multicomponent vaccine 4CMenB that consists of three highly immunogenic antigens (fHbp, NadA and NHBA) combined with outer membrane vesicles [16]. Despite considerable success in vaccine development, effectiveness of immunization to prevent IMD is always challenged by the genetic adaptability of *N. meningitidis*. Horizontal gene transfer of naturally competent meningococci as well as phase and antigenic variation affect most pathogenicity factors including the capsule and can lead to rapid and reversible switching of population phenotype [17, 18].

1.2 *Neisseria meningitidis*: Pathogenesis

Pathogenesis of *N. meningitidis* stems from the bacterium's ability to colonize the nasopharyngeal niche, cross the epithelial nasopharyngeal barrier, disseminate systemically via the bloodstream, and infiltrate various tissues including the meninges [19] (**Figure 1**).

1.2.1 Colonization of the nasopharyngeal niche

After transmission, meningococci colonize the mucosal surfaces of the nasopharyngeal epithelial cell layer. This environment provides several layers of natural immunity, which *N. meningitidis* must contend with, including mucociliary clearance, nutrient restriction in the mucosal layer, and factors of humoral immunity such as secreted IgA and cationic antimicrobial proteins (CAMPs) [20]. Metabolic adaptations of meningococci include the ability to use carbon sources available in the nasopharyngeal niche such as lactate, glucose, maltose and pyruvate [21]. Furthermore, *N. meningitidis* possesses various mechanisms to acquire and utilize extracellular iron and zinc, that are mostly found sequestered by secreted human proteins. Multiple uptake systems including TonB-dependent transporters allow meningococci to utilize iron carrier proteins transferrin, lactoferrin, hemoglobin, and haptoglobin as sources of essential iron [22]. Meningococcal receptors such as CbpA and ZunD enable utilization of host zinc [23]. For protection against host antibodies that can enhance phagocytosis or complement mediated killing, *N. meningitidis* expresses IgA proteases that can cleave IgA1 as well as IgG3 [24]. Host CAMPs are short peptides that bind negatively charged lipopolysaccharide (LPS) of the outer membrane of Gram-negative bacteria and disrupt membrane

integrity [25]. Enzymatic changes in the lipid A headgroup of meningococcal lipooligosaccharide (LOS) are one of the pathogen's many resistance mechanisms, along with interference by capsular polysaccharides, binding of human factor H on the bacterial surface, CAMP efflux mediated by Mtr pumps, and shedding of outer membrane blebs [25].

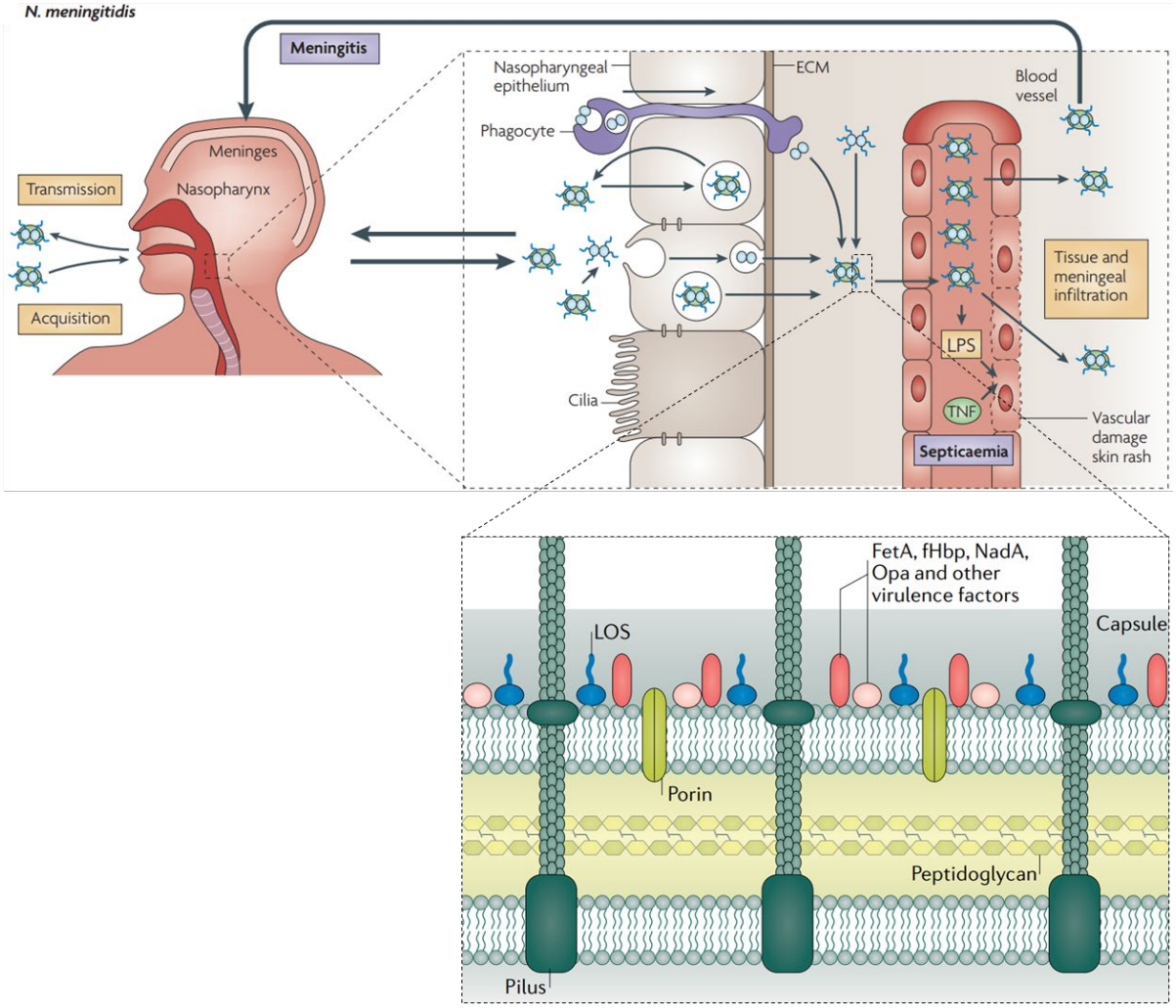

Figure 1. Stages of *Neisseria meningitidis* pathogenesis and virulence factors of the meningococcal outer membrane. Adapted from Virji 2009 [19], and Caugant & Brynildsrud 2020 [14].

Finally, the nasopharyngeal niche is occupied by diverse microbiota, mostly dominated by species of the *Fusobacterium, Streptococcus, Moraxella, Staphylococcus, Corynebacterium,* and *Dolosigranulum (Alloiococcus)* genera [26]. Both synergistic and antagonistic effects have been observed between *N. meningitidis* and *Streptococcus species*. *S. pneumoniae* produces bactericidal hydrogen peroxide and a neuraminidase affecting meningococcal LOS [27]. *S. mitis* has been shown to degrade mucins, aiding stable meningococcal colonization of the nasopharyngeal epithelial surface [28]. Apart from distinct bacterial genera, *N. meningitidis* may also compete with other commensal *Neisseria* species such as *N. lactamica* and *N. cinera* [20]. *N. cinera* has been shown to impair meningococcal host cell association and survival [29, 30]. To compete with other bacteria, *N. meningitidis* can secrete polymorphic toxins

CdiA and MafB (via the distinct TspABI and MafABI systems), which can have various effects including nucleic acid degradation and membrane disruption [31, 32].

1.2.2 Interaction with the nasopharyngeal epithelium

During colonization, *N. meningitidis* can also interact directly with the nasopharyngeal epithelial barrier, which consists of stratified squamous epithelium and columnar respiratory epithelium [28]. The major cell types of the columnar respiratory epithelium are ciliated cells, undifferentiated columnar, secretory, and basal cells [33]. Early studies using *ex vivo* tissue culture have suggested that meningococci preferentially attach to non-ciliated columnar cells of the nasopharynx [34, 35]. Initial adhesion to respiratory epithelial cells is mediated by meningococcal Type IV pili (Tfp) [36, 37] – long filamentous structures consisting of multiple subunits that extend past the outer edge of the polysaccharide capsule and conduct various functions including twitching motility [38]. Tfp also play a major role in bacterial aggregation and microcolony formation on the host cell surface [39]. Recent data suggests that this process is supported by virulence-associated meningococcal prophage MDAΦ, which stabilizes inter-bacterial interactions [40]. Following initial attachment, expression of Tfp and polysaccharide capsule is downregulated [41]. This allows for intimate adhesion and cellular invasion governed by opacity proteins Opa – which binds CEACAM receptors [42] – and Opc [43]. Additionally, several minor adhesins including *Neisseria* adhesin A (NadA; [44]), *Neisseria* hia/hsf homologue (NhhA; [45]), autotransporter meningococcal serine protease A (MspA; [46]), adhesion and penetration protein (App; [47]), hemagglutinin/hemolysin-related protein A (HrpA [48]), and Neisserial Heparin Binding Antigen (NHBA; [49]) are involved in epithelial cell adhesion and invasion. Previous research has shown that *N. meningitidis* can, then, cross the nasopharyngeal epithelial barrier via a microtubule-dependent, transcellular pathway without disruption of cellular junctions [50-52]. Meningococcal transcytosis may be facilitated by changes in polar architecture of the epithelial barrier and subversion of intracellular trafficking pathways [50].

1.2.3 Proliferation in the bloodstream

Upon crossing of the nasopharyngeal epithelial barrier, *N. meningitidis* enters the bloodstream and encounters a physiologically different environment. Here, meningococcal survival is challenged by innate and adaptive immunity of the host, particularly the complement system, which encompasses multiple effector proteins that can target bacterial pathogens for immune cell mediated killing or disrupt bacterial membranes directly. An intact complement system is necessary to kill *Neisseriae* in the blood, and complement deficiencies are correlated with increased risk of IMD [53]. Various mechanisms of meningococcal immune evasion have been described including common factors that also support colonization of the nasopharyngeal niche. Expression of the polysaccharide capsule, sialylation of LOS, cleavage of effector proteins and recruitment of inhibitors can interfere with the

complement system (reviewed in [53]). For example, the presence of a capsule reduces IgG/IgM antibody binding and C4b deposition, inhibiting the classical complement pathway [54]. Structural modulation of LOS such as sialylation of the α-chain can mediate resistance to all three pathways of complement [53]. The meningococcal autotransporter protease NalP can cleave the α-chain of the human complement factor C3 [55]. *N. meningitidis* Porin A (PorA) has been shown to recruit the human complement inhibitor C4b-binding protein (C4BP) [56]. The invasion Opc and minor adhesin NhhA can bind extracellular matrix (ECM) component vitronectin, which reduces formation of the membrane attack complex [57]. Finally, the recruitment of human factor H to the bacterial surface is an effective process of complement inhibition and is primarily mediated by *N. meningitidis* factor H binding protein (fHbp) [58]. Interestingly, it was recently found that temperature may be a relevant environmental cue to activate some of these mechanisms such as capsule biosynthesis, fHBP expression, and LOS sialylation [59].

Other mechanisms of immune evasion by *N. meningitidis* include antigen masking and genetic variation. For instance, molecular modeling has shown that glycosylation of class II pilin subunits of Tfp strongly decreases antibody access to the polypeptide chain [60]. All major virulence factors (over 100 genes), including the ones mentioned above, can undergo genetic adaptation in *N. meningitidis* (reviewed in [17]). Opa and major Tfp subunit PilE are subject of antigenic variation via gene conversion mediated by recombination events between multiple allelic variants [17]. Phase variation – a mechanism of rapid on and off switching of gene expression – directly affects relevant molecular structures such as the capsule, Opc, PorA, and NadA [17, 18, 61]. Phase variation can also influence posttranslational modification of antigens like the capsule or Tfp by controlling expression of the relevant enzymes [18, 62].

In addition to survival in the bloodstream, bacterial adherence to endothelial cells is a crucial step in the pathogenesis of *N. meningitidis*. Attachment and proliferation on peripheral endothelial cells lead to advanced meningococcemia, and can cause microvessel thrombosis and hemorrhagic necrosis particularly in the skin but potentially affecting other organs as well – a clinical syndrome known as purpura fulminans [63]. The ability of *N. meningitidis* to cause meningitis relies on its ability to adhere to and travers highly specialized endothelial barrier cells of meningeal microvessels, which is subject of this study and will be discussed in greater detail below.

1.3 The blood-CNS interface

A complex vasculature connects the brain and surrounding meninges to the circulatory system. The presence of a blood-CNS barrier was first recognized by Paul Ehrlich. In a study published in 1885, Ehrlich demonstrated that tracer dyes injected intravenously into rodents stained peripheral organs but not the brain or spinal cord [64]. Since then, several distinct cellular barriers that contribute to

brain homeostasis and restrict passage of toxins, drugs, and pathogens to the CNS have been described. This includes the meningeal blood-CSF barriers, the classical blood-brain barrier (BBB), the choroid plexus blood-CSF barrier, and the circumventricular organ barrier [65].

The most studied blood-CNS barrier is the classical BBB, which is primarily composed of brain endothelial cells that line blood vessels in the brain parenchyma. With a total surface area of 12 to 18 m^2 for the average human adult, this microvasculature constitutes the largest blood-CNS interface [66]. BBB microvessels are surrounded by basal lamina, astrocytes, pericytes, microglial cells and neurons, which collectively comprise what is known as the neurovascular unit (NVU) [67]. Compared to peripheral endothelial cells, BECs form a much more restrictive barrier due to the lack of fenestration, presence of tight junctions, and highly regulated transcellular transport [68]. Other cells of the NVU such as astrocytes, and pericytes support the barrier phenotype of BECs during and after development [67, 68]. Choroid plexus and circumventricular organs (CVOs) contain fenestrated blood vessels that lack tight junctions and are relatively permeable by solutes form the peripheral circulation [69, 70]. The choroid plexus is a spongy structure that is located in the ventricular system of the brain and produces CSF. It is composed of a single layer of microvilli-containing epithelial cells that are connected by tight junctions and separated from the endothelium by a thin layer of connective tissue called stroma [69]. The epithelial barrier at the choroid-plexus is commonly referred to as the blood-CSF barrier. CVOs located along the ventricular midline possess tight junction expressing ependymal cells (tanycytes) that restrict diffusion of macromolecules between the organ and the CSF [70, 71].

1.3.1 The meningeal blood-CSF barrier

Three meningeal layers encompass the human brain: the dura, the arachnoid, and the pia mater (**Figure 2**a). The dura forms the outermost layer closest to the scull and is composed of approximately 1 mm thick fibrous tissue that densely packed collagen fibers as well as vascularization and lymphatics [72]. Dural blood vessels are fenestrated, lack tight junctions, and permit passage of large solutes (43 kDA) [73, 74]. The arachnoid and pia are collectively referred to as the leptomeninges. The arachnoid mater is a roughly 200 µm thick layer of closely packed leptomeningeal cells connected via desmosomes and separates the dura from the CSF filled subarachnoid space (SAS) [72, 75]. Leptomeningeal cells of the arachnoid, particularly in the outer layer closest to the dura, contain tight junctions and efflux pumps, and act as a barrier to passage of CSF, solutes, and cells between the SAS and the permeable vasculature of the dura [75-77]. The arachnoid barrier restricts invasion of immune cells from dural blood vessels into the CSF and contains inflammatory cells in the SAS in cases of leptomeningitis [72]. Collagen fibers (trabeculae) coated with leptomeningeal cells span across the SAS connecting arachnoid and pia mater, and suspend arteries and veins within the SAS [72, 75] (**Figure 2**bI). The pia is a thin, mostly monolayer of LMCs joined by gap junctions and sometimes desmosomes

that is most closely situated to the CNS yet separated by a small subpial space [72, 75, 78]. Arteries pass the pia and enter the subpial space either perpendicular or parallel to the surface of the brain [79] (**Figure 2**bII). Vessels entering or exiting the brain parenchyma and/or the subpial space are coated by a complete layer of LMCs [80]. Pial LMCs are permissive to the passage of immune cells entering the SAS from the blood and tracers injected into the CSF [72, 81, 82]. Endothelial cells that comprise blood vessels of the subarachnoid and subpial spaces possess barrier characteristics similar to the BBB without contact to astrocytes, pericytes or other NVU cell types but LMCs instead [74] (**Figure 2**). In this study, the term meningeal blood-CSF barrier (mBCSFB) will be used in reference to this microvascular environment.

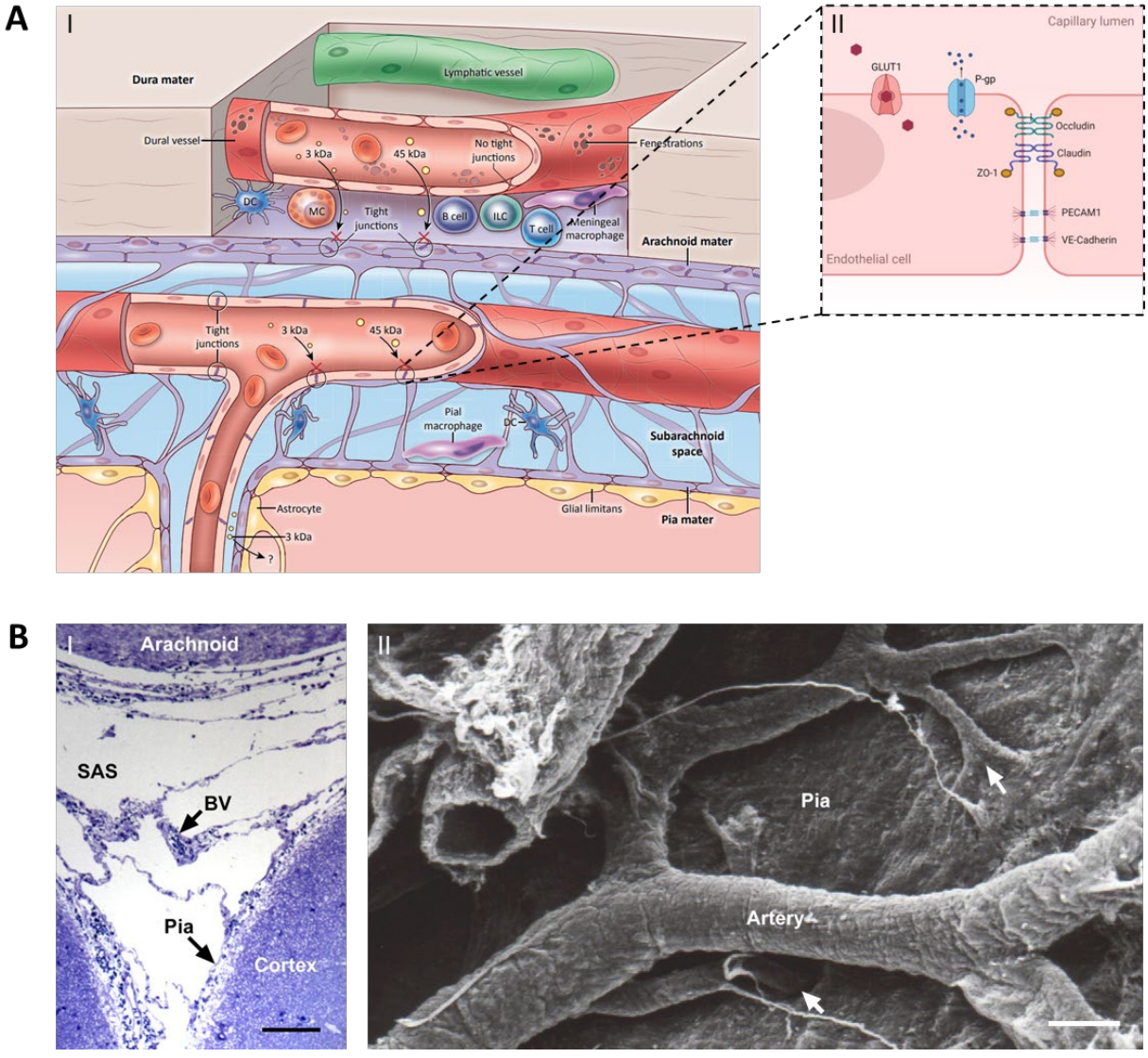

Figure 2. The meningeal blood-CSF barrier. **a**) Schematic representation of steady state meningeal anatomy (I, from Rua & McGavern 2018 [74]) and the BEC phenotype (II, created with BioRender.com). **b**) Leptomeninges of the adult human CSN. I) Tissue section stained with toluidine blue depicting the subarachnoid space (SAS) over the human cerebral hemispheres including blood vessels (BV) suspended by trabeculae. Scale bar 200 µm. II) Scanning electron micrograph showing blood vessels within the SAS entering the pial layer and brain cortex (arrows). Scale bar 150 µm. Adapted from Weller et al. 2018 [72].

1.3.2 Brain endothelial cells

BECs that line blood vessels in the leptomeningeal spaces and the brain parenchyma display a barrier phenotype that is distinct from peripheral endothelial cells to maintain CNS homeostasis. BECs are polarized cells that physically restrict diffusion of substances across the barrier by the absence of fenestra, generally low rates of endocytosis, and the presence of complex intercellular tight junctions [68] (**Figure 2**a). Tight junction complexes are found on the apical part of the cell membrane and contain transmembrane components that homo- and heterotopically interact with each other to connect adjacent cells and are linked to the cytoskeleton by cytoplasmic adaptor proteins [83]. The membrane spanning proteins present in BECs include claudins, tight junction-associated marvel proteins (TAMPs), and junctional adhesion molecules (JAMs) [84]. Several of the 27 identified members of the claudin family have been described to be expressed in BECs [85]. A particularly important role has been assigned to claudin-5 due to its specific and comparatively high expression in CNS endothelial cells and its major functional involvement in BBB stability during health and disease [86]. Three TAMPs have been identified at the mammalian BBB, namely occludin, tricellulin, and marvelD3 [84]. Occludin was the first described transmembrane component of tight junctions and is involved in many regulatory processes that can affect tight junction integrity and BBB permeability [83, 87, 88]. In the cytosol, adaptor proteins such as members of the zona occludens family (ZO-1, ZO-2, ZO-3) bind the c-terminal cytosolic domain of most transmembrane molecules including claudins, occludin, and JAMs [89-91]. ZO-1 and ZO-2 also bind directly to F-actin and other cytoskeletal proteins and regulate assembly of endothelial and epithelial intercellular junctions [92, 93]. Downregulation of tight junction components such as claudin-5, occludin, and ZO-1 are described in the pathology of most neurological disorders [83]. In addition to tight junctions, adherens and gap junctions can be found on BECs [94]. Adherens junction proteins such as endothelial (VE) cadherin are part of the junction complexes and important in their formation and maintenance [95, 96]. They are connected to the cytoskeleton via catenins but also interact with tight junction components such as ZO-1 [93, 96]. Finally, adhesins such as endothelial marker PECAM-1 (CD31) are found outside of organized tight and adherence junction complexes and can function as adhesive stress-response proteins to maintain vascular barrier integrity [96, 97].

In addition to forming a physically tight barrier, BECs contribute to maintaining proper CNS function by selectively regulating the movement of essential nutrients and toxins in and out of the brain (reviewed in [98]). ATP-binding cassette (ABC) transporters expressed in BECs mostly act as efflux pumps for the clearance of toxins and drugs from the CNS or endothelial cell lumen. This includes P-glycoprotein (P-gp, ABCB1, or multidrug resistance protein 1, Mdr1), breast cancer resistance protein (BCRP, or ABCG2), and multidrug-associated resistant proteins (MRPs, or ABCCs). The classical multidrug efflux transporter, P-gp, limits the entry of a large variety of drugs of different sizes and

structures [99]. Expression of P-gp is modulated under many conditions of neurological disease, including downregulation under bacterial infection [100, 101]. Members of the solute carrier (SLC) superfamily facilitate the transport of a wide range of substrates including organic ions, peptides, monocarboxylates, steroids, signaling molecules, and drugs [102]. For example, SLC2A transporters such as GLUT1 facilitate the transport of glucose to various tissues including the brain [103]. Finally, macromolecules including insulin or iron transport protein, transferrin, are transported across the BEC barrier via receptor mediated endocytosis [104, 105]. This mechanism has been taken advantage of for the CNS delivery of larger medicinal compounds such as monoclonal antibodies [106].

1.4 *N. meningitidis* interaction with the mBSCFB

While post-mortem studies have shown *N. meningitidis* adherence to endothelial cells of choroid plexus capillaries, no bacteria were found penetrating the choroidal epithelial barrier [107]. Furthermore, meningococci specifically adhered to leptomeninges and meningeal blood vessels but not to cortical brain tissue *in vitro* [108]. These observations suggest that meningococcal meningitis is the result of bacterial interaction with leptomeningeal microvessels, followed by infiltration of the SAS and interaction with LMCs. The ensuing inflammation of the leptomeninges and CSF-filled spaces is characterized by a plethora of host response molecules and rapid infiltration of polymorphonuclear leukocytes, which leads to gross cell and tissue necrosis [72].

1.4.1 *N. meningitidis* interaction with BECs

Adherence to BECs of the mBCSFB is mediated by Tfp that bind host cell receptor CD147, a member of the immunoglobulin superfamily, via PilE and PilV subunits [109] (**Figure 3**). CD147 forms hetero-oligomeric complexes with β2-adrenergenic receptor (β2AR), which belongs to the G protein coupled receptor family [110]. Complex formation increases the binding strength of *N. meningitidis* to BECs under shear stress and is governed by the scaffolding protein α-actinin-4 that binds the cytosolic tail of CD147 [110]. Following initial Tfp mediated attachment, several other meningococcal factors have been shown to enhance and/or modulate adhesion. Opa can interact with CEACAM receptors, although this may be more relevant in meningococcal interaction with nasopharyngeal epithelial cells compared to BECs as endogenous CEACAM expression is relatively low in endothelial cells [43, 111]. Opc directly binds extracellular matrix and serum components vitronectin and fibronectin and mediates adhesion to BECs via their respective receptors, αVβ3 and α5β1 integrin [112, 113]. NadA interacts with β1 integrins and LOX1 [44, 114]. PilQ and PorA may facilitate binding via the laminin receptor 1–galectin 3 complex [115]. Other meningococcal outer membrane proteins such as adhesin complex protein (ACP; [116]), MspA [46], and fructose-1, 6-bisphosphate aldolase (FBA; [117]) may enhance adhesion to BECs.

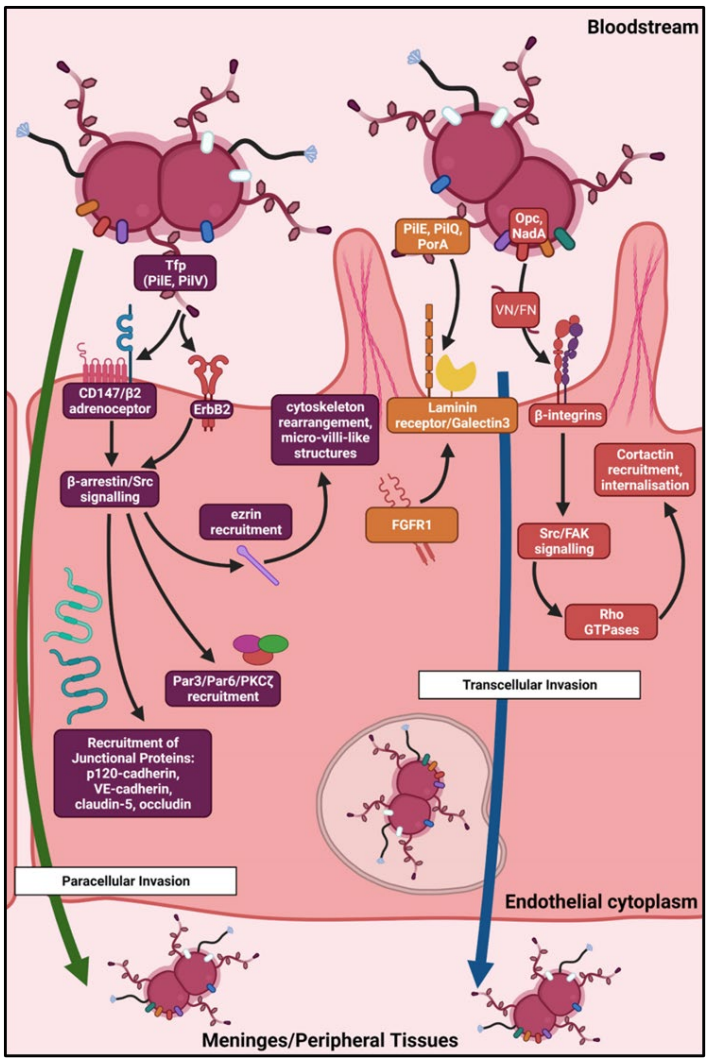

Figure 3. *N. meningitidis* interaction with brain endothelial cells. Schematic summary of meningococcal interaction with their cognate receptors, induction of signalling mechanisms, cortical plaque formation, transcytosis, and disruption of cellular junctions. From Mikucki et al. 2022 [20].

After adhesion, *N. meningitidis* interaction with host cell receptors promotes cell signaling events that lead to formation of membrane domains known as cortical plaques at the site of bacterial adhesion. Cortical plaque formation includes bulk accumulation of cellular components and cytoskeletal rearrangement that are thought to support vascular colonization and influence penetration of the BEC barrier. Interaction with Tfp subunits PilE and PilV activates β2AR, which leads to recruitment of molecular adaptor and signaling factor β-arrestin along with β-arrestin-binding molecules such as p120-catenin, VE-cadherin, and sarcoma tyrosine kinase (Src) [118]. Additionally, local production of membrane phospholipid phosphatidylinositol 4,5-bisphosphate (PIP2) is induced, probably through binding of the PIP2-producing enzyme PIP5K to β-arrestins [119]. PIP2 production allows the recruitment of ezrin and moesin, two members of the ezrin-radixin-moesin family (ERM), along with ezrin-binding proteins such as endothelial adhesins (E-Selectin, ICAM-1, ICAM-2, VCAM-1, and CD44) and tyrosine kinase transmembrane receptor ErbB2 [119, 120]. Enrichment of receptors such as ErbB2 is also promoted by the formation of ceramide-rich platforms, which is triggered by activation of acid

sphingomyelinase (ASM) [121]. ASM is shuttled to the outer leaflet of the membrane via lysosomal exocytosis induced by calcium flux triggered upon Tfp mediated meningococcal adhesion [122]. Cytoskeletal rearrangement and actin polymerization at the cortical plaque are facilitated by PIP2 activated ERM proteins that bind to F-actin, GTPases such as Cdc42 and Rho, and phosphorylated cortactin, an actin-binding protein which stimulates nucleation of actin filaments [123, 124]. Cytosolic cortactin is recruited to the cell cortex beneath adherent bacteria via a phosphoinositide-3-kinase (PI3K)/Rac1 pathway that depends on interaction of bacterial LOS with an unknown receptor [124]. Cortactin phosphorylation is mediated by Src kinase, which is activated by β-arrestin and ErbB2 binding [118, 120]. Cytoskeletal remodeling at the cortical plaque leads to the formation of microvillus-like cellular membrane protrusions around adherent bacteria and alongside Tfp fibres and may protect *N. meningitidis* against shear-forces exerted by the blood flow [110, 123, 125, 126].

Cortical plaque formation, membrane rearrangement, along with many of the signaling events and effector molecules described above also affect internalization of meningococci by endothelial cells [113, 120, 121, 123, 124]. In addition to Tfp mediated events, cellular invasion is strongly influenced by the indirect interaction of OpC with αVβ3 and α5β1 integrin via vitronectin and fibronectin, a process that seems to follow downregulation of the bacterial polysaccharide capsule after initial adhesion to unmask OpC [112, 113, 127]. Upon bacterial interaction, integrin signaling leads to activation of various kinases including c-Jun N-terminal kinases 1 and 2 (JNK1 and JNK2) and focal adhesion kinase (FAK) [128, 129]. FAK directly associates with integrins and acts in concert with Src to phosphorylate cortactin [128]. Activation of these kinases along with cortactin expression and phosphorylation are critical for efficient uptake of *N. meningitidis* [128, 129]. Although the fate of internalized meningococci is not entirely clear, a study has shown that *N. meningitidis* can survive and replicate inside cellular vacuoles [130]. Together, these observations have suggested a transcellular pathway for meningococcal traversal of the mBCSFB. However, disruption of cellular junctions and BEC barrier function upon *N. meningitidis* infection has also been reported, suggesting a paracellular route. Tfp mediated adhesion to BECs and the following signaling events lead to recruitment of the Par3/Par6/PKCζ polarity complex and cell junction components such as VE-cadherin and p120-catenin, which has been shown to increase paracellular permeability and bacterial transmigration [118, 131]. Furthermore, *N. meningitidis* infection induced proteolytic cleavage of TJ transmembrane protein occludin mediated by metalloproteinase MMP-8, which lead to occludin depletion at the cell periphery and weakening of the paracellular barrier [132]. Similar effects were observed in a recent study using induced pluripotent stell cell (iPSC)-derived BECs as a novel model to study *N. meningitidis* infection [133]. In conclusion, the pathway of mBCSFB traversal has not yet been fully elucidated, despite the wealth of *in vitro* data on *N. meningitidis* interaction with BECs.

Finally, a variety of other cellular responses to *N. meningitidis* infection have been observed including calcium flux, transcriptional regulation of apoptosis-related genes, and immune activation [119, 122, 129, 133-137]. Although expression of apoptosis-related gene was upregulated in different endothelial and brain endothelial *in vitro* models under infection, transcription of factors exerting cytoprotective effects such as TNFα-induced proteins (TNFAIP2, TNFAIP3) was also increased [133, 136, 137]. Additionally, elevated expression and secretion of proinflammatory cytokines including neutrophilic chemokines such as IL-8 have been observed in these models (although to varying extent) [129, 133, 135-137]. Mechanistically, it has been suggested that the activation of MAP kinase plays a role in the release of IL-6 and IL-8 [129]. In addition to transcriptional regulation, accumulation of adhesion molecules such as E-Selectin, ICAM, VCAM, and CD44 to the cortical plaque may also affect immune cell activation and recruitment at the brain endothelium, as these receptors play key roles in leukocyte rolling and arrest [119]. Lastly, transcript analysis from infected iPSC-derived BECs has recently revealed differentially expressed genes related to ion homeostasis and hypoxia including vascular endothelial growth factor A (VEGFA), which is important in angiogenesis and can increase vascular permeability [133].

1.4.2 *N. meningitidis* interaction with LMCs

To infiltrate the SAS, *N. meningitidis* must cross the BEC barrier, followed by a thin layer of connective tissue and a coat of leptomeningeal cells surrounding vessel [72]. Relatively little is known about meningococcal traversal of the LMC sheet enclosing the brain vascular endothelium and *N. meningitidis* interaction with LMCs of the arachnoid and pia mater. *N. meningitidis* specifically adheres to LMCs of fresh human brain sections and cells derived from human meningiomas [108]. The primary ligand that mediates meningococcal adhesion to LMCs is the Tfp. It was shown that Opa can increase association of capsulated bacteria with LMCs, however, only in strains expressing low-adhesive pili. Meningococci lacking a polysaccharide capsule were observed to interact more intimately with the host cells, likely due to exposition of outer membrane adhesins/invasins such as Opa and Opc. However, invasion of LMCs was not detected [108]. Additional bacterial factors described to contribute to *N. meningitidis* adhesion to meningeal cells are T-cell stimulating protein A (TspA) and ACP [116, 138]. Upon meningococcal challenge, meningioma derived LMCs secrete proinflammatory cytokines and chemokines IL-6, IL-8, and MCP-1, RANTES, and the GM-CSF [139]. Tfp-mediated adherence and bacterial components such as LOS and the capsule have varying effects on cytokine release [139]. More specifically, immune activation can occur independently of LOS-mediated toll-like receptor (TLR) 4 and TLR2 signaling [140]. Compared to other meningitis-causing bacteria, *N. meningitidis* induces a distinct inflammatory response profile upon interaction with human meningeal cells [141].

1.5 Modeling *N. meningitidis* interaction with the mBSCFB

The human-exclusive tropism of *N. meningitidis* and the specific barrier phenotype of BECs have presented unique challenges in modeling this complex host-pathogen interaction, particularly meningococcal traversal of the mBSCFB. Knowledge of the infection process of *N. meningitidis* has been primarily derived from *in vitro* studies using organ culture, primary or immortalized endothelial cells isolated from peripheral of brain-associated vessels [111]. Major drawbacks from using primary cells and tissue include limited availability of healthy tissue from the human brain and loss of barrier phenotype once cells are removed from the brain microenvironment [142, 143]. Immortalized cell lines can retain much of the BEC phenotype and eliminate the issue of limited scalability. Most research regarding *N. meningitidis* interaction with BECs of the mBCSFB has been conducted on immortalized cell lines including human bone-marrow-derived endothelial cells [109, 110, 120, 124, 144], human brain microvascular endothelial cells (HBMECs) [113, 121, 122, 128-130], human cerebral microvascular endothelial cells (hCMEC/D3) [109, 118, 131], and BB19 cells [109, 145]. Isolated from cerebral capillaries and immortalized using SV40 large T antigen, the HBMEC cell line was one of the first models to study bacterial interaction with brain endothelium [146, 147]. hCMEC/D3s were generated using transformation of microvascular cells from the temporal lobe of an epileptic patient with hTERT telomerase and SV40 [148]. The hCMEC/D3 model recapitulates most of the phenotypic features of BECs including expression of adherens and tight junction components and presence of functional transporter systems [148, 149]. Therefore, hCMEC/D3s have been a robust and widely utilized *in vitro* model to examine interaction with *N. meningitidis* and various other infectious agents including bacteria, viruses, fungi, and even parasites [109, 118, 150-155]. However, immortalized cell lines including HBMECs and hCMEC/D3s still lack certain key BEC characteristics such as continuous expression of tight junction proteins localized at the cell-cell borders and physiologically relevant paracellular tightness, indicated by high TEER [149, 156].

Recent advances in stem-cell technologies have generated model BEC-like cells derived from human iPSCs that possess superior barrier properties including continuous tight junction staining and high TEER [142, 157, 158]. Since then, iPSC-derived BECs (iBECs) have been used to study drug delivery and CNS diseases such as Huntington's disease and MCT8 deficiency (causing Allan-Hurndon-Dudley syndrome) [159-161]. Furthermore, an increasing number of studies show application of the iBEC model to examine bacterial and viral pathogens with neurotropism such as *Streptococcus agalactiae* (group B *streptococcus*) [101, 162, 163], Zika virus [164], and SARS-CoV2 [165]. Recently, our group has demonstrated that this model is also suitable to evaluate interaction with the human-specific bacterium *N. meningitidis* [133].

While BEC monoculture models are useful for testing simple parameters of host–microbe interactions, they cannot capture certain physiological and three-dimensional aspects of the native microenvironment that may be important when assessing pathogenesis. Such factors include presence of shear forces in the blood and supporting structures and cells around the blood vessels. Shear stress can be introduced via microfluidic pump systems and has been shown to affect the phenotype of peripheral and brain endothelial cells, although cellular response seems to be different between cell types and model used [166-168]. Certain aspects of meningococcal pathogenesis such as adherence and proliferation on ECs have previously been examined under shear stress [110, 126]. Co-culture systems that include model BECs and other cell types of the NVU, namely astrocytes and pericytes, have been increasingly implemented for modeling drug permeability and BBB function in health and disease [142, 169]. Astrocytes and pericytes have also been shown to induce BBB properties in primary bovine, porcine, rodent, or primate BEC models, however human primary and immortalized BEC lines were relatively non-responsive and remained at sub-physiological levels of paracellular tightness [142, 156, 170]. While iBECs alone can exhibit high paracellular tightness, co-culture with other NVU cell types has been reported to assert stimulating as well as stabilizing effects on iBEC barrier properties [142, 157, 158, 170-175]. Multicellular BBB models have not been used for infection studies with CNS pathogens yet, and co-culture with leptomeningeal cells, which are important in the context of the human mBCSFB, has not been explored before. Only direct interactions of *N. meningitidis* and other bacterial pathogens with LMCs have been investigated using meningioma derived LMCs [108, 141]. The meningioma cells were isolated from benign leptomeningeal tumors and share many features with normal LMCs including cell morphology and expression of desmosomal desmoplakin, intermediate filaments of cytokeratin and vimentin, and epithelial membrane antigen [108].

In vivo study of *N. meningitidis* infection is limited to humanized rodent models. Transgenic mice expressing CEACAMs have been used to investigate immune response and meningococcal interaction with the nasopharyngeal mucosa [176-178]. Mice engrafted with human dermal microvessels have been developed to assess *N. meningitidis* adhesion to the microvasculature and disease progressions such as purpura or meningitis [109, 179-181]. Nevertheless, translatability and scope of interactions that may be studied is limited in these models. Therefore, complex multicellular *in vitro* models that more closely resemble native physiology may be useful to study this complex human-specific host-pathogen mechanisms such as *N. meningitidis* interaction with the mBCSFB.

1.6 Aim of the study

The aim of this study was the development of a physiologically relevant *in vitro* model of the human mBCSFB using BECs derived from iPSCs in co-culture with meningioma derived LMCs to examine *N. meningitidis* interaction. In parallel, BEC-LMC co-culture models using the established infection model cell line hCMEC/D3 were developed and characterized for reference. To achieve this, the following topics were addressed:

- Establishment of iBEC-LMC and hCMEC/D3-LMC co-culture on transwell inserts
- Characterization of iBEC-LMC and hCMEC/D3-LMC co-culture models using electron and immunofluorescence microscopy
- Assessment of paracellular tightness using TEER and sodium fluorescein permeability assays
- Examination of meningococcal adherence, invasion, and traversal of the BEC-LMC co-culture models using gentamicin protection and transmigration assays as well as electron and super-resolution immunofluorescence microscopy
- Evaluation *N. meningitidis*-induced effects on the barrier integrity using TEER and analysis of cell-junction expression via qPCR and immunofluorescence staining
- Analysis of immune activation in response to infection of BECs co-cultured with LMCs using qPCR and ELISA

2 MATERIALS

2.1 Laboratory equipment

Table 1. Devices.

Description	Source
Centrifuge (Heraeus Megafuge 1.0R; Rotor: Heraeus #2704)	Thermo Scientific
Class II biosafety cabinet (LabGard)	Nuaire, ref. NU-437-400E
Class II biosafety cabinet (Safe 2020)	ThermoFisher Scientific
CO2 Air-Jacketed Incubator (DHD Autoflow)	Nuaire
Confocal microscope (Eclipse Ti2)	Nikon
Epithelial Volt-Ohm Meter (Millicell ERS-2) with STX electrode	Merck (Millipore), ref. MERS00002
Fluoresence microscope (Eclipse Ti)	Nikon
Inverted microscope (Wilovert)	Hund (Will Wetzlar)
JEM-1400Flash transmission electron microscope	JEOL
MACSQuant X	Miltenyi
Microcentrifuge (CT15E/CT15RE; Rotor: T15A61-3305/3519)	VWR Hitachi
Microplate reader (Infinite F200 PRO)	Tecan
ChemiDoc MP Imaging System	BioRad
NanoDrop One^{C}	Thermo Scientific
PCR Thermocycler (T3000)	Biometra
Pipette boy (Accu-Jet Pro)	Brand
RT-PCR thermocycler (StepOnePlus)	Applied Biosystems, ref. 4376600
Shaking incubator (Certomat H)	B. Braun Biotech

Table 2. Consumables.

Description	Source
Cell Culture Plates And Flasks	Sarstedt
Columbia Agar + 5 % Sheep Blood	Biomerieux, 43049
Costar Transwell Polyester Filters (0.4 µm; 12- / 24-Well)	Corning, 3460 / 3470
Cuvettes	Sarstedt, 67.742
Hemacytometer (Neubauer)	A. Hartenstein, Zk06
Microscope Cover Glasses	A. Hartenstein
Microscope Slides	A. Hartenstein, OTMM
qPCR Film (Microamp Optical Adhesive Film)	Applied Biosystems, 4211971
qPCR Plates (Microamp Fast 96-Well)	Applied Biosystems, 4346907
Reagent reservoirs (25/50 ml)	Carl Roth, EKX0.1
Serological Pipettes 5 ml, 10 ml, 25 ml	Sarstedt
Thincert Cell Culture Inserts (3 µm; 12- / 24-Well)	Greiner, 665630 / 662630

2.2 Chemicals and reagents

Table 3. Chemicals and reagents.

Designation	Source	Identifier
Accutase (1x)	Sigma	Ref. A6964
Acetic acid	Sigma	A6283
Agarose	Invitrogen	16500-500
B-27™ Supplement (50X), serum free	Gibco	17504044
Bacto Proteose Peptone	BD Biosciences	211684
BD OptEIA Set Human IL-8	BD Biosciences	555244
beta-mercaptoethanol	Merck (Sigma-Aldrich)	805740
Collagen I, rat tail	Corning	354236
Collagen I, rat tail	Gibco	A1048301
Collagen IV	Sigma	C5533
Control siRNA (FITC Conjugate)-A	SantaCruz	sc-36869
D(+)-Glucose	Merck (Sigma-Aldrich)	G8270
DAPI	Invitrogen	D1306
DMEM, high glucose, GlutaMAX™ Supplement, pyruvate	Gibco	31966021
DMEM/F12	Gibco	31330-038
DMSO	Carl Roth	A994.1
Dulbecco's phosphate-buffered saline (DPBS)	Gibco	21600-069
Durcupan	Sigma	
EndoGRO-MV Complete Culture Media Kit	Merck / Millipore	SCME004
Erythromycin	Sigma-Aldrich	53889
Ethanol, 100 %	Carl Roth	9065.2
Ethanol, 96 %	Carl Roth	P075.4
$Fe(NO_3)_3$	Carl Roth	5632,1
Fetal Calf Serum (FCS)	Life Technologies	10270
Fibronectin	Sigma	F1141
Fluoroshield™	Sigma	F6182-20ML
Gentamicin	Biochrom by Merck Millipore	A2712
GlutaMAX	Gibco	35050038
Glutaraldehyde Grade I (25%)	Sigma	G5882-50ML
Human basic fibroblast growth factor (bFGF)	PeproTech	100-18B
Human Endothelial Serum Free Medium (hESFM)	Gibco	11111-044
Isopropanol	Carl Roth	6752.4
K_2HPO_4	Merck Chemicals	7758-11-4
KH_2PO_4	Merck Chemicals	7778-77-0
Knockout serum replacement (KOSR)	Gibco	10828-028
L-Glutamine	Thermo Scientific	25030024
LunaScript RT SuperMix Kit	NEB	E3010L
Matrigel, growth factor reduced	Corning	354230
MEM Non-Essential Amino Acids (NEAA)	Gibco	11140-035
Methanol	Carl Roth	4627,5
$MgCl_2$	Carl Roth	KK36.1
Na_2CO_3	Carl Roth	A135.2
NaCl	Carl Roth	P029.2
$NaHCO_3$	Carl Roth	6329
Natriumfluorescein (NaF)	Sigma-Aldrich	F6377
NucleoSpin RNA isolation kit	Machery-Nagel	740955
OsO4	Electron Microscopy Sciences	19110
Paraformaldehyde (PFA)	Carl Roth	0335.2
Penicillin-Streptomycin	Gibco	15140122
Phalloidin-Alexa Fluor 543	Invitrogen	A22283
Phalloidin-ATTO 643	ATTO-Tec	AD643-81
Platelet poor plasma-derived serum, bovine (PDS)	Fisher	50-443-029

Designation	Source	Identifier
PowerUp SYBR Green Master Mix	Applied Biosystems	A25742
ProLong™ Glass Antifade Mountant	Invitrogen	P36982
Proteose-peptone (Bacto™)	Gibco	211684
Recombinant Human FGF-basic (bFGF)	PeproTech	100-18B-250UG
Retinoic acid (RA)	Sigma	R2625
ROCK inhibitor, Y27632 dihydrochloride	Tocris	1254
Saponin	SERVA	34655.02
Sodium borohydrate ($NaBH_4$)	Sigma-Aldrich	452882
Starch	Sigma-Aldrich	85642
StemFlex™ Medium	Gibco	A3349401
Sulfuric acid (H_2SO_4)	Carl Roth	4623.4
Thiamine pyrophosphate	Sigma	C8754-5G
TMB Substrate Kit, Pierce™	Thermo Scientific	34021
TransIT-siQUEST® Transfection Reagent	Mirus	MIR 2110
Triton-X 100	Carl Roth	3051.4
Trypan Blue Solution, 0.4%	Gibco	15250061
Trypsin-EDTA (0.05%), phenol red	Gibco	25300054
Tween 20	Carl Roth	9127.1
Uranyl acetate	Merck	
Versene	Gibco	15040-033

2.3 Cells and bacterial strains

Table 4. Cells.

Designation	Description	Reference
IMR90-4	Human induced pluripotent stem cells (iPSC) reprogrammed from fetal lung fibroblasts by lentiviral transduction [186]	WiCell
hCMEC/D3	Human cerebral microvascular endothelial cells derived from human temporal lobe microvessels and immortalized using hTERT and SV40 [148]	Sigma, ref. SCC066
Meningioma cells	Meningioma cells of the meningothelial histological subtype derived from tumor biopsies [108]	Kindly provided by M. Christodoulides

Table 5. Bacterial strains.

Bacterial strain	Genotype/characteristics	Origin
MC58	Sg B strain of the ST-74 (ST-32 cc)	Kindly provided by E. R. Moxon [187]
MC58-GFP	GFP-expressing MC58, pEG2-GFP-ErmR plasmid, Erythromycin resistance	AG Schubert-Unkmeir [121]

2.4 Media, buffers, and solutions

Table 6. Cell culture media. Media were filter-sterilized and **stored at 4 °C**.

Medium	Contents		Storage
iPSC medium (StemFlex)	StemFlex basal medium	90 %	4 °C
	50x StemFlex supplement	10 %	-20 °C
Unconditioned medium (UM)	DMEM/F12	78.5 %	4 °C
	KOSR	20 %	-20 °C
	MEM-NEAA	1 %	4 °C
	GlutaMAX	0.5 % (1mM)	RT
	beta-mercaptoethanol	0.07 % (0.1mM)	RT
EC medium + bFGF + RA[a]	hESFM	99 %	4 °C
	PDS /or B-27	1 %	-20 °C
	bFGF	20 ng/ml	-20 °C
	RA[a]	10 µM	-20 °C, dark
hCMEC/D3 medium (EndoGRO[b])	EndoGRO™ Basal Medium	475 ml	4 °C
	EndoGRO-LS Supplement	1 ml	-20 °C
	rh EGF	0.5 ml	-20 °C
	L-Glutamine[c]	25 ml	-20 °C
	Hydrocortisone Hemisuccinate	0.5 ml	-20 °C
	Heparin Sulfate	0.5 ml	-20 °C
	Ascorbic Acid	0.5 ml	-20 °C
	FCS	25 ml	-20 °C
Meningioma cell (LMC) medium	DMEM	89 %	4 °C
	FCS	10 %	-20 °C
	Pen/Strep	1 %	-20 °C (4 °C)

[a]Thaw and add RA fresh to EC + bFGF when needed. [b]EndoGRO-MV Complete Culture Media Kit. [c]Thaw at 37 °C and mix vigorously to dissolve precipitate.

Table 7. Media and solutions for bacterial culture.

Designation	Contents		Notes
Kellogg's supplement I	Glucose L-Glutamine Thiamine pyrophosphate dH_2O	40 g 1 g 2 mg *to* 100 ml	
Kellogg's supplement II	Fe(NO3)3 dH_2O	50 mg *to* 100 ml	
Kellog´s Supplement for PPM +	Kellogg's supplement I Kellogg's supplement II	100 ml 10 ml	Filter-sterilize (0.2 µm filter)
Buffer solution for PPM	KH2PO4 K2HPO4 dH_2O	200 g 50 g *to* 1 L	Adjust pH to 7.25 – 7.5 and autoclave
Proteose peptone medium (PPM)	Proteose peptone NaCl Starch Buffer solution dH_2O	7.5 g 2.5 g 0.25 g 10 ml *to* 500 ml	Adjust pH to 7.2 and autoclave
PPM +	PPM Kellog´s Supplement MgCl2 (2 M) NaHCO3 (8.4 %)	10 ml 100 µl 50 µl 50 µl	Prepare fresh for liquid bacterial subculture
Freezing medium	Tryptic soy broth Glycerol (86%) dH_2O	30 g 465 ml 535 ml	Heat slightly to dissolve and autoclave

Table 8. Buffers and other solutions.

Designation	Contents		Notes
Cacodylate buffer	Cacodylate pH 7.2 KCl MgCl2	50 mM 50 mM 2.5 mM	
Cytoskeleton buffer	MES NaCl EGTA Glucose $MgCl_2$	10 mM 150 mM 5 mM 5 mM 5 mM	Adjusted to pH 6.11
ELISA coating buffer	$NaHCO_3$ Na_2CO_3 ddH2O	7.13 g 1.59 g *to* 1 L	Adjusted to pH 9.5
ELISA stop solution	H_2SO_4 (96%) ddH2O	2.77 ml 47.23	
ELISA wash buffer	PBS Tween-20	200 ml 100 µl	
Immunofluorescence blocking buffer	PBS FCS	90 % 10 %	

2.5 Antibodies and primers

Table 9. Antibodies used for immunofluorescence staining.

Target antigen	Dilution	Species and clonal information	Vendor
CD31	1:200	Rb, polyclonal, ref. ab32457	Abcam
VE-cadherin[a]	1:25	Ms, clone BV9	Santa Cruz
ZO-1[b]	1:100	Ms, clone ZO1-1A12	Invitrogen
Occludin[a]	1:200	Ms, clone OC-3F10	Invitrogen
Claudin-5[a]	1:50	Ms, clone 4C3C2	Invitrogen
Vimentin	1:100	Ms, clone V9	Invitrogen
Desmoplakin I/II	1:50	Ms, clone A-1	Santa Cruz
EMA (Mucin 1)	1:25	Ms, clone VU4H5	Santa Cruz
E-cadherin	1:100	Ms, clone G-10	Santa Cruz
Laminin	1:50	Rb, polyclonal, ref. PA1-16730	Invitrogen
Secondary antibodies			
IgG, Ms	1:200	Gt, polyclonal, Alexa Fluor 488, ref. A11001	Invitrogen
IgG, Rb	1:200	Dk, polyclonal, Alexa Fluor 555, ref. A31572	Invitrogen

[a]Stebbins et at. 2016 [182]. [b]Kim et al. 2017 [163].

Table 10. qPCR primers.

Gene	Forward sequence	Reverse sequence
18S rRNA[a]	GTAACCCGTTGAACCCCATT	CCATCCAATCGGTAGTAGCG
PECAM1	AAGTGGAGTCCAGCCGCATATC	ATGGAGCAGGACAGGTTCAGTC
CDH5	AAGGACATAACACCACGAAACG	CAAACTGCCCATACTTGACTGTG
TJP1	GTCCAGAATCTCGGAAAAGTGCC	CTTTCAGCGCACCATpAACC
OCLN	ATGGCAAAGTGAATGACAAGCGG	CTGTAACGAGGCTGCCTGAAGT
CLDN5	CTCTGCTGGTTCGCCAACAT	CAGCTCGTACTTCTGCGACA
SNAI1[b]	GGACCCACACTGGCGAGAAG	ATTCGGGAGAAGGTCCGAGC
CXCL8[c]	AGCTCTGTGTGAAGGTGCAG	AATTTCTGTGTTGGCGCAGT
CXCL1[d]	CTCTTCCGCTCCTCTCACAG	GGGGACTTCACGTTCACACT
CXCL2[d]	CTCAAGAATGGGCAGAAAGC	AAACACATTAGGCGCAATCC
IL6[d]	GGAGACTTGCCTGGTGAAAA	CAGGGGTGGTTATTGCATCT
CCL20[d]	GCGCAAATCCAAAACAGACT	CAAGTCCAGTGAGGCACAAA

[a]Rho et al 2010 [183]. [b]Han et al 2011 [184]. [c]Kim et al 2019 [101]. [d]van Sorge et al 2008 [185].

3 METHODS

3.1 Cell culture

All cells used in this project were cultured in a sterile tissue culture incubator at 37°C, 5% CO_2, and approximately 95% humidity. Handling of cells was conducted in a sterile class II biosafety cabinet. Enumeration of cells from a single-cell suspension was generally done using a hemocytometer after 1:1 dilution with 0.4% trypan blue to distinguish between live and dead cells. Cryopreservation of cells was generally achieved by suspension in medium with 10% DMSO and gradual freezing at – 80 °C o/n using a freezing container (Mr. Frosty) filled with isopropanol. The cryotubes were then moved to a liquid nitrogen tank for long term storage. Cultures were started from frozen stocks by rapid thawing followed by dilution in medium and seeding onto coated tissue culture plastic.

3.1.1 hCMEC/D3 culture

hCMEC/D3s were cultured on collagen 1 coated tissue culture (TC) flasks in EndoGRO-MV Complete Culture Media. Flasks were coated with 30 µg/ml collagen 1 (rat tail) in 60% ethanol, letting the coating solution evaporate in the sterile environment of a class II biosafety cabinet. hCMEC/D3 cultures were maintained up to passage 30 and split as needed – typically once a week when confluent and at a ratio of 1:100. When splitting, cells were washed once with PBS and dissociated enzymatically using Accutase (1 ml for a 25 cm² flask) for 4-5 min at 37 °C. Finally, cells were diluted in fresh EndoGRO medium and seeded at the desired density.

3.1.2 Meningioma cell culture

Human meningioma cells of the meningothelial histological subtype were kindly provided by Prof. Myron Christodoulides (University of Southampton). Isolation and immunohistochemical characterization were conducted as described [108]. Cells were grown on 30 µg/ml collagen 1 (rat tail) coated TC flasks and in DMEM with 10% FCS and 1% Pen/Strep for up to 10 passages or until showing signs of senescence. Cultures were split twice a week by enzymatic dissociation using Trypsin-EDTA or Accutase (2 ml for a 75 cm² flask) for 4-5 min at 37 °C after PBS wash and reseeding at a density of 4 x 10^3 cells/cm².

3.1.3 Matrigel coating of tissue culture plastic for iPSC culture

Matrigel, which rapidly forms a gel at room temperature (RT), was thawed in the fridge overnight (o/n) and aliquoted quickly at 2.5 mg per aliquot on ice. For coating of tissue TC multi-well plates and flasks, one aliquot of Matrigel was added to 30 ml of DMEM/F12. To prevent gel formation, the frozen Matrigel was thawed and diluted quickly by adding 1 ml of medium to the aliquot, pipetting up and down until thawed, and transferring immediately to the remaining DMEM/F12 medium. 1 ml of coating solution was used per well of a 6-well plate and 12 ml per 75 cm^2 flask. If not used the same day, an

additional equal amount of DMEM/F12 was added per well/flask to avoid drying out. Finally, the coated TC plastic was incubated at 37 °C for at least 1 h or until ready to use. Matrigel coated TC plastic can be prepared up to two weeks in advance and kept at 37 °C. To avoid the coating solution drying out, each well of a coated 6-well plate was topped up with 0.5 ml fresh DMEM/F12 after a week of incubation.

3.1.4 iPSC maintenance culture

Human iPSC line IMR90-4 was grown on Matrigel coated 6-well plates in StemFlex medium according to previously published protocols [182, 188]. iPSCs were maintained by changing medium daily and splitting twice a week. For each passage, cultures that reached approximately 80 % confluence with spaces remaining in between the colonies and no signs of spontaneous differentiation (clear edges around the colonies) were dissociated using 1 ml Versene at 37 °C for 7 min. Two or more wells were prepared for iPSC seeding by replacing the Matrigel coating solution with StemFlex medium. After incubation, the Versene solution was carefully removed, and iPSC colonies were completely detached by rinsing the well with 6 ml StemFlex. Finally, cells were seeded onto the prepared wells at the appropriate densities – typically 1:6 and 1:12 – and distributed evenly across the well by shaking the plate back and forth and left to right, pausing in between alternating shaking motions until the medium has settled. For successful reattachment and growth after passage, it is important to achieve appropriate density and avoid dissociating the colonies into a single cell suspension. Denser wells chosen for passage may require longer Versene treatment.

3.1.5 Cryopreservation of iPSCs

To start iPSC culture from frozen stock, cells were thawed quickly, diluted with 9 ml StemFlex in a 50 ml comical tube, and spun down at 1500 x g for 10 min. Matrigel solution on four wells of a coated 6-well plate was replaced with 2 ml StemFlex supplemented with 10 µM ROCK inhibitor Y27632. ROCK inhibition enhances survival of dissociated single stem cells and thereby improves efficiency of iPSC cryopreservation [189]. After centrifugation, the cells were resuspended in 2 ml StemFlex + ROCK and seeded onto the prepared wells at four different densities (1:2, 1:4, 1:8, rest). The cells were distributed evenly by linear shaking back and forth and incubated for 1 day before removing ROCK inhibitor by changing to fresh StemFlex medium. To generate a cryo-stock of iPSCs, cells from an approximately 80 % confluent well were dissociated using Versene as if splitting for passage. Dissociated iPSCs were collected in 5 ml StemFlex and spun down spun down at 1500 x g for 10 min. Then, cells were resuspended in 2 ml StemFlex with 10 % DMSO, distributed equally across two vials, and gradually frozen at - 80 °C o/n using a freezing container (Mr. Frosty) filled with isopropanol. For better cell survival, ROCK inhibitor may also be added to the freezing medium.

3.1.6 Generation of brain endothelial-like cells from iPSCs

iBECs were differentiated from iPSCs as previously described [182, 188]. Cells from IMR90-4 maintenance culture were dissociated enzymatically using 1 ml of Accutase for 7 min at 37 °C. Detached cells were collected using a p1000 pipette, diluted with at least equal volume of StemFlex medium, and spun down at 1500 x g for 10 min. After centrifugation, cells were resuspended in 1 ml StemFlex per well and mixed thoroughly to generate a single-cell suspension. iPSCs were counted using a hemacytometer and seeded onto Matrigel coated cell culture flasks at a density of 1 x 10^4 cells/cm². Prior to seeding, cells were diluted in StemFlex medium and supplemented with 10 µM ROCK inhibitor (1:1000 dilution from 10 mM stock) to enhance iPSC survival in single-cell suspension. Typically, 7.5 x 10^5 cells were added to 12 ml medium, followed by addition of ROCK and seeding onto a 75 cm² flask. One day after seeding, ROCK inhibitor was removed by changing media to fresh StemFlex. At this point, cells should be evenly distributed across the flask exhibiting a spread, mesenchymal-like morphology due to the ROCK inhibitor treatment [182, 188]. After seeding and attachment, iPSCs were expanded in StemFlex for an additional two days, during which the cells display typical colony growth. Once the appropriate density was achieved (typically 3 days after seeding), differentiation was induced by changing media to unconditioned medium (UM; day 0). Co-differentiation of neuronal and brain endothelial cells in UM was carried out for 6 days, changing medium daily. The cell layer becomes confluent in 2 to 3 days and a cobblestone-like appearance – indicating presence of nestin$^+$ "neural tracts" around fields of PECAM-1$^+$ cells [157, 158] – develop as the differentiation progresses. After 6 days, the medium was changed to endothelial cell (EC) medium with 20 ng/ml basic fibroblast growth factor (bFGF) and 10 µM all trans-retinoic acid (RA) for 2 days.

Finally, the differentiated iBECs were isolated by seeding onto a selective matrix of collagen IV and fibronectin. Cells were dissociated using Accutase for 30 to 60 min at 37 °C, diluted with hESFM, and counted using a hemacytometer. After removing Accutase by centrifugation (1500 x g for 10 min), cells were resuspended in EC medium with bFGF and RA and seeded onto collagen IV and fibronectin coated transwell inserts or TC plates with a seeding density of approximately 9 x 10^5 cells/cm² or 4.5 x 10^5 cells/cm², respectively. bFGF and RA as well as cells excluded by the matrix mediated purification of iBECs were removed after one day by changing the medium to basic EC medium. TEER measurement and immunofluorescence staining of characteristic BEC markers were conducted to control quality of differentiated iBEC layers.

3.1.7 Co-culture of iBECs and meningioma cells

Co-culture with meningioma cells was set up on the day of iBEC purification after expansion in EC medium – typically on day 8 of differentiation (**Figure 4**a). The day before, transwell inserts [0.4 µm inserts (Corning), or 3 µm inserts (Greiner)] were coated on top with collagen IV and fibronectin in

water (1:4:5 ratio) for iBEC purification as previously described [182, 188]. Additionally, transwells were coated with 150 µg/ml collagen 1 on the bottom for direct co-culture with meningioma cells. Coated inserts were prepared for cell seeding by aspirating the coating solution and letting TC plates and inserts dry in a biosafety cabinet. Meningioma cells were dissociated, counted, and seeded onto the underside of the transwell at a density of 3.6 x 10^4 cells/cm² (40K/12K per 12-/24-well transwell) in LMC medium with Pen/Step. For seeding onto inserts with a 3 µm pore size in particular, cell suspension was sandwiched between insert membrane and well bottom of a flipped TC plate to prevent adverse effect caused by medium leaking through the membrane (**Figure 4**a). As dimensions may vary depending on the type and manufacturer of TC plastic used, it is important to note that enough space between membrane and well bottom as well as adequate seeding volumes ensure proper attachment of cells on the transwell bottom. In this study, optimal seeding volumes were 200 µl and 60 µl for 12-/24-well inserts (Greiner) and plates (Sarstedt). For indirect co-culture, LMCs were seeded onto collagen 1 coated plates at 2.2 x 10^4 cells/cm². LMCs were incubated for 4 h at 37 °C prior to addition of iBECs. Transwells (and plates) were flipped back, LMC medium was aspirated, and 9 x 10^5 cells/cm² from the iBEC differentiation were seeded on top of the transwell membrane for ECM-induced BEC purification and start of co-culture. Co-cultures were kept in EC medium supplemented with 1% Pen/Strep to minimize risk of contamination during co-culture set-up. As per iBEC differentiation protocol, bFGF and RA were removed after one day and experiments were conducted on the second day of co-culture.

3.1.8 Co-culture of hCMEC/D3s and meningioma cells

For hCMEC/D3 and meningioma cell co-culture, transwells were coated with 150 µg/ml collagen 1 (top and bottom). Seeding of LMCs was performed as described for co-culture with iBECs. After 4h of incubation to allow for LMC attachment, transwells and plates were flipped back, LMC medium was aspirated, and hCMEC/D3 cells were added to the top of the inserts at a density of 9 x 10^4 cells/cm². hCMEC/D3s and LMCs were co-cultured in hCMEC/D3 medium (EndoGRO-MV) with 1% Pen/Strep, and experiments were conducted after 3 days.

3.2 Transendothelial electrical resistance

To monitor tightness and integrity of the cellular barrier non-invasively, TEER was measured using a volt-ohm meter as described previously [188]. Prior to use, the “chopstick” electrode was disinfected in 70% ethanol for at least 5 min (<15 min) and air-dried in the biosafety cabinet. Measurements were conducted immediately after retrieval of the cells from the incubator to minimize temperature induced artifacts. Both prongs of the electrode were placed around the transwell insert with the longer electrode lightly resting on the well bottom for consistent measurements. The volt-ohm meter applies an alternating current with a low frequency of 12.5 Hz between the electrodes to detect electrical

resistance of a confluent cell layer influenced by paracellular tightness. Raw measurements were corrected for blank resistance of a coated transwell and multiplied by the culture area of the insert to obtain TEER values ($\Omega \times cm^2$).

3.3 Sodium fluorescein permeability

In addition to TEER, permeability to sodium fluorescein (NaF) – a small 376 Da fluorescent tracer molecule – was evaluated following established protocols [182]. After TEER measurement for quality control, medium on both sides of the insert was replaced with fresh pre-warmed medium, and cells were incubated for 1 h at 37 °C. To start the permeability assay, baseline TEER was measured and medium on top of the transwells was replaced with pre-warmed 10 µM NaF solution (diluted in medium from 10 mM NaF stock). Cells were incubated for 1 h at 37 °C with samples (150 µl) being taken from the basolateral compartment and transferred to a clear-bottom 96-well plate every 15 min. Volume removed during sampling was immediately replaced with fresh pre-warmed medium. At the 60 min time point, additional samples were collected from the top compartments and diluted 1:10 to prevent oversaturated signal. Fluorescence (485 nm excitation/530 nm emission) was measured using a fluorescent plate reader. After signal correction by removing background and accounting for signal loss from sampling, NaF permeability values were calculated using linear regression of clearance volume vs. time for each transwell with cells and a blank insert. For detailed description of the calculations refer to Stebbins et al. 2016 [182].

3.4 Immunofluorescence

Immunocytochemistry on co-culture models was adapted from published protocols for iBEC and LMC staining [108, 182, 188]. Cells were washed once with PBS and fixed with ice-cold methanol for 15 min at RT. After three more washes in PBS, inserts were incubated in 10% FCS (in PBS) blocking solution for 1 h at RT. For immunofluorescent labeling of epithelial membrane antigen (EMA/Mucin 1) and E-cadherin, 4% paraformaldehyde was used as the fixation agent, and cells were blocked and permeabilized with 10% FCS containing 0.1% saponin. PET membranes were carefully removed from the transwells using a scalpel and transferred to a multi-well plate (24-/48-well for 12-/24-well inserts) containing primary antibody diluted in blocking solution. Samples were incubated with primary antibody o/n at 4 °C. The next day, inserts were washed three times in PBS before adding secondary antibody in 10% FCS for 1 h at RT. After secondary antibody staining, samples were washed twice and incubated with DAPI (1:5000 in PBS) for nucleus labeling for 15 min at RT. Excess DAPI was removed by a final PBS wash and inserts were removed from the multi-well plate for mounting. On a glass slide, membranes were carefully cut in half using a scalpel and placed onto a clean slide facing opposite directions for proper imaging of both cell layers. After adding a drop of Fluoroshield mounting medium onto the sections, a cover slip was placed on top, and the mounting medium was allowed to harden at

RT for at least 20 min. Finally, images of the cell staining were acquired and analyzed on a Nikon Eclipse T*i*2 confocal microscope using NIS Elements image software version 5.02. Junction coverage was determined for occludin expression using the JAnaP junction analyzer program [190], in co-operation with Mustafa Divyapicigil and Asst. Prof. Brandon J. Kim (University of Alabama).

3.5 Bacterial culture

Serogroup B strain MC58 was predominately used to model infection with virulent *Neisseria meningitidis*. Meningococci were cryopreserved in freezing medium containing (40% glycerol in TBS) at – 80 °C. From frozen stock, bacteria were streaked on Columbia agar with 5% sheep blood and grown at 37 °C and 5% CO_2 overnight. The following day, 10 ml of proteose peptone medium (PPM) was freshly supplemented with 1% Kellogg's supplement, 10 nM $MgCL_2$ and 10 nM $NaHCO_3$, and inoculated with a fraction of the o/n culture. Liquid subculture of *N. meningitidis* was conducted at 37 °C and 200 rpm for 60 to 90 min, before bacteria were used for infection. GFP-expressing mutant strain MC58-GFP was grown on GC agar plates and in PPM+ supplemented with 7 µg/ml Erythromycin to apply selection pressure to retain the GFP-expression plasmid.

3.6 Infection assays

One day prior to infection, cellular co-cultures were washed twice with PBS and fresh medium without antibiotics was added. On the day of the experiment, medium was replaced once more at least 1 h before adding bacteria. Meningococci were prepared for infection as described previously [188]. Bacteria from liquid subculture were spun down at 4000 x g for 10 min and resuspended in PBS. To achieve the desired multiplicity of infection (MOI), density of the bacterial suspension was determined using OD600 measurements and adjusted either in PBS followed by dilution in cell culture medium or directly in cell culture medium. Finally, cells in the co-culture models were infected by adding 100 µl of the adjusted bacterial suspension onto the apical side of the transwell inserts. Unless specifically noted otherwise, an MOI of 10 was used for infection experiments.

3.7 Gentamicin protection assay

BEC layers on transwell inserts with or without LMC co-culture were infected with *N. meningitidis* strain MC58 for 2 h or 8 h using an MOI of 100. These infection parameters are consistent with previous studies on meningococcal interaction with BECs [110, 118, 122, 126, 129]. Gentamicin protection assays were used to quantify bacterial adherence and invasion of the endothelial cell layer at the indicated time point post-infection (p.i.). For enumeration of cell-associated bacteria, co-cultures washed once with PBS before BECs on top of the inserts were dissociated and lysed Trypsin-EDTA saponin. Specifically, in the 12-well format, cells were treated 100 µl of 0.05% Trypsin-EDTA and incubated for 5 min before 200 µl of 1.5% saponin in PBS was added on top for an additional 15 min at

RT. Samples were collected, diluted in PBS in a 1:10 dilution series, and plated onto blood agar plates. After o/n incubation at 37 °C, the number of colony-forming units (cfu) per BEC layer was determined from cfu counts of countable dilutions. To quantify invasive bacteria, cells were washed with PBS and incubated with cell culture medium containing 200 µg/ml Gentamicin at 37°C for 2 h to kill extracellular bacteria. After that, cell lysates were collected, diluted, and plated as described above.

3.8 Transmigration assay

Cells were cultured on transwell inserts with a 3 µm pore to allow for bacterial traversal of the artificial membrane and infected with *N. meningitidis* for the indicated time frames of 2 h to 30 h. At each time point, the rate of bacterial transmigration was determined by quantification of cfu crossing the model cell barrier within one hour. Inserts were washed twice with PBS exclusively on the basolateral side, transferred to fresh medium, and incubated for 1 h at 37 °C and 5% CO_2. Finally, samples were collected from the bottom compartment and plated from a dilution series. Transmigration rates were calculated from the cfu counts.

3.9 Structured illumination microscopy

BEC-LMC co-culture models were infected with GFP-expressing mutant of *N. meningitidis* strain MC58 for 24 h. After infection cells were washed once with PBS and permeabilized with 0.25% glutaraldehyde (GA) and 0.25% Triton X-100 in cytoskeleton buffer (CB) for 1-2 min at 37 °C. Models were fixed with 2% GA in CB for 10 min at RT. Following two washing steps in PBS, samples were quenched in 0.1% sodium borohydride ($NaBH_4$) in PBS for 7 min at RT. After another PBS wash, insert membranes were cut out, transferred to a multi-well plate, and incubated with 5 U/ml phalloidin-Alexa Fluor 543 or 100 nM phalloidin-ATTO 643 in PBS overnight at 4 °C. Nuclei were stained with DAPI (1:5000 in PBS) for 15 min at RT and washed once in ddH_2O. Finally, membranes were halved using a scalpel and mounted on a clean glass slide using ProLong™ Glass Antifade Mountant and clean high precision coverslips. The halves were mounted with either the BEC or the LMC side facing the coverslip, and the mounting medium was cured o/n at RT before being stored at 4 °C.

Structured illumination microscopy (SIM) was performed in collaboration with Marvin Jungblut and Prof. Markus Sauer (Department of Biotechnology and Biophysics). SIM was performed on a Zeiss Elyra 7 with Lattice SIM²with 9 or 13 phase-shifts of the lattice SIM pattern. A 40x (Plan-Apochromat 40x/1.4 Oil DIC M27) or a 63x (Plan-Apochromat 63x/1.4 Oil DIC M27) oil immersion objective and four different excitation lasers (405 nm diode, 488 nm OPSL, 561 nm OPSL, and 642 nm diode) were used. Z-stack images were taken in 3D Leap mode with optimal z-steps and appropriate band-pass and long-pass filters sets controlled by a piezo stage. Super-resolved images were reconstructed using ZEN 3.0 SR FP2 (black) (Version 16.0.10.306; Zeiss) with SIM and SIM^2 processing modules. Processing of final images was performed using Imaris 9.2.1. (Bitplane).

3.10 Transmission electron microscopy

To prepare BEC-LMC co-cultures for TEM at the indicated time points with or without infection, inserts were, first, washed with PBS and fixed with 2.5% glutaraldehyde in cacodylate buffer for 1 h at RT. Fixative was removed by washing three times in cacodylate buffer. Then, transwell membranes were cut out using a scalpel and transferred to glass vials for the following steps. Samples were processed for TEM by technical staff at the imaging core facility (Prof. Christian Stigloher, Biocenter, Würzburg), as previously published [191]. Briefly, samples were fixed in 2% OsO_4 buffered with 50mM cacodylate for 2 h at 4 °C, washed in H_2O, and stained using uranyl acetate (0.5% in H_2O) o/n at 4 °C. After dehydration, samples were infiltrated and embedded in Durcupan. Electron micrographs of ultrathin sections were recorded on a JEM-1400Flash transmission electron microscope (JEOL) with a Matataki camera system.

3.11 Quantitative RT-PCR

3.11.1 RNA extraction

BECs from monoculture and BEC-LMC co-culture with or without *N. meningitidis* infection were dissociated from the transwell membrane using Accutase for 15 min (iBEC) or 5-7 min (hCMEC/D3) at 37 °C. RNA was purified using the Machery-Nagel NucleoSpin RNA kit according to the manufacturer's instructions. Dissociated cells were collected in microcentrifuge tubes, diluted with PBS, and spun down at 1500 x g for 5 min. Cells were lysed in RA1 lysis buffer supplemented with 1% beta-mercaptoethanol. Lysates were either processed immediately, stored o/n at 4 °C, or stored at -20 °C for multiple days. To adjust RNA binding conditions, samples were mixed with 70% ethanol before being loaded onto NucleoSpin RNA columns followed by 30 s of centrifugation at 11 000 x g. Together with high amounts of chaotropic ions from the lysis buffer, these conditions favor association of RNA to the silica in the membrane. Next, MDB buffer containing chaotropic salt and ethanol was added to remove salt and improve conditions for DNase digestion. After 1 min of centrifugation at 11 000 x g, silica columns were incubated with rDNase reaction mixture for 15 min at RT. DNAse digestion was followed by multiple washing steps with two different ethanol-based buffers to remove salts, metabolites, and macromolecular cellular components. Finally, pure RNA was eluted with RNase free H_2O and immediately put on ice.

3.11.2 cDNA synthesis

Concentration or RNA was measured for each sample using a Nanodrop spectrophotometer. cDNA was generated by reverse transcription using the NEB LunaScript RT SuperMix, which contains the reverse transcriptase enzyme, optimized buffer, nucleotides (dNTPs), RNase inhibitor as well as random-hexamer and oligo-d(T) primers. In a PCR tube, nuclease free H_2O, 500 ng of RNA, and 4 µl of LunaScript RT SuperMix were combined to a total reaction volume of 20 µl and cDNA synthesis was run using a

standard PCR cycler and the following protocol (**Table 11**). Smaller amounts of RNA can also be used, if kept consistent between samples that are to be compared via qPCR later.

Table 11. PCR cycling protocol for cDNA synthesis.

Step	Temperature	Time
Primer annealing	25 °C	2 min
cDNA elongation	55 °C	10 min
Enzyme deactivation	95 °C	1 min
Storage	4 °C	∞

3.11.3 Quantitative PCR

Finally, SYBR green quantitative PCR (qPCR) was performed to quantify relative amounts of target cDNA and thereby determine gene expression levels. In principle, DNA of a target gene is amplified in a standard PCR reaction using specifically designed primers. The reaction mix also contains SYBR green – a dye that exhibits substantially increased fluorescence when it intercalates nonspecifically into double stranded DNA. As amplification proceeds, SYBR green signal increases proportionally to synthesized product. The number of PCR cycles required to reach a threshold level is known as the Ct value and can be used to determine relative amount of target cDNA in a sample normalized to expression level of a housekeeping gene.

qPCR reactions were set up as follows (**Table 12**). Typically, 1 µl of 1:10 diluted cDNA was used per qPCR reaction. Larger amounts can be used for genes with low expression levels. First, cDNA and nuclease free water are combined and added to a 96-well qPCR plate. Next, primers are added to PowerUp SYBR Green Master Mix and pipetted onto the designated wells. Finally, the plate is sealed using clear adhesive film and spun down briefly. The sealed plate can be stored at 4 °C for up to 24 h until needed. qPCR was run on a StepOnePlus real-time PCR thermocycler (**Table 13**). Fold change in gene expression relative to control and normalized to 18S was determined using the cycle threshold ($\Delta\Delta C_t$) calculation [192]. qPCR primers (listed in **Table 10**, p.29) were validated by primer efficiency analysis and agarose gel electrophoresis of the qPCR product.

Table 12. qPCR reaction mix [1x; 25 µl].

Reagent	Volume
Nuclease free H_2O	10.5 µl
cDNA	1 µl
SYBR Green Master Mix	12.5 µl
Forward primer	0.5 µl
Reverse primer	0.5 µl

Table 13. qPCR thermocycler protocol.

Stage	Temperature	Time
Holding	95 °C	10 min
Cycling [45x]	95 °C	15 sec
	60 °C	1 min
Melt curve	60 – 95 °C	
	0.3 °C increments	

3.12 *SNAI1* knockdown

SNAI1 transcription was knocked down in hCMEC/D3 cells using RNA interference (RNAi) mediated by a specifically designed short interfering RNA (siRNA). In this process, cells are chemically transfected with siRNA that has become part of a multi-protein complex called the RNA-induced silencing complex (RISC). Based on the antisense strand of the siRNA, RISC identifies and sequence-specifically cleaves the target mRNA, which ultimately leads to its degradation.

hCMEC/D3 cells were seeded onto a 24-well plate at a density of 2 x 10^5 cells/well. The next day, cells were transfected with *SNAI1* siRNA or scrambled, FITC conjugated siRNA at a final concentration of 50 nM using TransIT-siQUEST® Transfection Reagent according to manufacturer's instructions. Appropriate amounts of siRNA were mixed with EndoGRO basal medium (50 µl/well) and TransIT-siQUEST® transfection reagent (1.5 µl/well), incubated for 30 min at RT to allow for RISC formation, and added to each well for 24 h. Then, medium was changed, and cells were infected with *N. meningitidis* MC58 at an MOI of 10. After 24 h of infection, cells were lysed, and mRNA expression was analyzed using qPCR. Propidium iodide (PI) staining of uninfected cells was performed to evaluate cell viability after transfection. Cells were dissociated using Trypsin-EDTA, diluted in PBS, and spun down at 1500 x g for 5 min. Cells were resuspended in 100 µl 1 mg/ml PI solution (in PBS). As a control, 10 µl of 2.5% Triton-X was added to one sample of non-transfected cells. After 10 min of incubation at RT, unbound PI was diluted by adding another 100 µl of PBS to each sample. Flow cytometry was performed on a MACSQuant, and results were analyzed using FlowJo software.

3.13 IL-8 ELISA

IL-8 levels in supernatants of infected or uninfected BEC monoculture and BEC-LMC co-culture models were quantified using a sandwich enzyme-linked immunosorbent assay (ELISA). The target antigen is captured between a surface-attached antibody and biotin-carrying detection antibody, to which a streptavidin-horseradish peroxidase conjugate (HRP) is bound. Upon incubation with HRP substrate tetramethylbenzidine (TMB), the reaction product is detected using absorbance spectrophotometry.

ELISA was performed using antibodies, enzyme and standards from a BD Human IL-8 ELISA Set according to the manufacturer's instructions. Capture antibody was diluted 1:250 in 0.1 M sodium carbonate coating buffer and added to a clear, flat-bottom 96-well plate (100 µl/well). The plate was sealed and incubated o/n at 4°C. Well surfaces were blocked with 10% FCS (200 µl/well) for 1 h at RT. After appropriate dilution in 10% FCS, cell culture supernatants and IL-8 standards were transferred to the plate in duplicates (100 µl/well) and incubated sealed for 2 h at RT. Working detector containing detection antibody and streptavidin-HRP conjugate (1:250 in 10% FCS; 100 µl/well) was added for 1 h at RT before incubation with TMB substrate solution (100 µl/well) for 15-30 min at RT. The plate was washed multiple times with 0.05% Tween-20 in PBS (200 µl/well) between each step. Finally, the enzymatic reaction was stopped using 2N H_2SO_4 solution (50 µl/well) and absorbance was measured on an absorbance plate reader. Protein concentrations were calculated from wavelength-corrected absorbance values (450 nm – 570 nm) using a standard curve.

3.14 Statistics

Statistical analysis was performed using GraphPad Prism software (version 6.01). Student's t test or Analysis of variance (ANOVA) followed by Dunnett's multiple comparisons test were used for pairwise or multiple comparisons, respectively. Statistical significance was accepted at a P value of less than 0.05.

4 RESULTS

4.1 Development and characterization of BEC-LMC co-culture models

To establish the iBEC-LMC co-culture models, iPSCs were differentiated into iBECs as described previously [157, 158, 182, 188] (**Figure 4**). This protocol employs a co-differentiation step of endothelial and neuronal cells in unconditioned medium, providing a microenvironment comparable to the embryonic brain. The endothelial cell population was, then, expanded in endothelial medium supplemented with growth factor bFGF and retinoic acid for improved maturation of BEC phenotypes. Four hours prior to iBEC purification, LMCs were seeded onto coated tissue culture plates or the underside of transwell inserts. Co-culture was initiated by iBEC purification onto the selective collagen IV/ fibronectin matrix on top of the transwells. iBECs were generally co-cultured with LMCs in EC media for 2 days (**Figure 4**a).

Transmission electron microscopy was performed to morphologically characterize the iBEC-LMC co-culture model (**Figure 4**b). In addition to TEM on ultrathin cross-sections of embedded samples, brightfield images of semithin sections were taken. Two confluent monolayers that are morphologically distinct from each other were observed (**Figure 5**a). Electron dense regions between adjacent cells in the dense iBEC layer indicated the presence of complex cell-cell junctions such as tight junctions, adherens junctions, and desmosomes. In contrast to iBECs, LMCs displayed a more flat, spread-out morphology with a proportionally larger cytosol extending out to other cells in the monolayer. Here, TEM was able to resolve the structures of cytosolic components such as Golgi apparatus, endoplasmic reticulum, vesicles, lamellar bodies, and mitochondria. Although cell layer thickness was in part dependent on seeding density (data not shown), general morphology of each cell type was consistent. Immunofluorescences staining and confocal whole-mount imaging was conducted to evaluate expression of cell type specific markers. Within the iBEC layer, junctional expression of brain endothelial markers such as adherens junction proteins CD31, VE-cadherin, and tight junction components claudin-5, ZO-1, and occludin was observed (**Figure 5**b). The meningioma derived LMCs displayed characteristic features of the meningothelial subtype such as a large spread-out morphology with curvy-linear edges and expression of histopathological markers vimentin, desmoplakin, and epithelial membrane antigen (EMA). LMCs were also immunopositive for tight junction proteins ZO-1 and E-cadherin, which is reportedly expressed in arachnoid barrier forming leptomeningeal cells [64]. However, junctional expression of ZO-1 in LMCs was not as clear and quite distinct from the expression pattern in iBECs. E-cadherin was not localized at the cell-cell junction, potentially due to the tumorigenic nature of the cells. In summary, these results demonstrate successful co-culture of iPSC derived BECs with meningioma derived LMCs, as both cell types remain distinct in culture and retain their characteristic features.

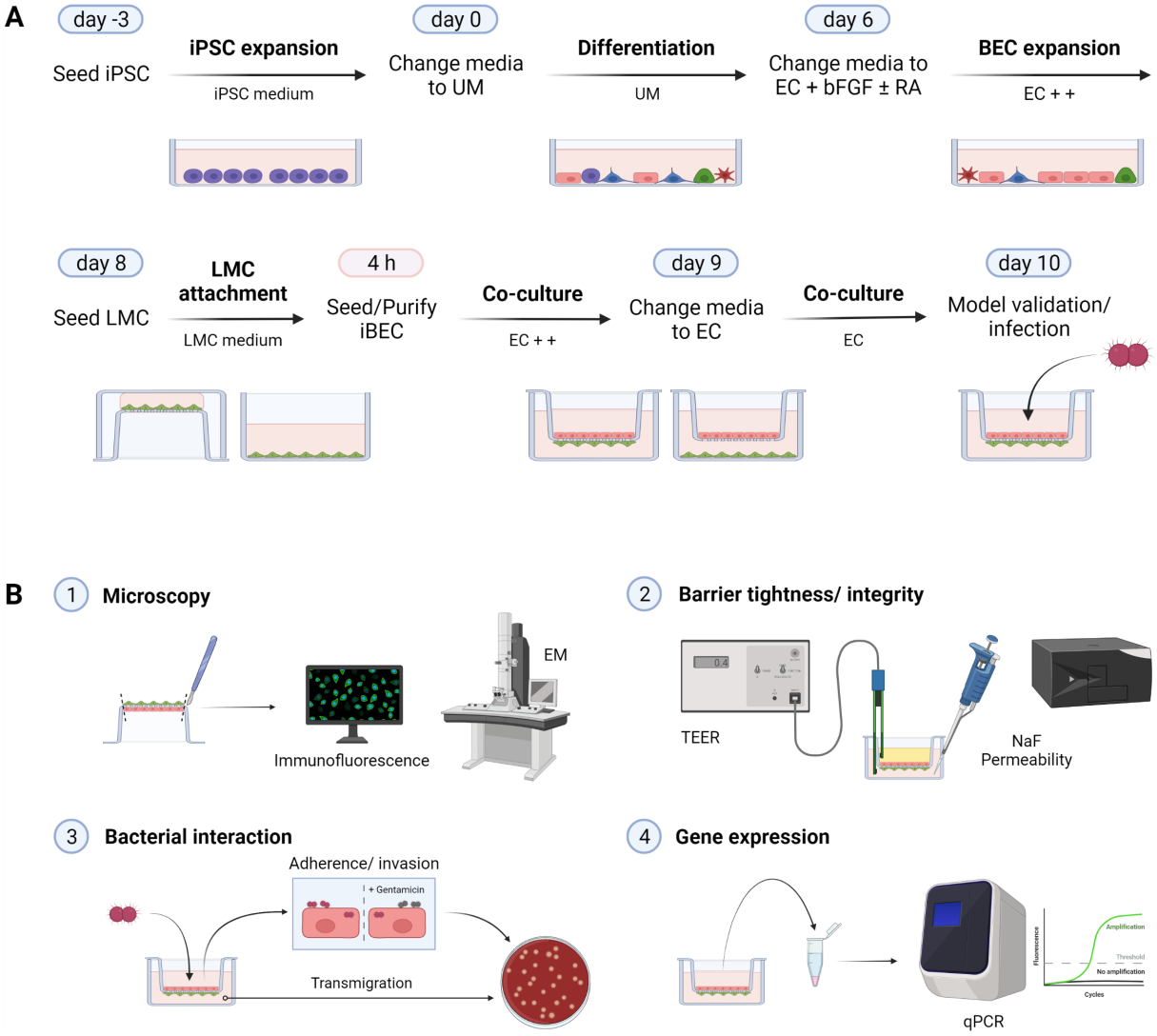

Figure 4. Set-up and application of the iBEC-LMC co-culture model. **a**) Schematic representation of iPSC-derived brain endothelial-like cell (iBEC) differentiation and co-culture with leptomeningeal cells (LMCs). iBEC differentiation as previously described [188]. On day 8, LMCs are seeded on the underside of transwells or on standard tissue culture plates. After 4h of incubation, iBECs are purified onto the apical side of the transwells. Co-cultures are cultivated in EC medium with Pen/Strep for 1 day, before changing to basal EC medium without supplements. Experiments were conducted on day 10 of differentiation (day 2 of co-culture). **b**) Schematic representation of methods used for model characterization and infection studies with *N. meningitidis*: immunofluorescence staining, electron microscopy (EM), transendothelial electrical resistance (TEER), sodium fluorescein (NaF) permeability, gentamicin protection (adherence/invasion) and transmigration assays, and quantitative RT-PCR (qPCR). Figure created with BioRender.com.

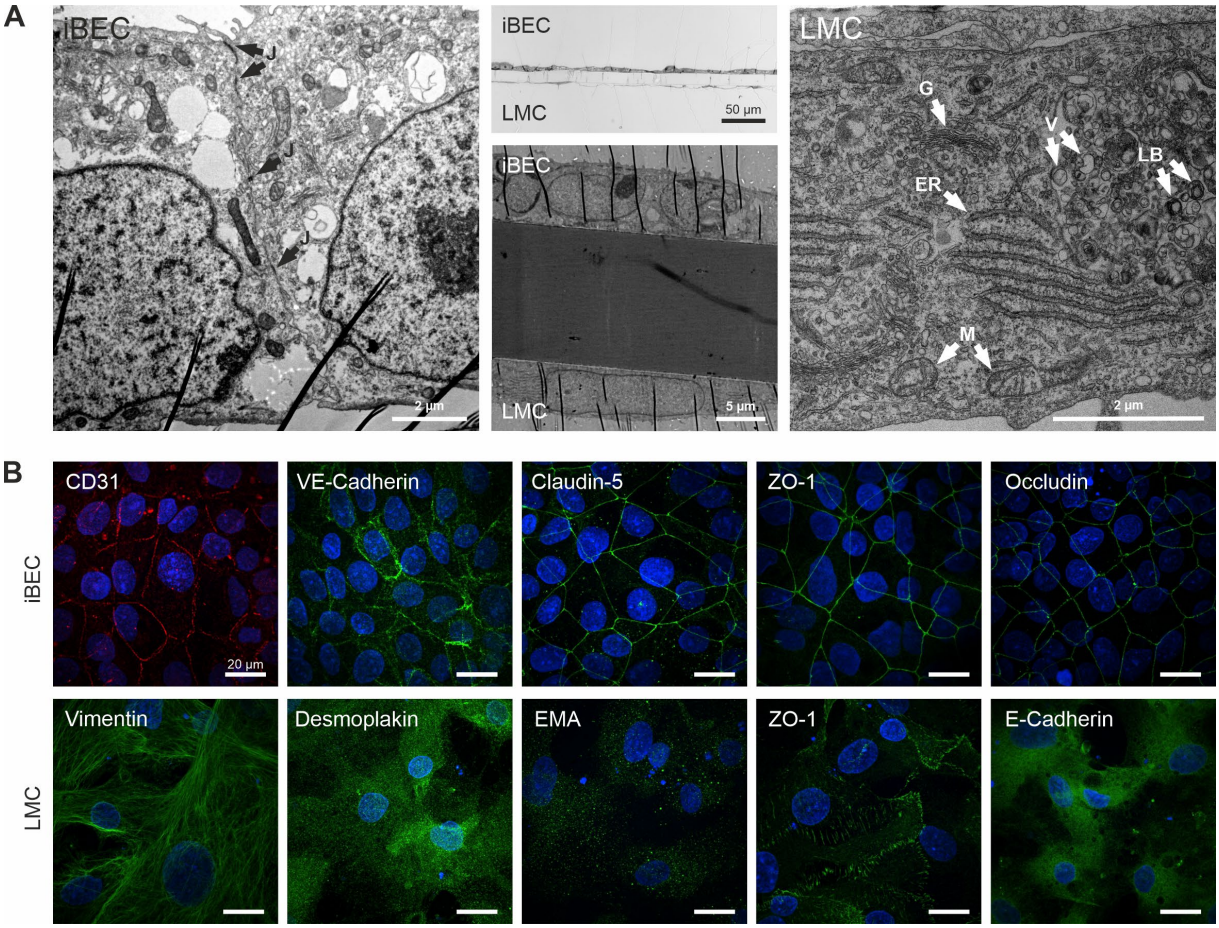

Figure 5. Characterization of the iBEC-LMC co-culture model. **a**) Transmission electron microscopy (TEM) of iBECs and LMCs co-cultured on transwell for 2 days. A widefield image of a semithin cross-section of the embedded model (middle, top) is presented in addition to electron micrographs of ultrathin sections. Labeled structures: cell junctions (J), Golgi apparatus (G), rough endoplasmic reticulum (ER), mitochondria (M), vesicles (V), lamellar bodies (LB). **b**) Immunofluorescence staining of iBEC (top) and LMC (bottom) monolayers on either side of transwell membranes for endothelial adherens junction proteins (CD31, VE-cadherin), tight junction components (claudin-5, ZO-1, occludin, E-cadherin), and meningioma markers (vimentin, desmoplakin I/II, epithelial membrane antigen), performed after 2 days of co-culture. Nucleus staining with DAPI (blue). Scale bars represent 20 µm.

In parallel to iBEC-LMC model development, co-culture using human cerebral microvascular endothelial cell line hCMEC/D3 and meningioma derived LMCs was to be established for reference. hCMEC/D3-LMC co-culture was set up similarly to the iBEC-LMC model (**Figure 4**). Four hours after LMC seeding, co-culture was initiated by adding hCMEC/D3s to the apical side of the transwell. Based on previous monoculture experiments, hCMEC/D3s were expected to reach confluence after two days and form a tight monolayer by day 3 of subculture. Therefore, experiments were generally performed after 3 days of hCMEC/D3-LMC co-culture. TEM performed on that day confirmed the presence of both cell types on either side of the transwell membrane (**Figure 6**a). With a few exceptions in denser areas, hCMEC/D3s generally stayed in a monolayer. Notably, hCMEC/D3s were capable of migrating through the PET membrane of transwell inserts with a pore size of 3 µm and populating the other side, as observed in hCMEC/D3 monocultures (data not shown). Although the presence of a mixed cell population on the LMC side in hCMEC/D3-LMC co-cultures cannot be excluded, both cell layers were structurally and immunocytochemically distinguishable. hCMEC/D3s displayed typical endothelial

morphology with smooth luminal surface, oval nucleus, thin and elongated cell shape. The LMC layer was distinguishable from the hMCEC/D3 layer particularly by large thin stretches of cytosolic portions and slightly higher abundance of cellular structures. Using confocal microscopy, expression of BEC markers CD31, VE-cadherin and ZO-1 was detected within the hCMEC/D3 layer (**Figure 6**b). However, clear and uniform immunofluorescence staining of junctional BEC markers at the cell-cell borders could not be achieved. Together, these results demonstrate successful co-culture of hCMEC/D3s with LMCs, which have not yet been included in studies of *N. meningitidis* interaction with the mBCSFB.

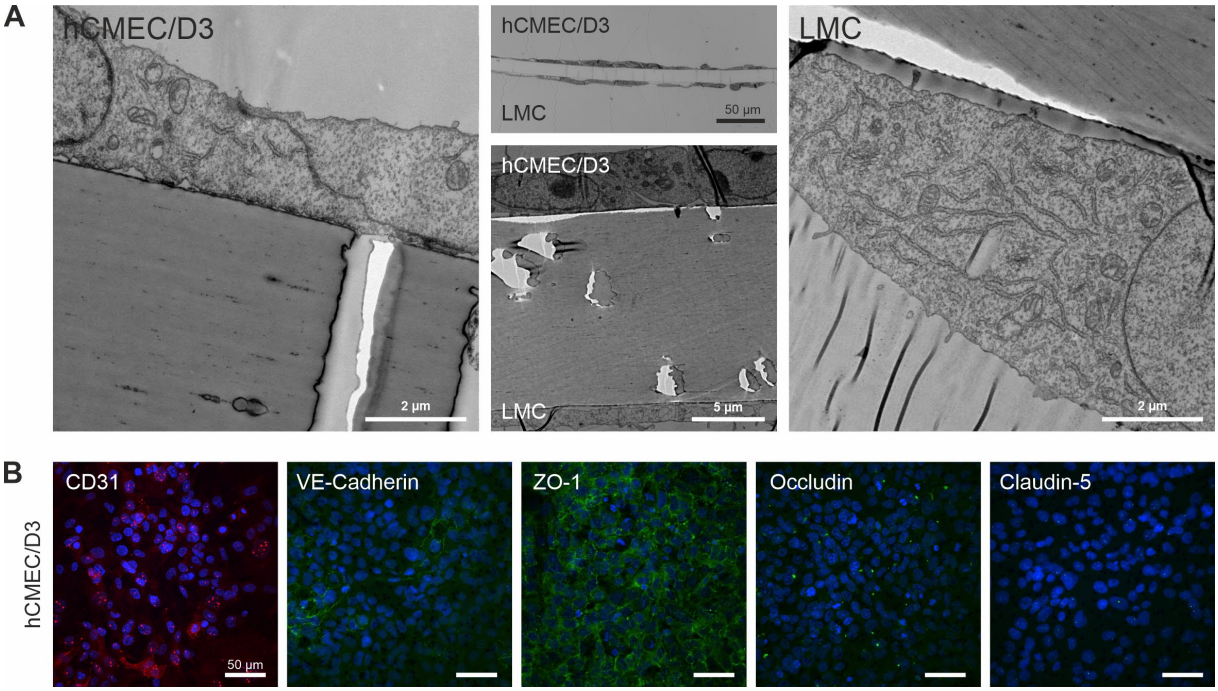

Figure 6. Characterization of the hCMEC/D3-LMC co-culture model. **a**) Transmission electron microscopy of hCMEC/D3 and LMCs co-cultured on transwell for 3 days. A widefield image of a semithin cross-section of the embedded model (middle, top) is presented in addition to electron micrographs of ultrathin sections. **b**) Immunofluorescence staining of the hCMEC/D3 layer for endothelial adherence junction proteins (CD31 and VE-cadherin) and tight junction components (ZO-1, occludin, and claudin-5), performed after 3 days of co-culture. Nucleus staining with DAPI (blue). Scale bars represent 50 µm.

4.2 Influence of LMC co-culture on tightness and stability of the BEC barrier

To evaluate whether LMC co-culture has an effect on the barrier properties of iBEC monolayers, TEER and NaF permeability were analyzed (**Figure 4**b). TEER was measured daily for 14 days following iBEC purification and start of co-culture. iBEC monoculture reached peak TEER (2820 ± 384 Ω x cm²) on day 2 (i.e., day 10 of differentiation) (**Figure 7**a), which is typical for iBECs generated using this differentiation protocol [182, 188]. After briefly dropping to lower levels yet remaining above 1500 Ω x cm², TEER increased again to near peak values on day 8 before continuously descending. Compared to monoculture, TEER of iBECs co-cultured directly or indirectly with LMCs was elevated slightly on day 2 (3389 ± 354 Ω x cm² or 3125 ± 393 Ω x cm²) (**Figure 7**a). TEER, then, remained stable and at

significantly higher levels in both direct and indirect iBEC-LMC co-culture models compared to iBEC monoculture for 7 days, reaching peak values of 3599 ± 738 Ω x cm² and 3488 ± 562 Ω x cm², respectively. Consistent with iBEC monoculture, a continuous decrease in TEER was observed after day 8. While TEER of direct iBEC-LMC co-culture models remained significantly higher for the entire experiment, indirect co-cultures reached near-monoculture levels by day 12. LMCs grown in monoculture on the underside of transwell inserts, did not generate TEER higher than 37 ± 17 Ω x cm² over a 14-day period (**Figure 7**b). In addition to TEER, permeability of the cell layers to small (376 kDa) fluorescent tracer sodium fluorescein (NaF) was analyzed on day 2 and day 4 of co-culture to assess barrier function of the models. On day 2, NaF permeability of both direct (1.96 ± 0.38 x 10^{-7} cm/s) and indirect (2.02 ± 0.58 x 10^{-7} cm/s) iBEC-LMC co-culture was slightly but significantly lower than iBEC monoculture (2.85 ± 0.73 x 10^{-7} cm/s) (**Figure 7**c). Significantly reduced NaF permeability was also observed in both co-cultures on day 4 (**Figure 7**d). Compared to day 2, permeability values recorded in this set of experiments, were higher in iBEC monoculture (4.57 ± 0.90 x 10^{-7} cm/s), similar in direct (1.82 ± 0.38 x 10^{-7} cm/s) and slightly elevated for indirect (2.84 ± 0.56 x 10^{-7} cm/s) iBEC-LMC co-culture. Together, these data demonstrate that co-culture with LMCs increased iBEC barrier tightness and stability over time.

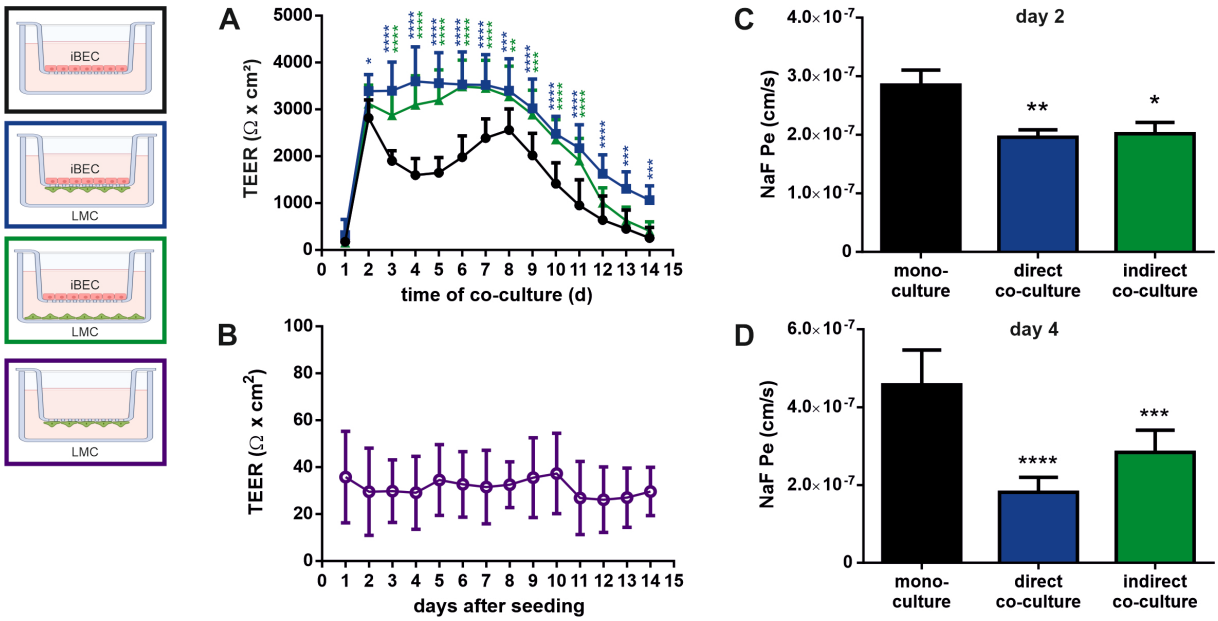

Figure 7. Barrier properties of iBEC-LMC co-culture models. **a**) Transendothelial electrical resistance (TEER) of iBEC monoculture (black), direct (blue) and indirect (green) iBEC-LMC co-culture over a time-course of 14 days. **b**) TEER of LMC monolayers cultured on the underside of transwell inserts. **c**) Sodium fluorescein permeability (NaF Pe) of iBEC mono and co-culture models on day 2 of co-culture. Data from three independent experiments performed in triplicate (n = 9) (a-c). **d**) NaF Pe of iBEC mono and co-culture models on day 4 of co-culture. Data from two independent experiments performed in triplicate (n = 6). All data presented as mean ± SD. *p < 0.05, **p < 0.01, ***p < 0.001, **** p < 0.0001; ANOVA followed by Dunnett's multiple comparisons test; direct (blue) and indirect (green) co-culture vs monoculture.

Barrier properties of the hCMEC/D3 based models were evaluated similarly by determining TEER and NaF permeability. TEER was relatively low and stayed consistent for the 14-day period (**Figure 8**a). After 3-4 days, peak values of 23 ± 4 Ω x cm², 30 ± 8 Ω x cm², and 24 ± 9 Ω x cm² were recorded for HMCE/D3 monoculture, direct and indirect hCMEC/D3-LMC co-culture. While TEER of hCMEC/D3 monolayers indirectly cultured with LMCs was statistically indifferent from hCMEC/D3 monoculture, elevated TEER was observed with direct hCMEC/D3-LMC co-culture for 11 days. In line with TEER data, NaF permeability measured on day 3 of co-culture was lower in the direct co-culture model (2.25 ± 0.36 x 10^{-5} cm/s) compared to indirect co-culture (3.62 ± 0.11 x 10^{-5} cm/s) and hCMEC/D3 monoculture (4.57 ± 0.24 x 10^{-5} cm/s) (**Figure 8**b). However, considering that LMC monocultures reached TEER values of up to 37 ± 17 Ω x cm² (**Figure 7**b), this effect may be a result of the added LMC layer on the transwell membrane.

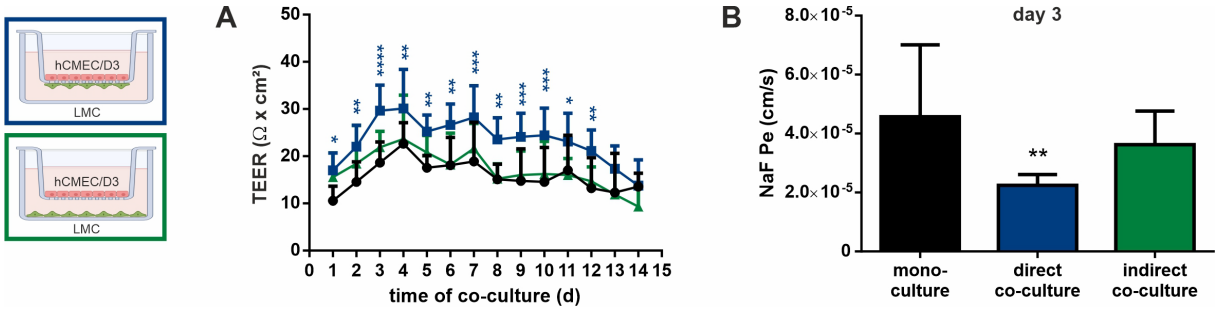

Figure 8. Barrier properties of hCMEC/D3-LMC co-culture models. **a**) TEER of hCMEC/D3 monoculture (black), direct (blue) and indirect (green) hCMEC/D3-LMC co-culture measured daily over a time-course of 14 days. **b**) NaF permeability of hCMEC/D3 mono and co-culture models on day 3 of co-culture. All data presented as mean ± SD from three independent experiments performed in triplicate (n = 9). *p < 0.05, **p < 0.01, ***p < 0.001, **** p < 0.0001; ANOVA followed by Dunnett's multiple comparisons test; direct (blue) and indirect (green) co-culture vs monoculture.

4.3 *N. meningitidis* interaction with and traversal of the BEC-LMC models

After development and characterization, the BEC-LMC co-culture models were used for infection studies with *N. meningitidis* (**Figure 4**b). The models were infected with *N. meningitidis* wild type serogroup B strain MC58 from apical side of the BEC layer after 2 (iBEC) or 3 days (hCMEC/D3) of direct co-culture with LMCs. BEC monoculture continued to be used as a control to assess whether addition of LMCs affects *N. meningitidis* interaction with the mBCSFB model.

First, meningococcal adherence and invasion of the BEC layer were determined using gentamicin protection assays 2 h and 8 h p.i. (**Figure 9**). Significant amounts of bacteria associated with the iBEC layer in iBEC-LMC co-cultures were already detected 2 h p.i. (3.58 ± 1.53 x 10^6 cfu/monolayer) (**Figure 9**a; blue bars). Longer infection time of 8 h lead to a relatively small increase in adherence (1.75 ± 0.80 x 10^7 cfu/monolayer). Comparatively little bacterial invasion of iBECs was detected. Numbers of intracellular bacteria recovered after 8 h of infection (2.06 ± 1.12 x 10^4 cfu/monolayer) were

approximately 10-fold higher than 2 h p.i. (1.26 ± 0.60 x 10^3 cfu/monolayer). Adherence and invasion data obtained from iBEC-LMC co-culture models was comparable to iBEC monoculture data. Using the hCMEC/D3-LMC co-culture models, enumeration of extra- and intracellular bacteria in the BEC layer yielded similar results (**Figure 9**b; blue bars). Meningococcal adherence to hCMEC/D3s was highly comparable 2 h (5.19 ± 2.25 x 10^6 cfu/monolayer) and 8 h p.i. (1.39 ± 0.54 x 10^7 cfu/monolayer). Counts of recovered intracellular bacteria were much lower after 2 h (42 ± 33 cfu/monolayer) but on par with data from the iBEC models after 8 h of infection having increased roughly 1000-fold (4.43 ± 5.38 x 10^4 cfu/monolayer). No significant difference in adherence or invasion was observed between hCMEC/D3-LMC co-culture and hCMEC/D3 monoculture.

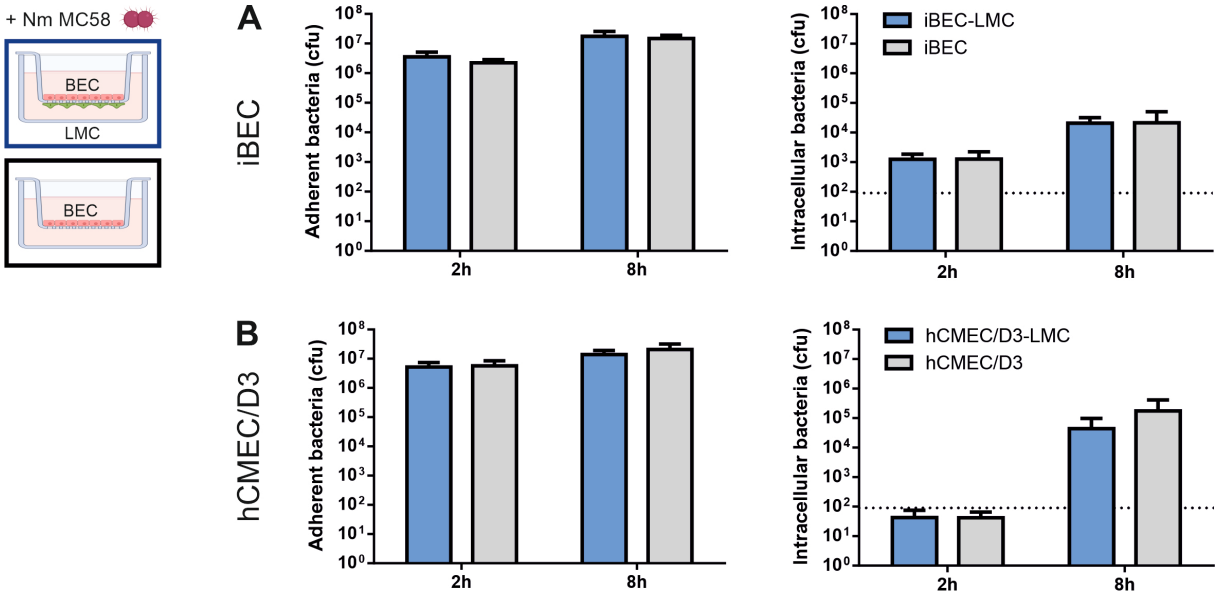

Figure 9. *N. meningitidis* interaction with BECs from the BEC-LMC co-culture models. Adherent and intracellular CFU per BEC monolayer 2 h or 8 h post-infection, quantified using gentamicin protection assays. iBEC (**a**) or hCMEC/D3 (**b**) layers infected at an MOI of 100 on day 2 (**a**) or day 3 (**b**) of subculture or co-culture with LMCs. Data presented as mean ± SD from at least three independent experiments and iBEC differentiations performed in duplicate (**a**, n = 6; **b**, n = 8). *p < 0.05, **p < 0.01, ***p < 0.001; Student's t test; direct co-culture (blue) vs monoculture (grey).

Next, meningococcal traversal of the BEC-LMC co-culture models was evaluated using transmigration assays (**Figure 10**). Transmigration rates 2 h, 6 h, 24 h, and 30 h p.i. were determined by sampling the basolateral compartment of the transwell system after 1 h of incubation in fresh basolateral media, followed by plating, and counting of cfu. In the iBEC-LMC co-culture model, bacterial traversal was mostly undetectable 2 h p.i. (**Figure 10**a). After 6 h, bacteria crossing the barrier were detected more frequently and in greater numbers (> 100 cfu/h). By 24 h of infection, substantially higher transmigration rates were observed (0.16-1.76 x 10^6 cfu/h), which kept increasing slightly for the remainder of the 30-h time course (0.94-2.92 x 10^6 cfu/h). Overall, transmigration data obtained from infected iBEC monocultures was comparable. However, higher rates of bacterial traversal were detected at the early infection time points (0.43-4.84 x 10^3 cfu/h at 6 h p.i.). Compared to the iBEC based models, *N. meningitidis* already crossed the cell layers of the hCMEC/D3-LMC co-culture model

much more frequently at 2 h p.i. (0.02-1.08 x 10^6 cfu/h) (**Figure 10**b). Transmigration rates increased slightly up to 6 h p.i. (1.52-5.28 x 10^6 cfu/h) and stayed consistent for the remainder of the experiment (1.64-8.40 x 10^6 cfu/h, 24 h p.i.). Similar results were obtained using hCMEC/D3 monoculture models, although slightly higher numbers of bacteria traversing the barrier were observed at 2 h p.i. (0.06-1.8 x 10^6 cfu/h) and slightly lower cfu/h were recorded at 24 h p.i. (0.24-4.8 x 10^6 cfu/h).

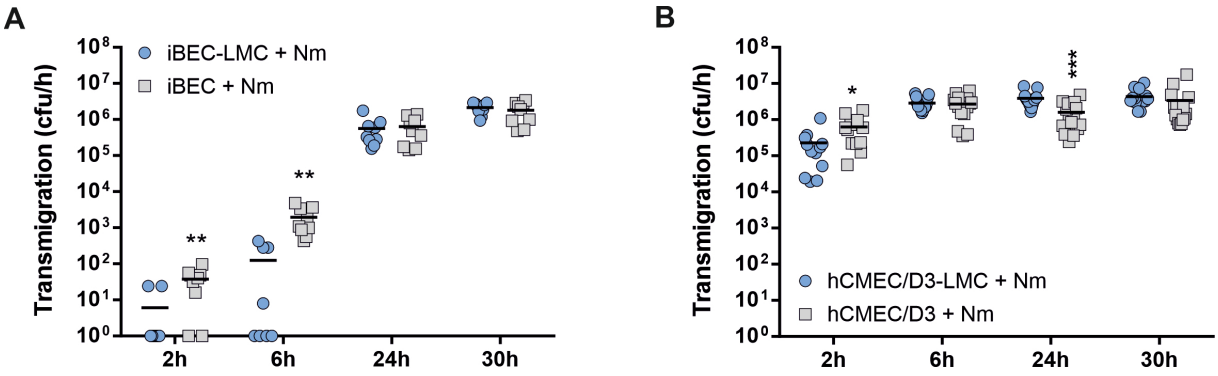

Figure 10. *N. meningitidis* traversal of BEC and BEC-LMC barrier models. *N. meningitidis* transmigration rates after the indicated time of infection determined by enumeration of cfu in the basolateral compartment after 1 h of incubation in fresh basolateral media. iBECs (**a**) or hCMEC/D3s (**b**) infected from the apical side (MOI = 10) on day 2 (**a**) or day 3 (**b**) of subculture with or without LMCs. Data from three independent experiments and iBEC diffeentiations performed in triplicate (n = 9). Data presented as mean ± SD. *p < 0.05, **p < 0.01, ***p < 0.001; Student's t test; direct co-culture (blue) vs monoculture (grey).

Finally, *N. meningitidis* interaction with and traversal of the iBEC-LMC co-culture model was examined using TEM and structured illumination microscopy (SIM) (**Figure 11**). The iBEC-LMC model was chosen due to its elevated barrier properties. TEM was performed on ultrathin cross sections of embedded iBEC-LMC co-cultures after 6 h, 24 h, and 30 h of infection. Meningococci were mostly detected on the apical surface of the iBECs, often tightly associated with the cellular membrane sitting on small indentations that fit the bacterial shape (**Figure 11**aI, II). Additionally, cytoplasmic protrusions often surrounded adherent bacteria that appeared mostly in clusters, commonly described as microcolonies. Consistent with data from the transmigration assays performed in this study, bacteria traversing the iBEC-LMC co-culture model and interacting with the LMC layer could be detected almost exclusively at the later infection time points using TEM, with the highest chance of detection at 30 h p.i. (**Figure 11**aIII, IV). Interestingly, intact tight junctions were still observed 24 h p.i. (**Figure 11**aII). SIM analysis of iBEC-LMC models, stained for F-actin after 24h of infection with GFP-expressing *N. meningitidis* strain MC58, revealed mostly adherent bacteria including meningococcal microcolonies on top of the iBEC layer (**Figure 11**b, left panels). Small numbers of meningococci were observed on the apical side or in the process of crossing the LMC layer (**Figure 11**b, right panels).

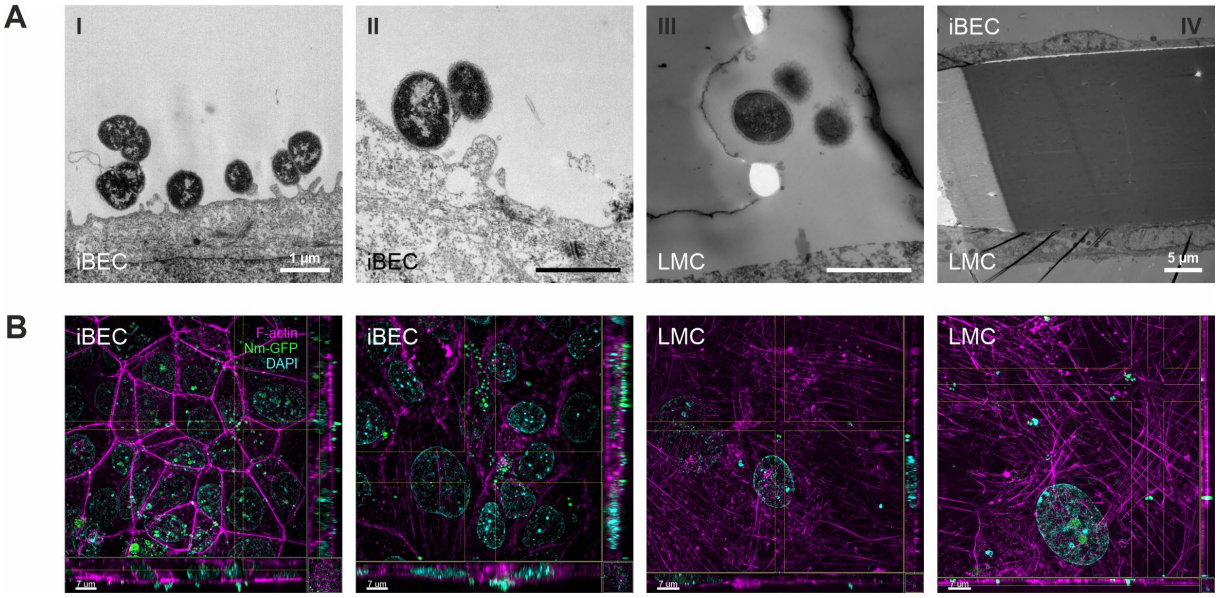

Figure 11. Microscopic analysis of *N. meningitidis* interaction with the iBEC-LMC direct co-culture model. iBECs were infected from the apical side (MOI = 10) on day 2 of co-culture with LMCs. **a**) TEM of iBEC-LMC co-culture models infected with *N. meningitidis* for 6 h (I), 24 h (II), and 30 h (III, IV). Scale bars represent 1 µm, unless labeled otherwise. **b**) Structured illumination microscopy showing iBEC or LMC layers from iBEC-LMC co-culture, stained for f-actin (phalloidin-546, magenta) and DNA (DAPI, blue) after 24 h of infection with GFP expressing *N. meningitidis* strain MC58-GFP. Images presented as maximum intensity projection in Z and including maximum intensity projections in X and Y(orthoslices) as indicated by the crosshairs. Scale bars represent 7 µm.

In summary, *N. meningitidis* adhered to and invaded BECs in iBEC-LMC and hCMEC/D3-LMC co-culture models and did so to an extent that was comparable between the models and their respective BEC monoculture controls. *N. meningitidis* traversal of the iBEC-based *in vitro* models, especially iBEC-LMC co-culture, occurred at significantly lower rates at the early infection time points. Transmigration increased substantially over 24 h of infection, at which point transmigration rates were comparable between iBEC and hCMEC/D3 models. Microscopic analysis of infected iBEC-LMC co-culture models showed typical *N. meningitidis* interaction with BECs as well as meningococcal traversal of the barrier model at the late infection time points.

4.4 Barrier deterioration upon prolonged *N. meningitidis* infection

Previous research has demonstrated *N. meningitidis*-induced disruption barrier disruption in BEC monolayers [118, 131-133]. To evaluate whether *N. meningitidis* infection affects barrier integrity of the novel BEC-LMC co-culture models, TEER was monitored over a 32 h time course post-infection. TEER of infected iBEC-LMC co-cultures remained at high levels for approximately 24 h (**Figure 12**a). After that, TEER decreased continuously until a significant loss of TEER compared to the uninfected control was detected after 30 h of infection. Similar effects were observed with infected iBEC monocultures, although overall TEER was lower compared to iBEC-LMC co-culture. Of note, absolute TEER values recorded during this experiment were lower than what was initially observed during the

iBEC-LMC co-culture establishment (**Figure 12**a). However, this was likely due to the change in transwell system. While 12-well inserts with 0.4 µm pores were used during model development, 24-well inserts with 3.0 µm pores were used for most of the infection experiments to ensure possible transmigration of meningococci with an approximate size of 1 µm. TEER of infected hCMEC/D3-LMC co-culture and hCMEC/D3 monoculture models also remained stable for up to 24 h of infection, after which point significantly lower values were recorded compared to the uninfected control (**Figure 12**b). As observed in the previous experiments, total TEER was substantially lower compared to iBEC based models. Together, these data demonstrate disruption of BEC-LMC barrier function upon prolonged *N. meningitidis* infection.

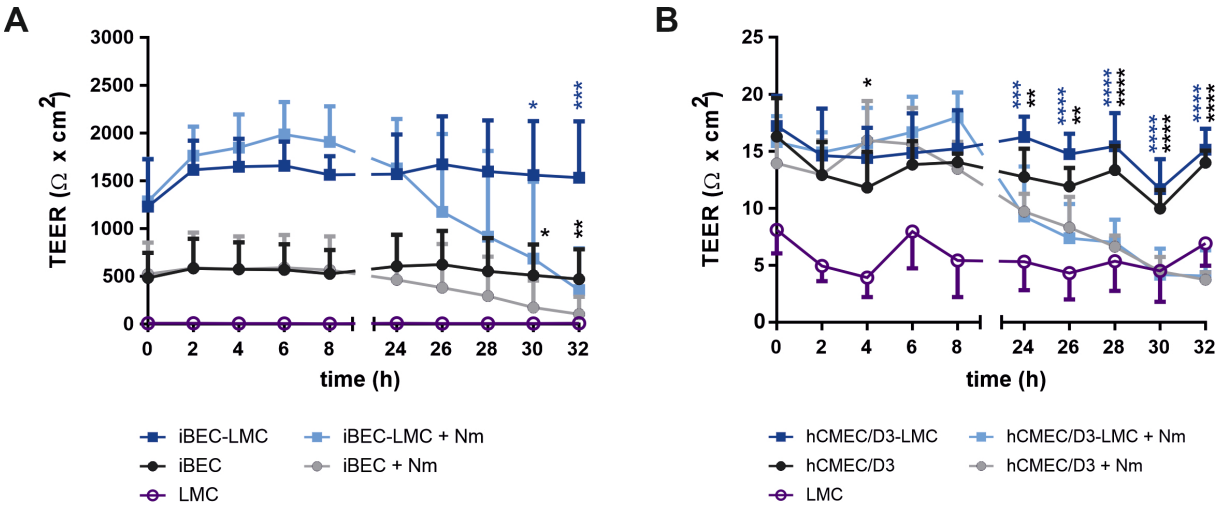

Figure 12. Effects of *N. meningitidis* infection on barrier integrity of BEC-LMC co-culture models. Transendothelial electrical resistance (TEER) of infected and uninfected BEC monoculture (black) and BEC-LMC co-culture (blue) models over a time-course of 32 h post-infection. iBEC (**a**) or hCMEC/D3 (**b**) layers infected at an MOI of 10 on day 2 (**a**) or day 3 (**b**) of subculture with (light blue) or without (grey) LMCs. Data presented as mean ± SD from three independent experiments and iBEC differentiations performed in triplicate (n = 9). *p < 0.05, **p < 0.01, ***p < 0.001; Student's t test; infected vs uninfected control.

To investigate potential mechanisms behind *N. meningitidis* induced barrier deterioration, expression of cell-junction components was analyzed in the BEC-LMC co-culture models. First, qPCR was used to examine expression of genes encoding for tight junction proteins ZO-1 (*TJP1*), claudin-5 (*CLDN5*), and occludin (*OCLN*) as well as endothelial adherens junction proteins VE-cadherin (*CDH5*) and CD31 (*PECAM1*) in infected BECs from BEC-LMC co-culture and BEC monoculture models (**Figure 4**b). In the iBEC-LMC co-culture model, expression of *TJP1*, *CLDN5*, and *CDH5* was downregulated in infected iBECs compared to the uninfected control (**Figure 13**). *TJP1* expression was slightly reduced 8 h p.i. (79 ± 19%) and significantly downregulated 24 h (45 ± 26%) and 30 h p.i. (39 ± 12%). The strongest effect was observed with *CLDN5* expression, which was already significantly lower after 8 h (59 ± 12%) and dropped even further 24 h (20 ± 12%) and 30 h p.i. (15 ± 8%). *CDH5* was downregulated at 24 h (55 ± 14%) and 30 h p.i. (40 ± 9%). *OCLN* and *PECAM1* were generally not differentially expressed under infection, although a slight reduction in *OCLN* expression was detected (82 ± 21%) and *PECAM1* mRNA

levels were slightly elevated (173 ± 56%) after 30 h of infection. To gain insights into potential mechanisms behind *N. meningitidis* induced downregulation of cell-junction gene expression, *SNAI1*, which encodes for Snail1, a transcriptional repressor of tight and adherens junctions [193-197], was included in this analysis. *SNAI1* expression was significantly upregulated in iBECs from iBEC-LMC co-culture 24 h (651 ± 311%) and 30 h p.i. (606 ± 206 %) (**Figure 13**). Overall, qPCR data from iBECs co-cultured with LMCs was comparable to iBECs from iBEC monoculture.

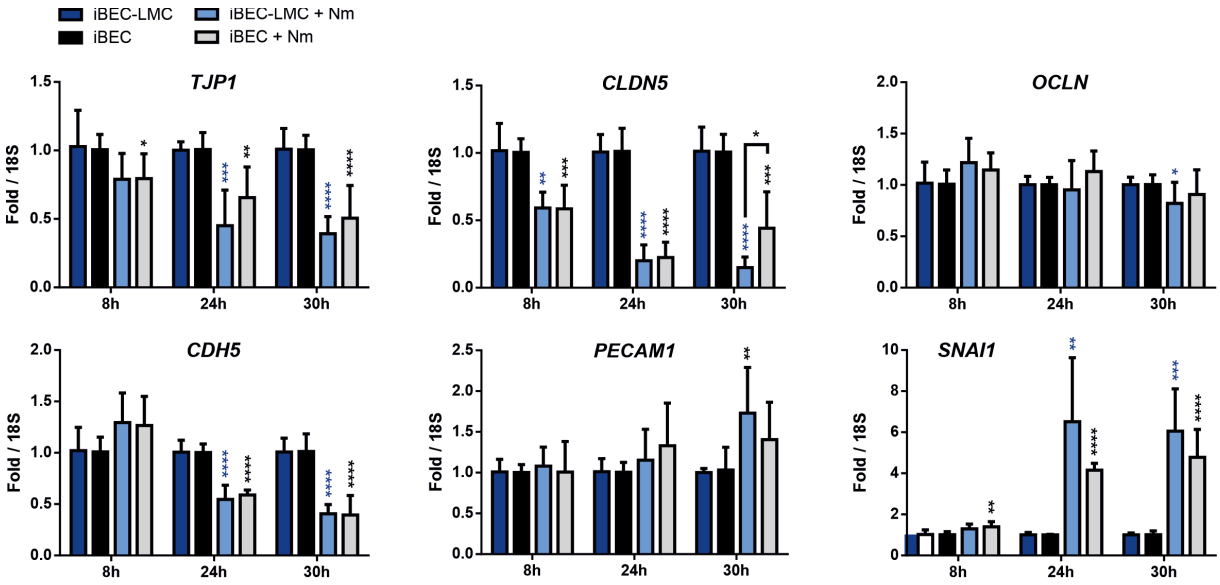

Figure 13. Effects of *N. meningitidis* infection on cell-junction expression in iBECs of mono- and co-culture models. Relative expression of genes for endothelial adherens junction proteins CD31 (PECAM1) and VE-cadherin (CDH5), and tight junction components ZO-1 (TJP1), occludin (OCLN), and claudin-5 (CLDN5) in iBECs from direct co-culture with LMCs (blue bars) and iBEC monoculture (black/gray bars), with (light bars) or without (dark bars) *N. meningitidis* infection, quantified by qPCR and normalized to 18S rRNA. Data presented as mean ± SD from four independent experiments and iBEC differentiations performed in duplicate (n = 6-8). *p < 0.05, **p < 0.01, ***p < 0.001, ****p < 0.0001; Student's t test; infected vs. uninfected control (blue/black asterisks directly over bars), mono vs co-culture (asterisks above brackets).

Next, the same panel of genes was analyzed using qPCR on hCMEC/D3s from hCMEC/D3-LMC co-culture and hCMEC/D3 monoculture after 8 h and 24 h of infection. As observed using the iBEC based models, transcription of claudin-5 and VE-cadherin was downregulated in infected hCMEC/D3s from hCMEC/D3-LMC co-culture (**Figure 14**). Although elevated mRNA levels of *CLDN5* were detected in infected hCMEC/D3s after 8 h of infection (162 ± 46%), expression was significantly reduced 24 h p.i. (39 ± 13%). In addition to the downregulation of *CDH5* at 24 h p.i. (51 ± 5%), adherence junction gene *PECAM1* was expressed at significantly lower levels in the hCMEC/D3 based model 8 h (66 ± 11%) and 24 h p.i. (30 ± 4%). *TJP1* expression was slightly lower at 24 h p.i. (77 ± 26%), although not quite to a degree of statistical significance. Interestingly, expression of *OCLN* was increased in infected hCMEC/D3s after 8 h (181 ± 44%) and 24 h of infection (206 ± 33%). *SNAI1* qPCR revealed reduced mRNA levels at 8 h p.i. (54% ± 7%) but upregulated expression at 24 h p.i. (155 ± 11%). Overall, data from hCMEC/D3 monocultures were consistent with the expression profiles in hCMEC/D3 from hCMEC/D3-LMC co-cultures. Significant reduction of *SNAI1* expression 8 h p.i. (87 ± 20%) was,

however, not recorded in the monoculture model. Despite part of the data set indicating elevation in junction gene expression, this could not be correlated with functional changes such as increased TEER, a phenomenon that was, however, occasionally observed at the early infection time points both in iBEC and hCMEC/D3 models (**Figure 12**). Taken together, the results from the qPCR analysis demonstrate *N. meningitidis*-induced downregulation of adherence and tight junction genes in BECs with and without LMC co-culture, along with upregulation of the transcriptional regulator Snail1.

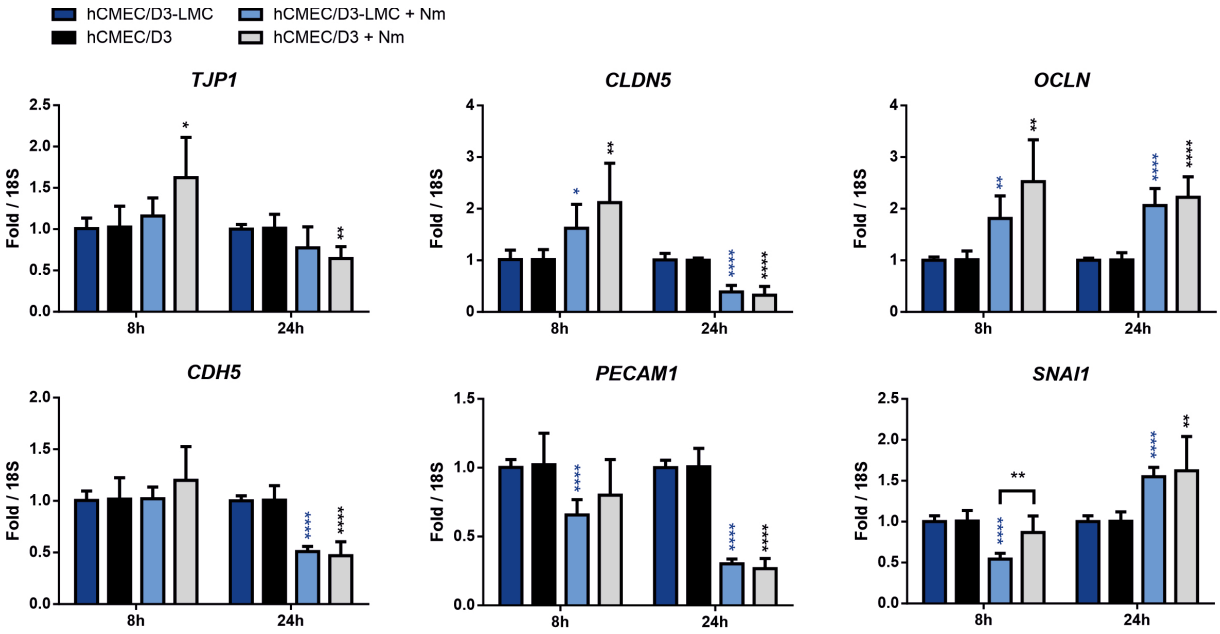

Figure 14. Effects of *N. meningitidis* infection on cell-junction expression in hCMEC/D3 from mono- and co-culture models. Relative expression of genes for endothelial adherence junction proteins CD31 (PECAM1) and VE-cadherin (CDH5), and tight junction components ZO-1 (TJP1), occludin (OCLN), and claudin-5 (CLDN5) in hCMEC/D3 from direct coculture with LMCs (blue bars) and hCMEC/D3 transwell monoculture (black/gray bars) with (light bars) or without (dark bars) *N. meningitidis* infection, quantified by qPCR and normalized to 18S rRNA. Data presented as mean ± SD from three independent experiments performed in duplicate (n = 6). *p < 0.05, **p < 0.01, ****p < 0.0001; Student's t test; infected vs. uninfected control (blue/black asterisks directly over bars), mono vs co-culture (asterisks above brackets).

To assess whether Snail1 plays a role in this mechanism, we performed siRNA knockdown of *SNAI1* and analyzed its effect on expression of cell-junction genes *CLDN5*, *TJP1*, *CDH5*, and *PECAM1* in hCMEC/D3 cells with and without *N. meningitidis* infection (**Figure 15**). hCMEC/D3 cells grown in a 24-well plate were transfected with 50 nM *SNAI1* siRNA or scrambled control siRNA for 24 h. After that, media with transfection mix was removed and cells were infected with *N. meningitidis* strain MC58 at an MOI of 10 for 24 h. Relative amounts of mRNA in cell lysates were quantified using qPCR. A knockdown of *SNAI1* expression by approximately 50% could be achieved using 50 nM *SNAI* siRNA (**Figure 15**a). Test experiments beforehand indicated a less efficient knockdown at 25 nM and only slightly lower *SNAI1* expression along with potential cytotoxic side effects such as perceptively lower density of the cell monolayer using 100 nM siRNA (data not shown). Cell viability was unaffected by *SNAI1* siRNA transfection at 50 nM, as determined by PI staining and flowcytometry (**Figure 15**b). *SNAI1* knockdown lead to increased expression of *CLDN5* (131 ± 24%), *CDH5* (269 ± 83%), and *PECAM1* (202 ± 38%) (**Figure**

15c), which are all Snail1 targets [198]. Despite this, no significant rescue of the substantially reduced *CLDN5* (20 ± 7%), *TJP1* (16 ± 4%), *CDH5* (64 ± 27%), and *PECAM1* (50 ± 13%) expression was observed in infected hCMEC/D3s. Together, these data suggest that Snail1 mediated repression was not solely responsible for the downregulation of cell-junction genes in hCMEC/D3s after *N. meningitidis* infection.

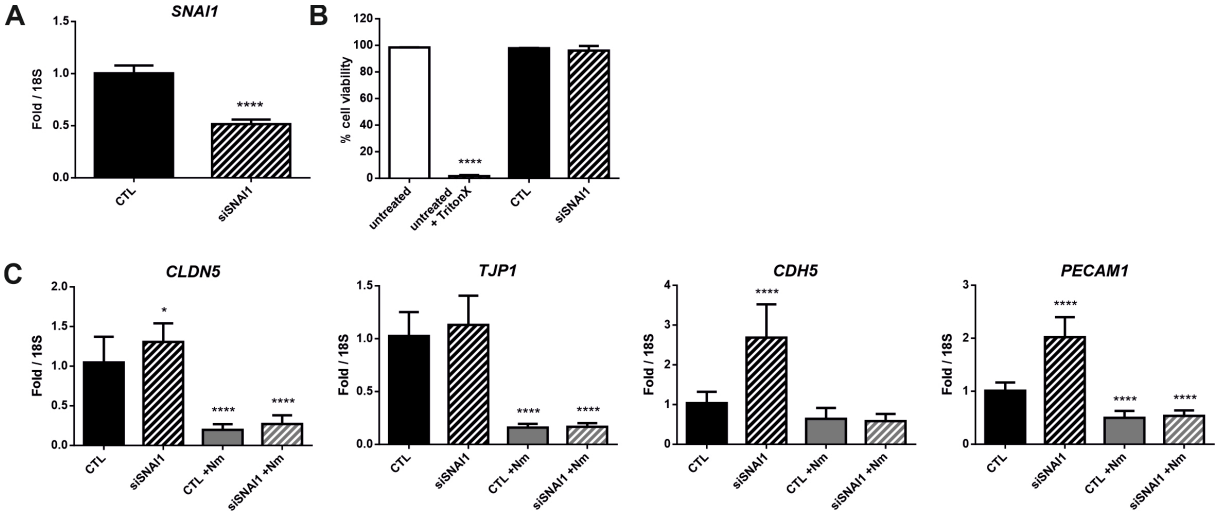

Figure 15. Effects of SNAI1 knockdown on *N. meningitidis* induced downregulation of cell-junction expression in hCMEC/D3s. **a**) Relative expression of SNAI1 after siRNA mediated knockdown (siSNAI1) compared to scrambled control siRNA (CTL), quantified by qPCR and normalized to 18S rRNA. **b**) Percentage of viable cells after siRNA transfection, determined via PI staining and flow cytometry using untreated hCMEC/D3 as controls. **c**) Relative expression of genes for tight junction components ZO-1 (TJP1) and claudin-5 (CLDN5), and endothelial adherence junction proteins VE-cadherin (CDH5) and CD31 (PECAM1) in hCMEC/D3 after siRNA knockdown of SNAI1 and with (light bars) or without (dark bars) *N. meningitidis* infection, quantified by qPCR and normalized to 18S rRNA. Data presented as mean ± SD from three independent experiments performed in triplicate (n = 9). ****p < 0.0001; Student's t test (**a**); ANOVAfollowed by Dunnett's multiple comparisons test (**b**, **c**).

Finally, to examine effects of prolonged *N. meningitidis* on expression and localization of tight junction proteins ZO-1, claudin-5, and occludin in the iBEC layer, immunofluorescence staining of infected and uninfected iBEC-LMC co-cultures was performed 24 h and 30 h p.i. (**Figure 16**). To determine junction coverage, confocal images (Z-stacks) were analyzed using recently developed junction analyzer software JAnaP [190]. This analysis revealed a significant reduction in junction coverage of occludin in infected iBEC layers from iBEC-LMC co-culture 24 h and 30 h p.i. (**Figure 16**). Junction coverage of claudin-5 was slightly reduced 24 h p.i., and no significant effect difference between infected and uninfected samples was detected 30 p.i. However, it must be noted that immunofluorescence staining of claudin-5 may not be well suited for JAnaP analysis due to its high levels of cytoplasmic background causing high degrees of variation and uncertainty. Interestingly, no significant change in junctional ZO-1 expression was observed with *N. meningitidis* infection, suggesting that transcriptional downregulation did not affect protein levels at iBEC cell-cell junctions in the iBEC-LMC co-culture model in this time frame.

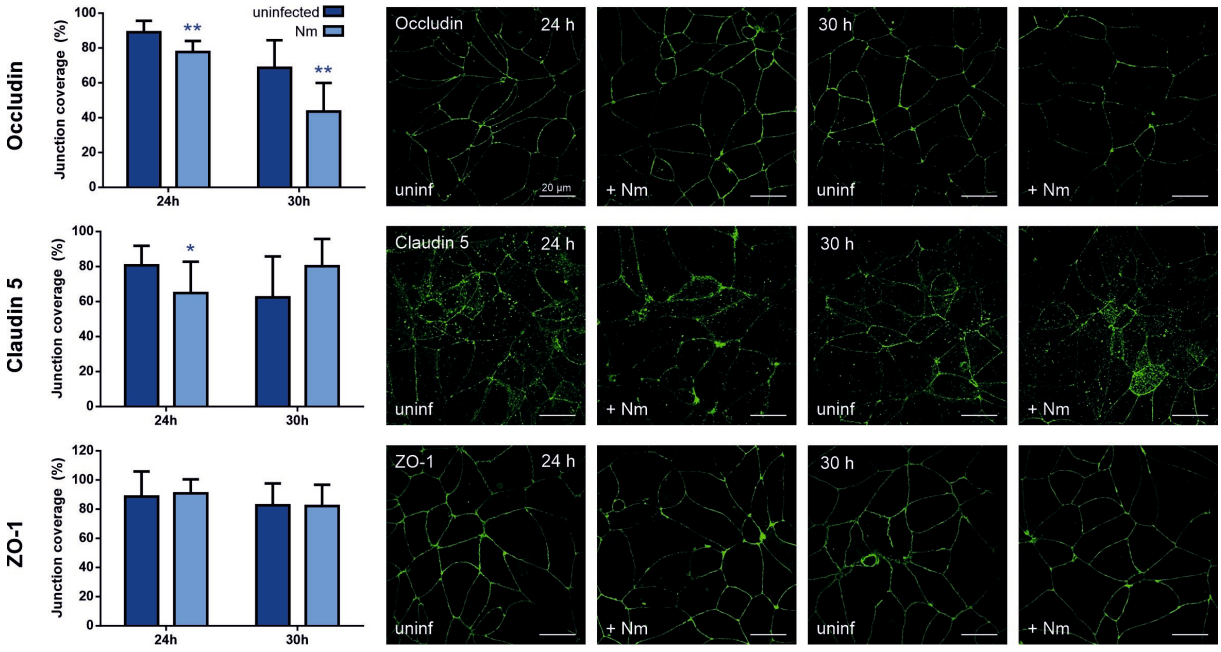

Figure 16. Effects of *N. meningitidis* infection on cell-junction protein expression in iBECs of mono- and co-culture models. Junction coverage of occludin, claudin-5, and ZO-1 in iBEC monolayers from iBEC-LMC co-cultures analyzed using confocal microscopy and JAnaP junction analyzer software [REF]. Data presented as mean junction coverage ± SD from three independent experiments, calculated using average junction coverage data from three images per experiment (n = 9). Representative images were chosen based on these calculations. *p < 0.05, **p < 0.01, ***p < 0.001, ****p < 0.0001; Student's t test; infected vs. uninfected control (blue/black asterisks directly over bars).

In summary, TEER of infected iBEC-LMC co-culture barrier models remained high for approximately 24 h (**Figure 12**), at which point intact tight junctions could still be observed using TEM (**Figure 11**). These results suggest a transcellular route of traversal by *N. meningitidis* considering that significant levels of bacterial invasion and transmigration were detected within 24h after infection (**Figure 9**, **Figure 10**). However, after 24 h, TEER of infected iBEC-LMC models dropped to significantly lower levels by 30 h p.i. irrespective of the barrier enhancing effect of LMC co-culture (**Figure 12**). Similar results were observed with the hCMEC/D3-LMC model. Furthermore, expression of tight and adherens junction genes was downregulated in BECs from both BEC-LMC co-culture models at the late infection time points (**Figure 13**, **Figure 14**), potentially but not solely mediated by Snail1 (**Figure 15**). While mRNA levels of occludin were not affected, junctional coverage of the protein was reduced in infected BEC layers from iBEC-LMC co-culture (**Figure 16**), suggesting post-transcriptional modification. Together these results suggest deterioration of mBCSFB barrier properties upon prolonged meningococcal challenge, which may enable paracellular bacterial traversal considering that higher transmigration rates were observed in models with lower TEER (**Figure 10**, **Figure 12**).

4.5 *N. meningitidis* induced immune activation of BECs

Immune activation of BECs at the mBCSFB presumably contributes to recruitment of leukocytes into the CSF and progression of bacterial meningitis [199]. To assess activation of BECs from the BEC-LMC co-culture models, gene expression of the neutrophilic chemoattractants IL8 (*CXCL8*), C-X-C motif chemokine 1 and 2 (*CXCL1*, *CXCL2*), and C-C motif chemokine 20 (*CCL20*), as well as the broad cytokine Interleukin-6 (*IL6*) was analyzed using qPCR on samples collected 8 h, 24 h, and 30 h p.i. (**Figure 17**). *CXCL8*, *CXCL1*, *CXCL2*, and *CCL20* were upregulated in iBECs from iBEC-LMC co-culture during the time course of infection. Highest increases in expression level were detected with *CXCL8* and *CCL20*. mRNA levels of both genes were approximately 6 times higher in infected samples at 8 h p.i. (*CXCL8*: 6.1 ± 3.8; *CCL20*: 6.8 ± 4.1). *CCL20* expression increased slightly further 24 h p.i. (7.8 ± 2.9) and 30 h p.i. (12.3 ± 12.2), although variance between replicates of four independent experiments was high. *CXCL1* and *CXCL2* were upregulated approximately 2-fold (±1) at 8 h p.i. (*CXCL1*: 1.9 ± 1.1; *CXCL2*: 1.9 ± 0.6). While similar values were recorded for *CXCL1* expression 24 h and 30 h p.i., *CXCL2* levels were statistically indifferent in infected and uninfected samples at these timepoints. No change in *IL6* expression was detected, except for slight reduction at 24 h p.i. (0.7 ± 0.3). This effect was not observed in iBECs from monoculture, which generated overall comparable results other than higher upregulation of *CXCL8* (24.2 ± 9.7) and *CXCL1* (4.3 ± 1.8) after 24 h of infection.

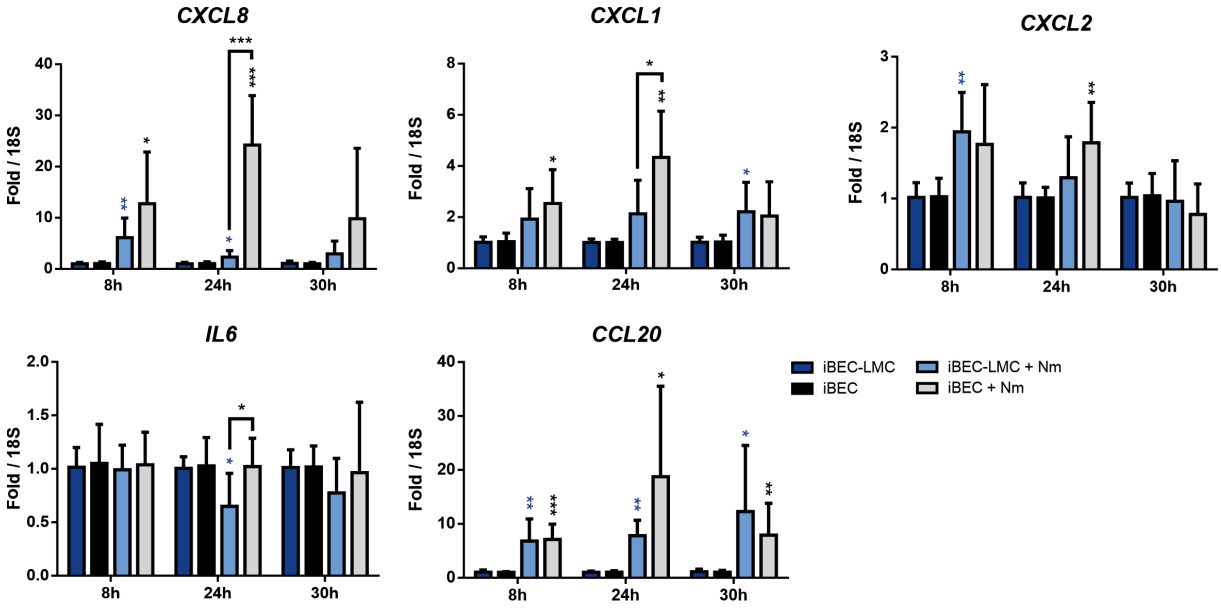

Figure 17. Effects of *N. meningitidis* infection on expression of proinflammatory cytokines in iBECs of mono- and co-culture models. Relative expression of CXCL8, CXCL1, CXCL2, CCL20, and IL6 transcripts in iBECs from direct co-culture with LMCs with (light bars) or without (dark bars) *N. meningitidis* infection, quantified by qPCR and normalized to 18S rRNA. Data presented as mean ± SD from four independent experiments and iBEC differentiations performed in duplicate (n = 6-8). *p < 0.05, **p < 0.01, ***p < 0.001; Student's t test; infected vs. uninfected control (blue/black asterisks directly over bars), mono vs co-culture (asterisks above brackets).

The same panel of genes was analyzed using qPCR on hCMEC/D3s from hCMEC/D3-LMC co-culture and hCMEC/D3 monoculture after 8 h and 24 h of infection. Significant upregulation of all cytokines and chemokines, including *IL6*, was observed at both time points, most prominently at 8 h p.i. (**Figure 18**). Compared to iBECs, mRNA levels were elevated much more substantially, but strongest changes were still observed with *CXCL8* and *CCL20*. 8 h p.i., a mean increase of approximately over 100-fold was recorded for *CXCL8* (131 ± 45) and *CCL20* (102 ± 51) expression. Levels of *CXCL1* (42 ± 6) and *CXCL2* (33 ± 3) mRNA were at least 30 times higher in infected cells after 8 h. At the same time, IL6 transcription was upregulated about 75-fold (± 27). Data collected from hCMEC/D3 monoculture samples was generally comparable, although relative fold-change was often a bit lower.

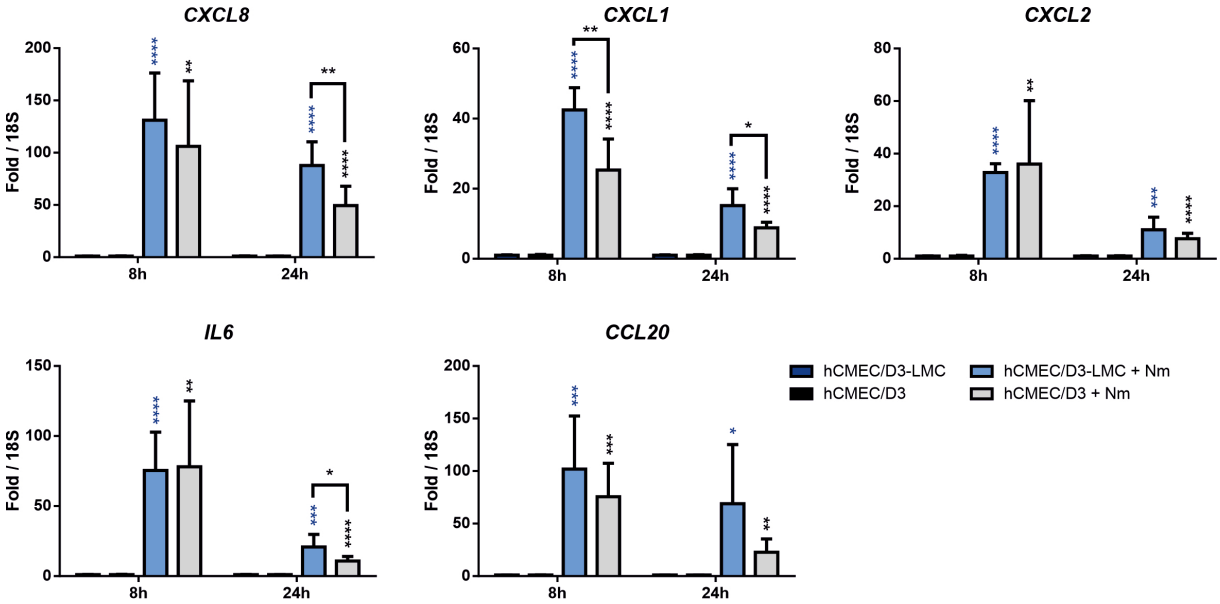

Figure 18. Effects of *N. meningitidis* infection on the expression of proinflammatory cytokines in hCMEC/D3 from monoand co-culture models. Relative expression of CXCL8, CXCL1, CXCL2, CCL20, and IL6 transcripts in hCMEC/D3 from direct co-culture with LMCs (blue bars) and hCMEC/D3 transwell monoculture (black/gray bars) with (light bars) or without (dark bars) *N. meningitidis* infection, quantified by qPCR and normalized to 18S rRNA. Data presented as mean ± SD from three independent experiments performed in duplicate (n = 6). *p < 0.05, **p < 0.01, ***p < 0.001, ****p < 0.0001; Student's t test; infected vs. uninfected control (blue/black asterisks directly above bars), mono vs co-culture (asterisks above brackets).

Finally, ELISAs were performed to evaluate secretion of IL-8, one of the most transcriptionally upregulated chemokines (**Figure 19**). After 8 h, 24 h, or 30 h of *N. meningitidis* infection, supernatants were collected from the apical and basolateral compartments of the transwell models and analyzed combined (BEC monoculture) or separately (BEC-LMC co-culture). IL-8 was barely detectable by ELISA in medium from iBEC monoculture (< 10 pg/ml) (**Figure 19**a). Slightly higher protein concentrations were measured in apical supernatants from iBEC-LMC co-cultures reaching peak values of around 50 pg/ml, particularly in samples from infected cells 24 h (55 ± 53 pg/ml) and 30 h p.i. (46 ± 58 pg/ml). However, variability between replicates of the four independent experiments was high and may have been influenced by IL-8 secretion from LMCs on the basolateral side. IL-8 secretion and upregulation under *N. meningitidis* infection has been demonstrated in meningioma derived LMCs previously [139].

Consistent with these observations, much higher levels of IL-8 were detected in basolateral medium from iBEC-LMC co-culture, and elevated protein concentrations were measured in infected samples 24 h (631 ± 365 pg/ml) and 30 p.i. (779 ± 437 pg/ml) (**Figure 19**a). In contrast to the iBEC models, IL-8 was substantially more abundant in hCMEC/D3 culture supernatants (**Figure 19**b). While concentrations of up to 1375 ± 596 pg/ml (24 h p.i.) were already measured in uninfected hCMEC/D3 monocultures, IL-8 levels were significantly increased by *N. meningitidis* infection 8 h (4290 ± 1067 pg/ml) and 24 h p.i. (4927 ± 1265 pg/ml). The greatest amounts of IL-8 were detected in apical supernatants from infected hCMEC/D3-LMC co-cultures reaching 13736 ± 1601 pg/ml (8 h p.i.) and 14065 ± 2131 pg/ml (24 h p.i.). High IL-8 concentrations were also found in basolateral medium from infected hCMEC/D3-LMC co-culture 8 h (8420 ± 2527 pg/ml) and 24 h p.i. (11684 ± 2938 pg/ml), suggesting contribution of chemokine secretion by the LMCs.

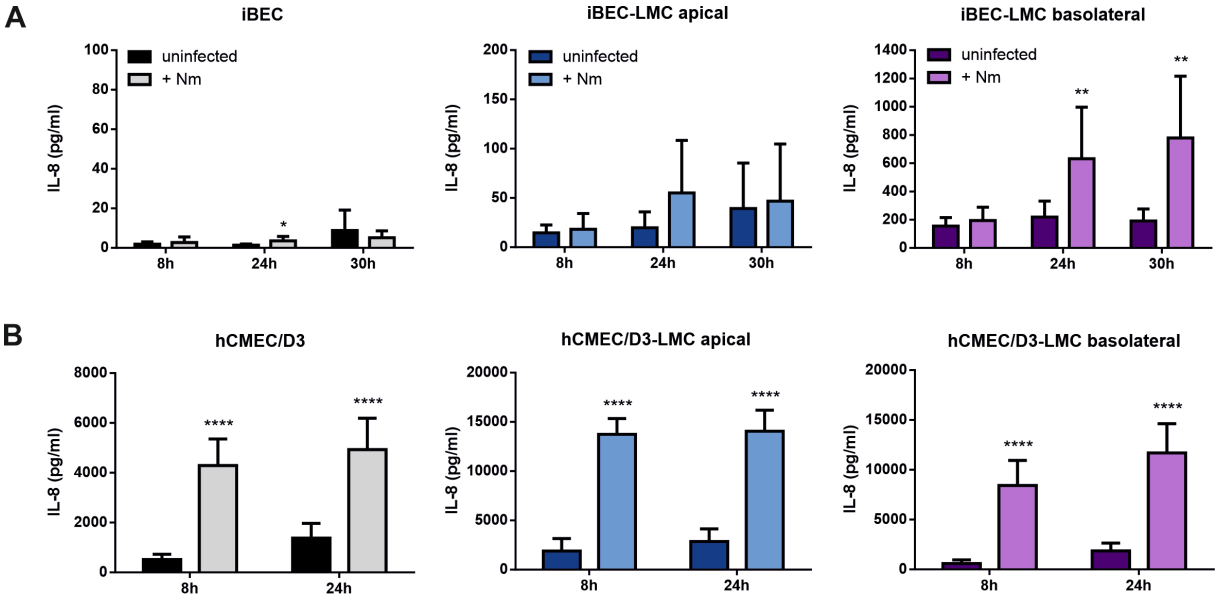

Figure 19. Effects of *N. meningitidis* infection on IL-8 secretion in the mBCSFB models. Concentration of IL-8 in the cell culture medium determined by ELISA. Supernatants from apical and basolateral compartment anlayzed separately in BEC-LMC co-cultures. **a**) iBEC monoculture and iBEC-LMC co-culture. **b**) hCMEC/D3 monoculture and hCMEC/D3-LMC co-culture. Data presented as mean ± SD from four independent experiments performed in duplicate (n = 6-8). *p < 0.05, **p < 0.01, ****p < 0.0001; Student's t test; infected vs. uninfected control.

In conclusion, these results demonstrate upregulation of relevant proinflammatory cytokines in infected iBECs and hCMEC/D3s co-cultured with LMCs, comparable to respective BEC monocultures, suggesting that BECs activate innate immune response mechanisms in response to bacterial infection. In comparison, gene expression was increased more substantially in hCMEC/D3 compared to iBEC based models. Furthermore, significant concentrations of secreted IL-8 were measured in supernatants of hCMEC/D3 culture, whereas secretion of this transcriptionally upregulated chemokine was almost undetectable in iBEC culture medium. Finally, elevated levels of IL-8 in basolateral supernatants of infected iBEC-LMC and hCMEC/D3-LMC co-culture models suggest immune activation of LMCs upon meningococcal interaction with the mBCSFB.

5 DISCUSSION

N. meningitidis (the meningococcus) is one of the main causes of bacterial meningitis worldwide, a severe disease that occurs when pathogens infiltrate CSF filled spaces within the meninges and elicit an exaggerated host immune response that leads to damage of CNS tissue [200]. Studies using post-mortem tissue have suggested that meningococci primarily enter the CSF by crossing meningeal microvessels and interact with leptomeningeal cells of the arachnoid and pia mater [107, 108]. Brain endothelial cells that compose these vessels are highly specialized cells that possess barrier characteristics similar to BBB endothelium but are surrounded by LMCs rather than brain parenchymal cell types such as astrocytes and pericytes found at the NVU [65, 72]. *N. meningitidis* interaction with this specific meningeal blood-CSF barrier has primarily been investigated *in vitro* using immortalized BECs alone, which retain much of the BEC phenotype but lack critical barrier characteristics such as high paracellular tightness [142, 156, 201]. Recent advances in stem-cell technologies have generated model BEC-like cells that form a highly restrictive barrier and can be used to examine pathogenesis of various meningeal pathogens [158, 201]. Direct interaction of meningococci with LMCs has been analyzed using meningioma derived cells [108, 139, 140]. As *in vitro* monoculture models only distantly represent the native microenvironment and the use of *in vivo* models to study interaction with human-specific *N. meningitidis* is limited to humanized rodents, more advanced and complex *in vitro* models could expand our understanding of this host-pathogen interaction. The aim of this study was the development and validation of novel BEC-LMC co-culture models to investigate meningococcal interaction with and penetration of the mBCSFB in a more physiologically relevant setting.

5.1 Development and characterization of the BEC-LMC co-culture models

5.1.1 Model development

iPSC derived BECs and hCMEC/D3 cells were used to develop two separate co-culture models with LMCs derived from meningioma. iBECs were differentiated from the iPSC line IMR90-4, which was originally generated using lentiviral reprogramming of human fetal fibroblasts and presented the highest differentiation potential and cell yield compared to other iPSC lines [158, 186]. The differentiation was performed according to published protocols [157, 158, 182], as previously described [188]. The procedure relies on a co-differentiation step, during which the presence of neuronal cells induces the BEC phenotype in developing endothelial cells, presumably via canonical Wnt/β-catenin signaling [158, 202, 203]. During the following expansion phase, endothelial medium was supplemented with all-trans retinoic acid. BECs specifically express retinol-binding proteins and its membrane receptor *STRA6* [158, 204]. Addition of RA has been shown to improve the BEC phenotype by increasing VE-cadherin and occludin expression at this stage of the differentiation as well as elevating tight junction continuity, TEER, and MRP efflux activity in purified, mature iBECs [157].

Subculture onto a selective collagen IV and fibronectin matrix finally leads to a pure iBEC monolayer as well as further EC maturation, as evident by induction of vWF expression [158]. Recognizing the advantage of a human *in vitro* BEC model exhibiting physiological barrier tightness, our group and others have recently demonstrated usefulness of iBECs to investigate how pathogens such as GBS, *N. meningitidis*, Zika virus, and SARS-CoV2 affect and penetrate blood-CNS barriers [101, 133, 162-165]. iBECs have previously been co-cultured with brain parenchymal cell types present at the NVU such as pericytes, astrocytes, and neurons derived from various sources including human and rodent primary and iPSC derived cells [142, 157, 158, 170-175]. Using iBECs differentiated with RA, co-cultures have typically been initiated immediately upon iBEC purification and maintained in EC medium, which provided the best conditions for co-culture induced barrier tightening effects on the iBEC layer [157, 171-175]. Therefore, iBEC-LMC co-culture was set up similarly in this project. After pre-seeding LMCs in wells of a TC plate or onto the underside of transwell inserts, the medium was changed to EC medium and iBECs were purified on top of the transwell membrane. The LMCs were isolated from benign leptomeningeal tumors and characterized following previously published methods [108], and kindly provided by Prof. Myron Christodoulides. Previously validated for infection studies with *N. meningitidis* [108, 138-140], these cells were deemed suitable for mBCSFB modeling in this project. In addition to the iBEC-LMC model, co-cultures were established using hCMEC/D3 cells and LMCs, for reference. Isolated from human cerebral microvessels of an epileptic patient and immortalized using hTERT and SV40, hCMEC/D3s possess many BEC phenotypes, especially compared to other human cell lines, although still lacking physiological levels of paracellular tightness [148, 149, 156]. Considering this, hCMEC/D3s have been a useful *in vitro* model to examine interaction with *N. meningitidis* and various other infectious agents [109, 118, 131, 201]. hCMEC/D3s have been co-cultured with astrocytes and pericytes to model the BBB [156, 205]. hCMEC/D3-LMC co-cultures were set-up similarly to the iBEC-LMC model by seeding hCMEC/D3s onto TC plastic pre-seeded with LMCs and incubation in hCMEC/D3 medium. Experiments were typically conducted on the BEC-LMC models on day 2 (iBEC) or day 3 (hCMEC/D3) of co-culture, one day after a confluent BEC layer had formed to allow for maturation of cellular junctions, which also corresponded to maximum or close-to-maximum TEER across all models.

5.1.2 Characterization of the BEC-LMC co-culture models

Electron microscopy, immunofluorescence staining of relevant markers, TEER, and sodium fluorescein permeability assays were performed to characterize and validate the BEC-LMC co-culture models according to some of the most relevant benchmarks [170]. Previous research, including studies from our group, have demonstrated that iBECs possess all major BEC phenotypes such as endothelial markers, tight junction expression, barrier properties, and functional efflux transporters [101, 133, 157, 158, 163, 171, 174, 182, 188]. Following co-culture with LMCs, clear junctional expression of BEC adherens and tight junction markers CD31, VE-cadherin, claudin-5, ZO-1, and occludin in the iBEC layer

was observed in this project. Furthermore, presence and polarized localization of complex cellular junctions including tight junctions between cells of the densely packed iBEC layer was detected using TEM. Similarly, ultrastructural analysis using freeze-fracture EM and TEM has previously revealed complex networks of tight junction particles between iBECs co-cultured with and without other cell types of the NVU [158, 171].

Although iBECs that were generated according to the co-differentiation protocol used in this thesis display important vascular characteristics along with superior barrier properties, recent studies have identified certain limitations, particularly regarding their endothelial phenotype [206]. Using transcriptomic analyses, expression of a substantial number of epithelial-associated genes has been detected in iBECs [169, 207-209]. RNAseq revealed lower expression levels of endothelial genes along with presence of an epithelial transcriptional signature in iBECs compared to generic iPSC-derived ECs [207]. Expression of both epithelial and endothelial transcripts was also observed in an RNAseq analysis of iBECs from a BBB-chip model [169]. Using both RNAseq and scRNAseq techniques, Lu and colleagues further demonstrated expression of epithelial genes and proteins, such as EPCAM [208, 209]. However, lack of CD31 (PECAM-1) and VE-cadherin (CDH5) protein expression was also reported in their work, which has conversely been demonstrated for iBECs using flow cytometry, western blotting, and immunofluorescence in a multitude of other studies [133, 157, 158, 163, 171, 172, 188, 206, 210]. In addition to antibody-based detection methods, a gene-edited human embryonic VE-cadherin-eGFP reporter stem cell line has recently been used to illustrate VE-cadherin expression after differentiation into iBECs [206]. Nevertheless, the mentioned transcriptomic studies indicate a mixed endothelial-epithelial phenotype for iBECs. Certain epithelial characteristics of iBECs could also be observed in this project, particularly related to the cytoarchitecture, such as small protrusions on the apical surface and larger cell height. However, the thickness of the iBEC layer was variable to some degree depending on seeding density. While it is important to consider these limitations when employing the model, iBECs remain suitable for various applications as they recapitulate critical BBB functions such as minimal paracellular transport better than other human *in vitro* models [142, 206]. Interestingly, despite the depressed vascular character, Delsing at al. demonstrated that iBECs recapitulated BBB function much better than generic iPSC-derived ECs in terms of passive barrier, efflux transport, and drug permeability [207]. Furthermore, from personal experience and other reports [206, 210], it should be noted that lack of proper marker expression including endothelial protein expression or localization may also be a result of suboptimal differentiation. For example, iPSC seeding density and timing of the differentiation are key variables for successful iBEC generation [158, 210, 211]. Thus, analyzing endothelial markers such as CD31 and VE-cadherin at the protein level is important for quality control of the iBEC differentiation, in addition to assessment of barrier properties. In conclusion, much research has been conducted on the iBEC model following publication of the original protocols,

uncovering advantages as well as weaknesses, and establishing alternative protocols and improvements [206, 212]. This will undoubtably lead to the generation of iBECs that model the BBB even more faithfully in the future.

Compared to the iBEC layer, LMCs displayed a distinct morphology such as a large spread-out cytosol with curvy-linear edges and formed a close-to-confluent monolayer. Additionally, the meningioma derived cells expressed histopathological markers vimentin, desmoplakin, and EMA, characterizing them to be of the meningothelial subtype, as previously described [108]. The LMCs were also immunopositve for tight junction proteins ZO-1 and E-cadherin, although junctional expression of ZO-1 was discontinuous and relatively uniform E-cadherin staining was observed over the entire cell, potentially due to the cancerous nature of the cells. For the most part, LMCs of the arachnoid and pia mater are connected by gap junctions and sometimes desmosomes but lack tight junctions, with the exception of a layer of arachnoid barrier cells closest to the dura mater [72, 75, 76]. Immunoreactivity for E-cadherin in this cell layer has been observed in mice, and expression of claudin-11 was shown in the developing human, rat, and mouse arachnoid barrier [213-215]. Pial LMCs, in particular, form a more permissive barrier that allows for the passage of immune cells entering the SAS from the blood and tracers injected into the CSF [72, 81, 82].

hCMEC/D3s co-cultured with LMCs displayed typical endothelial morphology evident by a smooth luminal surface and a thin elongated cell shape. However, multilayer formation was occasionally observed in areas of high cell density. Presence of electron dense regions indication complex paracellular junctions was seldomly observed between neighboring cells using TEM. Although expression of CD31, VE-cadherin, and ZO-1 was detected immunocytochemically, clear and uniform staining of BEC adherens and tight junction proteins could not be achieved. While it was observed here and in previous studies that hCMEC/D3s express many components that constitute the BEC phenotype on a transcriptional and protein level, junctional localization of these proteins is often missing, and TEER is relatively low [148, 149, 156, 216, 217]. During the original development of the model, junctional expression of proteins such as CD31, β-catenin, ZO-1, and JAM-A and claudin-5 was demonstrated [148]. However, claudin-5 expression was not as clear compared to the other proteins and occludin was not detected at the cell-cell contacts [148]. Claudin-5 expression in hCMEC/D3s was recently found to be significantly lower than in primary porcine BECs [216]. Elevation of claudin-5 expression was achieved via lentiviral transfection and lead to slightly improved barrier properties of hCMEC/D3s, but paracellular tightness comparable to the porcine BECs was not achieved [216]. A recent in-depth study of hCMEC/D3 culture under various conditions showed expression of VE-cadherin, ZO-1, claudin-5 and occludin, but junctional localization was incomplete or entirely absent, as in the case of claudin-5 and occludin [217]. In conclusion, data concerning BEC junctions in hCMEC/D3s varies slightly between literature, potentially due to differences in culture conditions, but

lack of continuous expression of certain tight junction components at the cell-cell borders is common. Considering that other models including iBECs exhibit clear junctional staining of tight junction proteins, this phenotype is likely necessary for formation of a tight paracellular barrier.

5.1.3 Influence of LMC co-culture on tightness and stability of the BEC barrier

High TEER inversely related to paracellular permeability of solutes is considered one of the key benchmarks for *in vitro* BBB models [170]. The relationship between these two parameters is non-linear (one-phase exponential decay), and varying cut-off values have been suggested for physiologically relevant studies depending on the specific application [170, 218, 219]. One-phase exponential decay was first demonstrated on primary rat BECs, where a constant permeability coefficient for sodium fluorescein of 2 x 10^{-6} cm/s was observed above a threshold TEER of 130 Ω cm² [218]. In a recent study using human iPSC derived BECs, it was shown that permeability of a larger molecule such as IgG did not significantly change above a TEER of 900 Ω cm² [219]. Although *in vivo* data are scarce, studies on brain surface microvessels of anesthetized frogs and rats have shown mean TEER values of at least 1870 Ω cm² and 800 Ω cm², respectively [220-222]. iPSC derived BECs typically reach TEER values above 1500 Ω cm² and NaF permeability values in the order of 10^{-7} cm/s [133, 157, 172, 173, 188, 223]. While iBECs alone can exhibit high paracellular tightness, many reports have shown stimulating as well as stabilizing effects on iBEC barrier properties caused by co-culture with cells of the NVU [142, 157, 158, 170-175]. For instance, TEER of iBEC layers was elevated together with junctional continuity of occludin when cultured together with iPSC-derived pericytes, astrocytes, and neurons in a recent study [174]. In this project, average peak TEER of 2820 Ω cm² was recorded for iBEC monocultures on transwell inserts with a 0.4 µm pore size two days after purification. Co-culture with LMCs increased iBEC barrier tightness and stability further, as reflected by consistently improved TEER and NaF permeability values over a subculture period of at least one week. Soluble factors were likely responsible for this effect as barrier properties were enhanced with both direct and indirect co-culture and TEER of LMC monoculture was insignificantly low. Similarly, barrier stimulating effects of astrocyte, pericyte, or neuron co-culture on iBECs have been observed in indirect co-culture systems [157, 158, 171, 172, 174, 175]. BBB induction, including increased TEER, has been observed in human and bovine ECs upon treatment with astrocyte conditioned medium [224]. Pericytes and pericyte conditioned medium improved barrier function of iBECs under stress conditions [173]. Generally, crosstalk between glial and endothelial cells involves various secreted factors that interact with their respective receptors [67, 225]. Several secreted glial factors that can induce BBB properties in BECs have been described, such as bFGF [226], GDNF [227, 228], and hydrocortisone [229]. Initial experiments with conditioned medium from LMCs performed in this project did not result in elevated TEER of iBEC monolayers. However, further investigation into the mechanism behind LMC-induced improvement of iBEC barrier tightness and stability is required. More complex crosstalk that requires

presence of both cell types may also be responsible for these effects. For example, platelet-derived growth factor (PDGF-BB) secreted by ECs binds to and activates its receptor PDGFR-β on pericytes, causing downstream signaling that is essential for pericyte induced regulation of BBB integrity in health and disease [230]. To investigate the mechanisms and factors involved in LMC-BEC crosstalk, RNAseq analysis could be performed comparing BECs and LMCs in monoculture and co-culture settings. Candidate molecules from the RNAseq analysis or from literature can be identified using immunolabeling methods, and, ultimately, subjected to further molecular analysis regarding their effects on the iBEC barrier. On a different note, in addition to biological factors and methodology of measurement, physical and physicochemical parameters including tissue culture geometry have been described to influence TEER of BEC models [222]. Interestingly, comparatively lower TEER across all models was measured in this project using inserts with a smaller diameter and a 3 µm pore size during infection experiments on day 2 of subculture. However, the barrier boosting effect induced by LMC co-culture was even more noticeable under these conditions.

Substantially lower levels of paracellular tightness were observed in the hCMEC/D3 based models, consistent with previous literature [156, 217]. Stimulation of the Wnt/β-catenin signaling by addition of activators such as lithium chloride has shown slight improvement of the barrier phenotype of hCMEC/D3s [231, 232]. Another study showed a significant increase in TEER as well as a slight reduction of paracellular permeability to solutes upon hydrocortisone supplementation [233]. However, hydrocortisone was a component of the hCMEC/D3 culture medium used in this project, and the addition of lithium chloride was tested but did not result in higher TEER of hCMEC/D3 monolayers (data not shown). Although co-culture of hCMEC/D3s with astrocytes was shown to slightly increase TEER in one study [205], others have shown that hCMEC/D3s were unresponsive to astrocyte or pericyte co-culture [156, 217, 234]. In this project, slightly higher TEER and lower NaF permeability was observed in hCMEC/D3-LMC direct co-cultures on 0.4 µm transwells compared to monoculture and indirect co-cultur. However, this was most likely due to the LMC layer on the underside of the transwell membrane, as similar TEER was measured on LMC monocultures. A similar observation was recorded recently using hCMEC/D3s in co-culture with a human astrocyte cell line [217]. Overall, these data suggest that iBEC based models may be better suited for studies of paracellular permeability or transport.

In conclusion, novel human *in vitro* models of the mBCSFB were established successfully using iBECs or hCMEC/D3 in co-culture with meningioma LMCs. While previous research has focused on modeling the classical BBB using BECs and cell types present at the NVU, these models resemble the physiological environment blood-CSF barrier in the leptomeninges and can be used not only for infection studies, pharmacological studies, and studies of CNS disease. Particularly the iBEC-LMC model can be useful for pharmacological transport studies due to its superior barrier function.

5.2 *N. meningitidis* interaction with the BEC-LMC co-culture models

5.2.1 Adherence and Invasion of the BEC layer

Upon characterization, the BEC-LMC co-culture models were validated for infection studies with *N. meningitidis*. First, meningococcal adherence and invasion of the BEC layer was analyzed. Shortly after infection, substantial amounts of adherent bacteria were observed in both the iBEC and the hCMEC/D3 based models, consistent with published data [109, 112, 113, 121]. Microcolony formation and close interaction with iBECs along with cytoplasmic protrusions around adherent bacteria was observed in the iBEC-LMC co-culture model using electron and structured illumination microscopy. Studies using immortalized BECs have shown that initial adhesion is mediated by meningococcal Tfp binding to host receptor CD147, which forms a complex with β2-adrenergenic receptor increasing strength of bacterial attachment [109, 110]. A previous study from our group has demonstrated presence of the cellular receptor CD147 on iBECs as well as its proximity to sites of bacterial attachment iBECs [133]. Bacterial aggregation and microcolony formation on the endothelial cell surface typical feature of *N. meningitidis* host-cell interaction and is primarily mediated by Tfp [179, 235]. Microvillus-like membrane protrusions that form around adherent bacteria alongside Tfp fibres may protect *N. meningitidis* against blood-flow induced shear-stress [110, 123, 125, 126]. Meningococcal invasion of human peripheral ECs as well as bone marrow, brain microvessel, and, recently, iPSC derived BECs has previously been demonstrated *in vitro* [112, 113, 121, 123, 124, 128-130, 133]. Accordingly, intracellular bacteria were detected in iBECs and hCMEC/D3s from BEC-LMC co-cultures. While relatively low at first, bacterial invasion increased significantly during prolonged infection. Similar observations have been previously described using the HBMEC model, and this dynamic may be attributed to downregulation of the polysaccharide capsule upon initial bacterial adhesion, which demasks critical adhesins and invasins such as Opc [113, 127]. A capsule deficient mutant *N. meningitidis* strain expressing OpcA and Opa has also been recently shown to be more invasive in iBECs compared to the wild type [133]. Overall, data gathered on meningococcal adhesion and invasion of iBECs and hCMEC/D3s co-cultured with LMCs in this project was statistically indifferent from iBECs and hCMEC/D3 monoculture, respectively, and comparable between the models. Consistent with previous literature, these findings validate the BEC-LMC models for infection studies with *N. meningitidis*.

5.2.2 Barrier disruption upon infection

Previous research has shown that *N. meningitidis* interaction with BECs induced barrier disruption through modulation of cellular junctions, proposing a paracellular route for bacterial traversal of the mBCSFB [118, 131-133]. Tfp mediated meningococcal interaction with hCMEC/D3s triggered β-arrestin signaling that lead to the recruitment of cytoskeletal and cell-junction components underneath adherent bacteria, effectively weakening the BEC barrier [118, 131]. Discontinuous junctional staining

of adherens junction protein VE-cadherin was detected together with increased permeability to lucifer yellow and correlated with *N. meningitidis* traversal of the hCMEC/D3 layer [118, 131]. Significantly elevated paracellular flux of FITC-labeled dextrans and cleavage of tight junction transmembrane protein occludin was observed upon prolonged meningococcal challenge using the immortalized HBMEC line [132]. Activated metalloprotease MMP8 was responsible for the cleavage of occludin, which resulted in its ablation from the cell-cell border [132]. A recent study using iBEC monocultures also shows *N. meningitidis* induced barrier disruption and modulation of tight junctions [133]. Loss of TEER along with an increase in NaF permeability after 24h of infection was described. Furthermore, altered junctional expression of occludin, ZO-1, and claudin-5 was observed in infected iBECs cultured on plate. While ZO-1 staining was continuous but appeared to be frayed, junction strands of occludin were clearly disrupted, and a potential cleavage product of the protein was detected [133]. Irrespective of the elevated barrier tightness of the iBEC-LMC co-culture models, a similar drop in TEER was observed, here, after 24 h of *N. meningitidis* challenge. This was also noticeable in the hCMEC/D3 based models, although overall TEER was extremely low. Additionally, junctional coverage of occludin was reduced slightly in iBEC layers from iBEC-LMC co-culture after 24 h and more substantially after 30 h of infection. While effects on claudin-5 were difficult to analyze due to a less defined junctional staining, ZO-1 expression appeared not to be altered when analyzed immunocytochemically. This could be influenced by the different culture geometry compared to iBEC monoculture on plate but may also be attributed to a co-culture effect. Interestingly, improved junction continuity of tight junction components such as occludin upon co-culture with NVU cells has been previously described [174, 175]. Nevertheless, *N. meningitidis* induced disruption of occludin, without a change in junctional ZO-1, was sufficient to significantly increase paracellular permeability in the HBMEC model [132].

In addition to disorganization and post-translational modulation of cellular junction components, transcriptional regulation relevant genes under meningococcal infection was examined in BECs from BEC-LMC co-cultures as a potential mechanism contributing to barrier deterioration. Downregulation of tight junction proteins ZO-1, occludin, and claudin-5 upon GBS infection, and mediated by zinc finger transcription factor Snail1 has previously been observed in immortalized BECs and in mice [195]. Thereafter, a similar mechanism for junction disruption was proposed in iBECs upon interaction with GBS [163]. In a recent study from our group, *N. meningitidis* also induced downregulation of genes coding for ZO-1 (*TJP1*), and especially claudin-5 (*CLDN5*) in iBEC monocultures after 24 h of infection, but no significant change in occludin (*OCLN*) transcription was observed upon interaction with this pathogen [133]. Consistent with these observations, expression of *TJP1*, and, most drastically, *CLDN5* was reduced in infected iBEC layers co-cultured with LMCs, predominantly 24 h p.i. or later. Additionally, downregulation of VE-cadherin (*CDH5*) was detected. Similar results were observed in hCEMC/D3 cells from hCMEC/D3-LMC co-cultures after 24 h of infection, although CD31 (*PECAM1*)

transcription was downregulated, too, in this model. Results from BEC monoculture and BEC-LMC co-culture were generally comparable. A question that remains is, how these changes in mRNA level affect protein expression and, ultimately, barrier integrity. Apart from dynamic, steady state processes, transcriptional changes do not necessarily lead to immediate alteration of protein levels outside of steady state, and post-transcriptional processes are more important for short-term adaptations [236]. Quantitative correlation of mRNA levels and protein abundance can be temporally separated by many hours [237]. Although tendencies towards lower levels of occludin, ZO-1, and claudin-5 were detected after 32 h of infection [133], quantification was difficult due to low abundance of reference proteins such as β-actin or COX IV. Future investigations using better suited reference proteins and including later timepoints could help elucidate this mechanism. However, barrier disruption has already progressed substantially at that stage in the infection process.

Together with the downregulation of cell-junction components upon *N. meningitidis* infection, simultaneous upregulation of Snail1 (*SNAI1*) was detected in BECs from BEC-LMC co-culture, most significantly in iBECs, consistent with previous data [133]. Snail1 is a zinc finger transcription factor that is most known for its role as a regulator of epithelial-mesenchymal transition (EMT) and cancer metastasis [238]. Snail1 can repress the expressions of genes coding for adherens and tight junction proteins such as E-cadherin (*CDH1*), claudins, and occludin by direct binding of E-box motifs in the promoter region [194, 196, 239]. Upregulation of Snail1 has been previously linked to BBB disruption caused by the meningeal pathogens GBS, *Streptococcus pneumoniae*, and *E. coli* K1 [195, 240, 241]. To investigate the influence of Snail1 on *N. meningitidis* induced downregulation of tight and adherence junction genes in BECs, siRNA mediated knockdown experiments were performed in this project using hCMCE/D3 monocultures. *SNAI1* knockdown led to a slight increase in *CLDN5* and substantial elevation of *CDH5* and *PECAM1. TJP1* levels were not significantly altered, which is consistent with previous literature suggesting that Snail1 does not regulate transcription of ZO-1 [194]. Furthermore, siRNA knockdown of *SNAI1* was not sufficient to rescue the significant downregulation of *CLDN5*, *CDH5*, and *PECAM1* in infected hCMEC/D3s. Together, these findings indicate that Snail1 mediated repression is not solely responsible for the reduction of cell-junction gene expression in BECs induced by *N. meningitidis* infection, and further investigation is required to elucidate this mechanism. Previous research suggests, for instance, that claudin-5 is transcriptionally repressed by forkhead box protein O1 (FoxO1) in concert with β-catenin under IL-1β induced inflammatory conditions [242]. Interestingly, VE-cadherin has been described to stimulate claudin-5 expression by inducing the phosphorylation of FoxO1 and by limiting the translocation of beta-catenin to the nucleus [243]. However, this protein is itself subject to *N. meningitidis* induced effects on its transcription and cellular localization. Regarding elevated Snail1 expression, other mechanisms outside of tight junction repression seem intriguing.

Snail1 can also act as an activator in concert with other factors, stimulating expression of fibronectin, metalloproteases such as MMP9, and the chemokine IL-8, for instance [244-246].

5.2.3 Meningococcal traversal of the mBCSFB

Meningeal pathogens such as *N. meningitidis, Streptococcus pneumoniae*, Group B *Streptococcus*, and *E. coli* K1 can translocate from the bloodstream into the CNS by crossing the endothelium at the mBSCFB via a transcellular or paracellular pathway or both [200, 247]. Transcellular barrier traversal follows tight interaction with and invasion of BECs, whereas paracellular translocation may be enabled by disruption of cellular junctions or cell damage induced by the pathogen [200, 247]. Although much research has elucidated mechanisms as well as cellular and bacterial factors involved in the interaction between *N. meningitidis* and BECs, the pathway of meningococcal penetration of the mBCSFB has been a matter of debate. As mentioned before, cellular internalization of meningococci, influenced by *N. meningitidis* induced host cell signaling events, has been observed using various peripheral and brain endothelial cell models [112, 113, 120-124, 128-130, 133]. Although the fate of the internalized bacteria is not entirely clear, intracellular survival and replication of *N. meningitidis* was shown using HBMECs [130], suggesting a transcellular route for meningococcal traversal of the mBCSFB. On the other hand, barrier disruption upon modulation of tight and adherens junction components was observed in infected hCMEC/D3s and HBMECs, proposing potential mechanisms for paracellular bacterial transmigration [118, 131, 132]. However, modeling of this complex host-pathogen interaction has been limited by the lack of human *in vitro* models that exhibit physiologically relevant paracellular tightness. BEC-like cells generated from human iPSCs overcome these limitations and have recently been used to model interaction with CNS pathogens such as GBS, *N. meningitidis*, and Zika virus, and SARS-CoV2, particularly to investigate how such pathogens affect and penetrate the blood-CNS barriers [101, 133, 162-165, 188]. While Zika virus crossed the BEC layer without compromising barrier integrity [164], GBS was shown to disrupt tight junctions and increase paracellular permeability [163]. Using iBECs in co-culture with LMCs, in this project, *N. meningitidis* transmigration rates were low at first, but increased substantially within 24 h of infection, while TEER was still high and intact tight junctions could still be observed. Together with increasing bacterial invasion of iBECs, detected with the first 8 h of infection, these observations support the notion of transcellular barrier traversal. However, deterioration of the iBEC-LMC barrier including gradual loss of TEER and modulation of cellular junction components such as occludin was detected after 24h h of infection, consistent with previous results from iBEC monoculture [133]. Furthermore, higher rates of bacterial transmigration often correlated with lower TEER. For instance, more meningococci were detected traversing the iBEC monoculture model compared to the iBEC-LMC co-culture model early on, although absolute counts were low. Additionally, transmigration rates in the hCMEC/D3 based models were already substantially higher than in the iBEC models at the earliest measured time point after infection. This demonstrates

the usefulness of models exhibiting physiological barrier tightness for studying bacterial traversal of cellular barriers, and it indicates that *N. meningitidis* is likely to cross the BEC barrier via a paracellular route if available. While meningococcal invasion of BECs potentially contributes to early migration through the mBCSFB, deterioration of barrier properties may open a more accessible paracellular route later during infection.

An intriguing thought is whether *N. meningitidis* interaction with basolateral host cell receptors upon transcellular passage may also influence junction modulation and barrier disruption. It was recently shown that *Helicobacter pylori* interaction with basolateral integrin-β1 receptor triggers secretion of the CagA oncoprotein which affects host cell signaling [248, 249]. However, disruption of cellular junctions is mediated by serine protease HtrA and occurs earlier in the infection process [248, 249]. While basolateral interactions have not been specifically explored during meningococcal interaction with BECs, *N. meningitidis* does interact with integrin receptors. Specifically, meningococcal Opc can bind host αVβ3 and α5β1 integrins indirectly via vitronectin and fibronectin [112, 113, 127]. This interaction has been shown to promote cytoskeletal rearrangement and promote bacterial invasion [112, 113, 127-129]. In addition to indirect Opc-mediated binding, direct association of the meningococcal adhesin NadA with β1 integrins has been demonstrated [44]. Furthermore, *N. meningitidis* can interact with laminin receptor 1 (LAMR1/RPSA) via Tfp subunits PilQ and PilE and the membrane porin PorA [115]. Like integrins, non-integrin laminin receptors such as LAMR1 (37/67 laminin receptor) or dystroglycan are involved in cellular adherence to the basal membrane by binding the ECM component laminin [250]. Previous studies on the interactions between these receptors and meningococcal factors have analyzed their effects on adherence and invasion of host cells, presuming presence of these receptors on the apical surface of BECs. While it is possible that predominantly basolateral receptors such as integrins are delivered to the apical membrane [251], previous studies have been limited by the use of EC or BEC models with low paracellular barrier function. Therefore, using the highly polarized iBEC model would be of interest to analyze localization of these receptors, interaction with meningoccocal factors, and effects on bacterial traversal of the cellular barrier. An additional receptor that would be interesting to investigate in this model is CD147, the receptor that mediates initial adhesion of *N. meningitidis* on endothelial cells [110]. It was previously shown using the hCMEC/D3 model that activation of the CD147-associated β2-adrenergenic receptor leads to recruitment of adherence junction components VE-cadherin and p120-catenin away from the cell-cell junction and to the site of infection [118]. Interestingly, CD147 contains basolateral sorting information contained in its cytoplasmic domain and is basolaterally expressed in most epithelia with certain exceptions such as retinal pigment epithelia [252, 253]. CD147 can interact with integrins including α5β1, influence cell polarity, and mediate MMP expression, which can lead to the cleavage of tight junction components and affect cellular attachment to the ECM [254-256].

5.2.4 *N. meningitidis*-induced immune activation

Meningococcal interaction with the mBCSFB and translocation into CSF filled leptomeningeal spaces evokes a strong inflammatory response, which is characterized by rapid influx of leukocytes – primarily neutrophiles – and is presumably triggered by immune activation of BECs and LMCs [72, 199, 200]. *N. meningitidis* has been shown to induce endothelial expression and accumulation of adhesion molecules that regulate leukocyte interaction such as E-Selectin, ICAM, VCAM, and CD44 [119, 257]. Additionally, increased cytokine expression and secretion was observed in HBMECs in response to meningococcal infection [129, 135, 137]. Compared to peripheral endothelial cells, significantly higher release of the general cytokine IL-6 and the neutrophilic chemokine IL-8 was observed in the BEC model [135]. Furthermore, it was shown that secretion of both immunological effector proteins was influenced by the *N. meningitidis* induced activation of MAP kinase [129]. Upregulation of proinflammatory cytokines and neutrophilic chemoattractants was also recently observed in iBECs after infection with *N. meningitidis* or *Group B Streptococcus* [133, 163]. Consistent with these findings, transcription of IL-8 (*CXCL8*), Gro-α (*CXCL1*), Gro-β (*CXCL2*) and MIP3A (*CCL20*) was elevated in iBECs from iBEC-LMC co-culture models upon meningococcal challenge. However, although iBECs are evidently immunologically activated in response to bacterial infection, previous studies have shown that cytokine secretion corresponding to these changes in gene expression was generally lacking [133, 163]. Similarly, IL-8 was barely detectable in iBEC supernatants in this project. While it is unclear whether this low abundance of secreted cytokines observed in iBECs is biologically relevant, future studies are going to be able to address this issue. Recently, an alternative protocol was published for the generation of iBECs with improved properties for the study of immune cell interaction including constitutive expression adhesion molecules ICAM-1/-2 and E-selectin and upregulation of ICAM-1, P-selectin and VCAM-1 in response to proinflammatory stimulation [258]. In contrast to the iBEC based models, much higher basal levels of extracellular IL-8 were observed in hCMEC/D3 cultures, in this project, together with substantially increased IL-8 secretion in addition to significant transcriptional upregulation of all evaluated cytokines upon *N. meningitidis* infection. Chemokine secretion under basal conditions (CCL2 and CXCL8) or following pro-inflammatory cytokine treatment (CCL5, CXCL10, fractalkine) has previously been demonstrated in hCMEC/D3s and primary human BECs [259, 260]. Therefore, hCMEC/D3s may currently be better suited for studying immune activation of BECs than iBECs. However, BECs are not the only cell type that contributes to meningeal inflammation upon interaction with bacterial pathogens such as *N. meningitidis*. LMCs are also activated by meningococcal interaction and secretion of proinflammatory cytokines and chemokines such as IL-6, IL-8, and MCP-1, RANTES, and the GM-CSF has been shown using meningioma derived LMCs [139-141]. Activation of LMCs was modulated by LOS and other meningococcal components and was independent of TLR2 and TLR4 signaling [139, 140]. Compared to other meningitis-causing bacteria, *N. meningitidis* showed the

highest levels of adherence and induction of the mentioned inflammatory mediators [141]. Consistent with these results, elevated levels of IL-8 were detected in basolateral supernatants of infected iBEC-LMC and hCMEC/D3-LMC co-culture models. IL-8 secretion by LMCs was most likely responsible for higher concentrations of the protein in the apical medium from BEC-LMC co-culture compared to BEC monoculture, as this effect was most pronounced in the leakier hCMEC/D3 models.

5.3 Conclusion and future perspectives

In this project, novel *in vitro* models of the mBCSFB were successfully developed using iBECs or hCMEC/D3s in co-culture with meningioma derived LMCs and validated for infection studies with *N. meningitidis*. iBECs, which form tight paracellular barriers on their own but have been shown to be responsive to co-culture cues from other NVU cell types such as astrocytes and pericytes, exhibited improved barrier tightness and stability when co-cultured with LMCs. Meningococci interacted with and penetrated the iBEC-LMC co-culture model, and induced barrier disruption upon prolonged infection by modulating expression of cell-junction components. These observations were consistent with previous data from BEC and iBEC monoculture studies, and the cellular response of iBECs to *N. meningitidis* infection was generally not affected by LMC co-culture. Furthermore, meningococcal challenge induced similar effects in iBEC and hCMEC/D3 based models. However, usefulness of hCMEC/D3s for studying meningococcal disruption and traversal of the mBCSFB was limited by low paracellular tightness and lack of clear tight junction expression. On the other hand, this cell line seemed particularly suitable for investigation of molecular mechanisms such as immune activation. Interestingly, the combined results from this study suggest that meningococcal invasion of BECs potentially contributes to early traversal of the mBCSFB, while barrier deterioration may open a more accessible paracellular route later on. In conclusion, the work conducted in this project demonstrates the usefulness of advanced *in vitro* models that more closely resemble native physiology to study interaction with human-exclusive pathogens such as *N. meningitidis.* Specifically, models exhibiting physiological barrier tightness can provide relevant insight into pathogenic modulation and penetration of blood-CNS barriers such as the mBCSFB.

Following this work, many avenues can be explored, including in the future including detailed mechanistic studies of some of the observed effects, application of the developed BEC-LMC co-culture models for other research questions, and further advancement of the models. Additional investigation is required to fully elucidate the mechanisms of *N. meningitidis* induced barrier disruption. For instance, signaling pathways and molecular factors involved in post transcriptional modulation of occludin are mostly unknown. The involvement of metalloproteinases such as MMP-8, which has been shown to mediate cleavage of occludin in HBMECs [132], could be examined in iBECs and hCMEC/D3s. Furthermore, the mechanism behind transcriptional downregulation of cell-junction components in

infected BECs and its effect on protein expression remain elusive. Further studies could clarify the role of Snail1 in this process or uncover involvement of other transcriptional regulators such as FoxO1 [242]. Here, gene knockdown or knock-out could be performed using methods such as siRNA transfection or CRISPR/Cas9, respectively. However, adverse side effects of knocking out/down multi-purpose regulators such as Snail1 must be considered. Nevertheless, other functions of Snail1 such as stimulating expression of fibronectin [245], metalloproteases such as MMP9 [246], and the chemokine IL-8 [244], seem intriguing in the context of *N. meningitidis* infection. Regarding a different mechanism of barrier destabilization, assessing meningococcal stimulation of basolateral cellular receptors would be interesting, especially in the iBEC model, and could initially be tested seeding BECs on the underside of transwells and infecting from the basolateral side. Super resolution immunofluorescence microscopy could be employed to investigate localization receptors and interaction with *N. meningitidis*. Bacterial factors involved in the interaction and their impact on adherence, invasion, and especially transmigration could be evaluated using knockout and overexpression strains. Further research is also required to elucidate the proposed transcellular crossing of the mBCSFB by *N. meningitidis*. BEC invasion and intracellular survival can be analyzed in iBECs and hCMEC/D3s as done before using the HBMEC model [130]. However, acquiring data that clearly indicates intracellular survival and transcellular passage has been difficult and will require multiple methods including electron and super-resolution microscopy as well as alternative approaches such as differential staining of extra- and intracellular bacteria [261, 262]. Finally, more physiologically relevant models such as the iBEC-LMC model offer the opportunity to investigate the capacity of other meningeal pathogens or clinical isolates of *N. meningitidis* to modulate and traverse the mBCSFB. Within such studies, meningococcal factors responsible for potentially enhanced or reduced invasiveness could be identified using mutant strains and molecular interference, for example.

Multiple options also remain for further development of advanced mBCSFB *in vitro* models that better reflect the complex native physiology. This includes adaptation of tissue culture geometry, addition of other relevant cell types such as immune cells, and introduction of physiological parameters such as shear stress exerted by blood flow. Microscopic analysis of BEC-LMC co-culture models on transwells was often challenged by presence of the 10 µm thick artificial PET membrane that interfered with signal detection and seemed to adversely affect cross-sectioning of embedded samples. Other strategies for construction of 3D tissue models are available including approaches using alternative scaffolds such as fibrous mesh created by electrospinning techniques and scaffold free strategies such as cell aggregation using hydrogel beds [263]. However, availability of such alternative scaffolds can be limited and different co-culture strategies may affect functional aspects of the model. In a recent study, seeding of iBECs together with or directly on top of pericytes resulted in a slight reduction of

TEER, which was, however, not observed when iBECs were added onto a hydrogel containing the pericytes [173].

Next, the introduction of leukocytes such as neutrophils and macrophages primarily from the blood-side of the BEC-LMC co-culture model could expand the scope of the model to study barrier modulation, immune cell migration, and disease progression. Recently, activation of neutrophils, transmigration across the 3D tissue model, recruitment to the site of *Neisseria gonorrhoeae* infection was demonstrated in a newly established perfusion bioreactor system using a triple co-culture model of epithelial cells, fibroblasts, and endothelial cells [264]. Microfluidic systems are useful to introduce shear stress, a physiologically relevant parameter caused by blood flow. Shear stress has been shown to affect the phenotype of peripheral and brain endothelial cells, although to varying extent depending on cell type and model [166-168]. Various aspects of pneumococcal interaction with endothelial cells such as bacterial adhesion or disruption of endothelial layer integrity have recently been investigated under circulatory flow [265, 266], and a detailed description of the methodology was published [267]. *N. meningitidis* adhesion and proliferation on ECs has also previously been examined under shear stress [110, 126], but BEC models such as iBECs have not been in a microfluidic system used to interrogate meningococcal interaction. Finally, novel organ-on-a-chip technologies that have been emerging in the tissue engineering field combine microfluidics with 3D tissues and possess great potential for more wholistic studies of disease progression and treatment [268]. Multiple tissues connected via microfluidics can be included on a single chip. Therefore, *N. meningitidis* infection and pathogenesis could potentially be modeled as a whole, from nasopharyngeal colonization to invasion and proliferation in the bloodstream, and infiltration of tissues such as the skin or the meninges.

REFERENCES

1. Pace, D. and A.J. Pollard, *Meningococcal disease: clinical presentation and sequelae.* Vaccine, 2012. **30 Suppl 2**: p. B3-9.
2. Wang, B., et al., *Case fatality rates of invasive meningococcal disease by serogroup and age: A systematic review and meta-analysis.* Vaccine, 2019. **37**(21): p. 2768-2782.
3. McNamara, L.A., et al., *Detection of Ciprofloxacin-Resistant, beta-Lactamase-Producing Neisseria meningitidis Serogroup Y Isolates - United States, 2019-2020.* MMWR Morb Mortal Wkly Rep, 2020. **69**(24): p. 735-739.
4. Potts, C.C., et al., *Antimicrobial Susceptibility Survey of Invasive Neisseria meningitidis, United States 2012-2016.* J Infect Dis, 2022. **225**(11): p. 1871-1875.
5. Zapun, A., C. Morlot, and M.K. Taha, *Resistance to beta-Lactams in Neisseria ssp Due to Chromosomally Encoded Penicillin-Binding Proteins.* Antibiotics (Basel), 2016. **5**(4).
6. Caugant, D.A. and M.C. Maiden, *Meningococcal carriage and disease--population biology and evolution.* Vaccine, 2009. **27 Suppl 2**: p. B64-70.
7. Christensen, H., et al., *Meningococcal carriage by age: a systematic review and meta-analysis.* Lancet Infect Dis, 2010. **10**(12): p. 853-61.
8. Peterson, M.E., et al., *Meningococcal carriage in high-risk settings: A systematic review.* Int J Infect Dis, 2018. **73**: p. 109-117.
9. Cooper, L.V., et al., *Risk factors for acquisition of meningococcal carriage in the African meningitis belt.* Trop Med Int Health, 2019. **24**(4): p. 392-400.
10. Jafri, R.Z., et al., *Global epidemiology of invasive meningococcal disease.* Popul Health Metr, 2013. **11**(1): p. 17.
11. Salomon, A., et al., *Influenza increases invasive meningococcal disease risk in temperate countries.* Clin Microbiol Infect, 2020. **26**(9): p. 1257 e1-1257 e7.
12. Harrison, O.B., et al., *Description and nomenclature of Neisseria meningitidis capsule locus.* Emerg Infect Dis, 2013. **19**(4): p. 566-73.
13. Maiden, M.C., et al., *Multilocus sequence typing: a portable approach to the identification of clones within populations of pathogenic microorganisms.* Proc Natl Acad Sci U S A, 1998. **95**(6): p. 3140-5.
14. Caugant, D.A. and O.B. Brynildsrud, *Neisseria meningitidis: using genomics to understand diversity, evolution and pathogenesis.* Nat Rev Microbiol, 2020. **18**(2): p. 84-96.
15. Pace, D. and A.J. Pollard, *Meningococcal A, C, Y and W-135 polysaccharide-protein conjugate vaccines.* Arch Dis Child, 2007. **92**(10): p. 909-15.
16. Serruto, D., et al., *The new multicomponent vaccine against meningococcal serogroup B, 4CMenB: immunological, functional and structural characterization of the antigens.* Vaccine, 2012. **30 Suppl 2**(0 2): p. B87-97.
17. Davidsen, T. and T. Tonjum, *Meningococcal genome dynamics.* Nat Rev Microbiol, 2006. **4**(1): p. 11-22.
18. Tzeng, Y.L., J. Thomas, and D.S. Stephens, *Regulation of capsule in Neisseria meningitidis.* Crit Rev Microbiol, 2016. **42**(5): p. 759-72.
19. Virji, M., *Pathogenic neisseriae: surface modulation, pathogenesis and infection control.* Nat Rev Microbiol, 2009. **7**(4): p. 274-86.
20. Mikucki, A., N.R. McCluskey, and C.M. Kahler, *The Host-Pathogen Interactions and Epicellular Lifestyle of Neisseria meningitidis.* Front Cell Infect Microbiol, 2022. **12**: p. 862935.
21. Derkaoui, M., et al., *Transport and Catabolism of Carbohydrates by Neisseria meningitidis.* J Mol Microbiol Biotechnol, 2016. **26**(5): p. 320-32.
22. Perkins-Balding, D., M. Ratliff-Griffin, and I. Stojiljkovic, *Iron transport systems in Neisseria meningitidis.* Microbiol Mol Biol Rev, 2004. **68**(1): p. 154-71.
23. Stork, M., et al., *Zinc piracy as a mechanism of Neisseria meningitidis for evasion of nutritional immunity.* PLoS Pathog, 2013. **9**(10): p. e1003733.

24. Spoerry, C., et al., *Neisseria meningitidis IgA1-specific serine protease exhibits novel cleavage activity against IgG3.* Virulence, 2021. **12**(1): p. 389-403.
25. Tzeng, Y.L. and D.S. Stephens, *Antimicrobial peptide resistance in Neisseria meningitidis.* Biochim Biophys Acta, 2015. **1848**(11 Pt B): p. 3026-31.
26. De Boeck, I., et al., *Comparing the Healthy Nose and Nasopharynx Microbiota Reveals Continuity As Well As Niche-Specificity.* Front Microbiol, 2017. **8**: p. 2372.
27. Shakhnovich, E.A., S.J. King, and J.N. Weiser, *Neuraminidase expressed by Streptococcus pneumoniae desialylates the lipopolysaccharide of Neisseria meningitidis and Haemophilus influenzae: a paradigm for interbacterial competition among pathogens of the human respiratory tract.* Infect Immun, 2002. **70**(12): p. 7161-4.
28. Audry, M., et al., *Airway Mucus Restricts Neisseria meningitidis Away from Nasopharyngeal Epithelial Cells and Protects the Mucosa from Inflammation.* mSphere, 2019. **4**(6).
29. Custodio, R., et al., *Type VI secretion system killing by commensal Neisseria is influenced by expression of type four pili.* Elife, 2021. **10**.
30. Custodio, R., et al., *Commensal Neisseria cinerea impairs Neisseria meningitidis microcolony development and reduces pathogen colonisation of epithelial cells.* PLoS Pathog, 2020. **16**(3): p. e1008372.
31. Arenas, J., et al., *Domain exchange at the 3' end of the gene encoding the fratricide meningococcal two-partner secretion protein A.* BMC Genomics, 2013. **14**: p. 622.
32. Jamet, A., et al., *A new family of secreted toxins in pathogenic Neisseria species.* PLoS Pathog, 2015. **11**(1): p. e1004592.
33. Crystal, R.G., et al., *Airway epithelial cells: current concepts and challenges.* Proc Am Thorac Soc, 2008. **5**(7): p. 772-7.
34. Read, R.C., et al., *Experimental infection of human nasal mucosal explants with Neisseria meningitidis.* J Med Microbiol, 1995. **42**(5): p. 353-61.
35. Stephens, D.S., L.H. Hoffman, and Z.A. McGee, *Interaction of Neisseria meningitidis with human nasopharyngeal mucosa: attachment and entry into columnar epithelial cells.* J Infect Dis, 1983. **148**(3): p. 369-76.
36. Bartley, S.N., et al., *Attachment and invasion of Neisseria meningitidis to host cells is related to surface hydrophobicity, bacterial cell size and capsule.* PLoS One, 2013. **8**(2): p. e55798.
37. Virji, M., et al., *Pilus-facilitated adherence of Neisseria meningitidis to human epithelial and endothelial cells: modulation of adherence phenotype occurs concurrently with changes in primary amino acid sequence and the glycosylation status of pilin.* Mol Microbiol, 1993. **10**(5): p. 1013-28.
38. Carbonnelle, E., et al., *Meningococcal interactions with the host.* Vaccine, 2009. **27 Suppl 2**: p. B78-89.
39. Imhaus, A.F. and G. Dumenil, *The number of Neisseria meningitidis type IV pili determines host cell interaction.* EMBO J, 2014. **33**(16): p. 1767-83.
40. Bille, E., et al., *A virulence-associated filamentous bacteriophage of Neisseria meningitidis increases host-cell colonisation.* PLoS Pathog, 2017. **13**(7): p. e1006495.
41. Deghmane, A.E., et al., *Down-regulation of pili and capsule of Neisseria meningitidis upon contact with epithelial cells is mediated by CrgA regulatory protein.* Mol Microbiol, 2002. **43**(6): p. 1555-64.
42. Sadarangani, M., A.J. Pollard, and S.D. Gray-Owen, *Opa proteins and CEACAMs: pathways of immune engagement for pathogenic Neisseria.* FEMS Microbiol Rev, 2011. **35**(3): p. 498-514.
43. Virji, M., et al., *Meningococcal Opa and Opc proteins: their role in colonization and invasion of human epithelial and endothelial cells.* Mol Microbiol, 1993. **10**(3): p. 499-510.
44. Nagele, V., et al., *Neisseria meningitidis adhesin NadA targets beta1 integrins: functional similarity to Yersinia invasin.* J Biol Chem, 2011. **286**(23): p. 20536-46.
45. Scarselli, M., et al., *Neisseria meningitidis NhhA is a multifunctional trimeric autotransporter adhesin.* Mol Microbiol, 2006. **61**(3): p. 631-44.

46. Turner, D.P., et al., *Characterization of MspA, an immunogenic autotransporter protein that mediates adhesion to epithelial and endothelial cells in Neisseria meningitidis.* Infect Immun, 2006. **74**(5): p. 2957-64.
47. Serruto, D., et al., *Neisseria meningitidis App, a new adhesin with autocatalytic serine protease activity.* Mol Microbiol, 2003. **48**(2): p. 323-34.
48. Schmitt, C., et al., *A functional two-partner secretion system contributes to adhesion of Neisseria meningitidis to epithelial cells.* J Bacteriol, 2007. **189**(22): p. 7968-76.
49. Vacca, I., et al., *Neisserial Heparin Binding Antigen (NHBA) Contributes to the Adhesion of Neisseria meningitidis to Human Epithelial Cells.* PLoS One, 2016. **11**(10): p. e0162878.
50. Barrile, R., et al., *Neisseria meningitidis subverts the polarized organization and intracellular trafficking of host cells to cross the epithelial barrier.* Cell Microbiol, 2015. **17**(9): p. 1365-75.
51. Lecuyer, H., X. Nassif, and M. Coureuil, *Two strikingly different signaling pathways are induced by meningococcal type IV pili on endothelial and epithelial cells.* Infect Immun, 2012. **80**(1): p. 175-86.
52. Sutherland, T.C., et al., *Transcellular passage of Neisseria meningitidis across a polarized respiratory epithelium.* Infect Immun, 2010. **78**(9): p. 3832-47.
53. Lewis, L.A. and S. Ram, *Complement interactions with the pathogenic Neisseriae: clinical features, deficiency states, and evasion mechanisms.* FEBS Lett, 2020. **594**(16): p. 2670-2694.
54. Agarwal, S., et al., *Inhibition of the classical pathway of complement by meningococcal capsular polysaccharides.* J Immunol, 2014. **193**(4): p. 1855-63.
55. Del Tordello, E., et al., *Neisseria meningitidis NalP cleaves human complement C3, facilitating degradation of C3b and survival in human serum.* Proc Natl Acad Sci U S A, 2014. **111**(1): p. 427-32.
56. Jarva, H., et al., *Binding of the complement inhibitor C4bp to serogroup B Neisseria meningitidis.* J Immunol, 2005. **174**(10): p. 6299-307.
57. Griffiths, N.J., et al., *Meningococcal surface fibril (Msf) binds to activated vitronectin and inhibits the terminal complement pathway to increase serum resistance.* Mol Microbiol, 2011. **82**(5): p. 1129-49.
58. Principato, S., M. Pizza, and R. Rappuoli, *Meningococcal factor H binding protein as immune evasion factor and vaccine antigen.* FEBS Lett, 2020. **594**(16): p. 2657-2669.
59. Loh, E., et al., *Temperature triggers immune evasion by Neisseria meningitidis.* Nature, 2013. **502**(7470): p. 237-40.
60. Gault, J., et al., *Neisseria meningitidis Type IV Pili Composed of Sequence Invariable Pilins Are Masked by Multisite Glycosylation.* PLoS Pathog, 2015. **11**(9): p. e1005162.
61. Schielke, S., et al., *Characterization of FarR as a highly specialized, growth phase-dependent transcriptional regulator in Neisseria meningitidis.* Int J Med Microbiol, 2011. **301**(4): p. 325-33.
62. Giltner, C.L., Y. Nguyen, and L.L. Burrows, *Type IV pilin proteins: versatile molecular modules.* Microbiol Mol Biol Rev, 2012. **76**(4): p. 740-72.
63. Lecuyer, H., et al., *Pathogenesis of meningococcal purpura fulminans.* Pathog Dis, 2017. **75**(3).
64. Ehrlich, P.U.h.b.g.d.b.i.P., *Das Sauerstoff-Bedürfniss des Organismus: eine farbenanalytische Studie*. 1885: August Hirschwald.
65. Mastorakos, P. and D. McGavern, *The anatomy and immunology of vasculature in the central nervous system.* Sci Immunol, 2019. **4**(37).
66. Abbott, N.J., et al., *Structure and function of the blood-brain barrier.* Neurobiol Dis, 2010. **37**(1): p. 13-25.
67. Abbott, N.J., L. Ronnback, and E. Hansson, *Astrocyte-endothelial interactions at the blood-brain barrier.* Nat Rev Neurosci, 2006. **7**(1): p. 41-53.
68. Daneman, R. and A. Prat, *The blood-brain barrier.* Cold Spring Harb Perspect Biol, 2015. **7**(1): p. a020412.
69. Kaur, C., G. Rathnasamy, and E.A. Ling, *The Choroid Plexus in Healthy and Diseased Brain.* J Neuropathol Exp Neurol, 2016. **75**(3): p. 198-213.

70. Morita, S., et al., *Heterogeneous vascular permeability and alternative diffusion barrier in sensory circumventricular organs of adult mouse brain.* Cell Tissue Res, 2016. **363**(2): p. 497-511.
71. Langlet, F., et al., *Tanycyte-like cells form a blood-cerebrospinal fluid barrier in the circumventricular organs of the mouse brain.* J Comp Neurol, 2013. **521**(15): p. 3389-405.
72. Weller, R.O., et al., *The meninges as barriers and facilitators for the movement of fluid, cells and pathogens related to the rodent and human CNS.* Acta Neuropathol, 2018. **135**(3): p. 363-385.
73. Balin, B.J., et al., *Avenues for entry of peripherally administered protein to the central nervous system in mouse, rat, and squirrel monkey.* J Comp Neurol, 1986. **251**(2): p. 260-80.
74. Rua, R. and D.B. McGavern, *Advances in Meningeal Immunity.* Trends Mol Med, 2018. **24**(6): p. 542-559.
75. Alcolado, R., et al., *The cranial arachnoid and pia mater in man: anatomical and ultrastructural observations.* Neuropathol Appl Neurobiol, 1988. **14**(1): p. 1-17.
76. Nabeshima, S., et al., *Junctions in the meninges and marginal glia.* J Comp Neurol, 1975. **164**(2): p. 127-69.
77. Yasuda, K., et al., *Drug transporters on arachnoid barrier cells contribute to the blood-cerebrospinal fluid barrier.* Drug Metab Dispos, 2013. **41**(4): p. 923-31.
78. Brightman, M.W. and T.S. Reese, *Junctions between intimately apposed cell membranes in the vertebrate brain.* J Cell Biol, 1969. **40**(3): p. 648-77.
79. Hutchings, M. and R.O. Weller, *Anatomical relationships of the pia mater to cerebral blood vessels in man.* J Neurosurg, 1986. **65**(3): p. 316-25.
80. Zhang, E.T., C.B. Inman, and R.O. Weller, *Interrelationships of the pia mater and the perivascular (Virchow-Robin) spaces in the human cerebrum.* J Anat, 1990. **170**: p. 111-23.
81. Morris, A.W., et al., *Vascular basement membranes as pathways for the passage of fluid into and out of the brain.* Acta Neuropathol, 2016. **131**(5): p. 725-36.
82. Schlager, C., et al., *Effector T-cell trafficking between the leptomeninges and the cerebrospinal fluid.* Nature, 2016. **530**(7590): p. 349-53.
83. Lochhead, J.J., et al., *Structure, Function, and Regulation of the Blood-Brain Barrier Tight Junction in Central Nervous System Disorders.* Front Physiol, 2020. **11**: p. 914.
84. Haseloff, R.F., et al., *Transmembrane proteins of the tight junctions at the blood-brain barrier: structural and functional aspects.* Semin Cell Dev Biol, 2015. **38**: p. 16-25.
85. Berndt, P., et al., *Tight junction proteins at the blood-brain barrier: far more than claudin-5.* Cell Mol Life Sci, 2019. **76**(10): p. 1987-2002.
86. Greene, C., N. Hanley, and M. Campbell, *Claudin-5: gatekeeper of neurological function.* Fluids Barriers CNS, 2019. **16**(1): p. 3.
87. Yuan, S., K.J. Liu, and Z. Qi, *Occludin regulation of blood-brain barrier and potential therapeutic target in ischemic stroke.* Brain Circ, 2020. **6**(3): p. 152-162.
88. Furuse, M., et al., *Occludin: a novel integral membrane protein localizing at tight junctions.* J Cell Biol, 1993. **123**(6 Pt 2): p. 1777-88.
89. Bazzoni, G., et al., *Interaction of junctional adhesion molecule with the tight junction components ZO-1, cingulin, and occludin.* J Biol Chem, 2000. **275**(27): p. 20520-6.
90. Nomme, J., et al., *Structural Basis of a Key Factor Regulating the Affinity between the Zonula Occludens First PDZ Domain and Claudins.* J Biol Chem, 2015. **290**(27): p. 16595-606.
91. Tash, B.R., et al., *The occludin and ZO-1 complex, defined by small angle X-ray scattering and NMR, has implications for modulating tight junction permeability.* Proc Natl Acad Sci U S A, 2012. **109**(27): p. 10855-60.
92. Fanning, A.S. and J.M. Anderson, *Zonula occludens-1 and -2 are cytosolic scaffolds that regulate the assembly of cellular junctions.* Ann N Y Acad Sci, 2009. **1165**: p. 113-20.
93. Tornavaca, O., et al., *ZO-1 controls endothelial adherens junctions, cell-cell tension, angiogenesis, and barrier formation.* J Cell Biol, 2015. **208**(6): p. 821-38.
94. Stamatovic, S.M., et al., *Junctional proteins of the blood-brain barrier: New insights into function and dysfunction.* Tissue Barriers, 2016. **4**(1): p. e1154641.

95. Giannotta, M., M. Trani, and E. Dejana, *VE-cadherin and endothelial adherens junctions: active guardians of vascular integrity.* Dev Cell, 2013. **26**(5): p. 441-54.
96. Tietz, S. and B. Engelhardt, *Brain barriers: Crosstalk between complex tight junctions and adherens junctions.* J Cell Biol, 2015. **209**(4): p. 493-506.
97. Lertkiatmongkol, P., et al., *Endothelial functions of platelet/endothelial cell adhesion molecule-1 (CD31).* Curr Opin Hematol, 2016. **23**(3): p. 253-9.
98. Al Rihani, S.B., et al., *Disease-Induced Modulation of Drug Transporters at the Blood-Brain Barrier Level.* Int J Mol Sci, 2021. **22**(7).
99. Abdullahi, W., T.P. Davis, and P.T. Ronaldson, *Functional Expression of P-glycoprotein and Organic Anion Transporting Polypeptides at the Blood-Brain Barrier: Understanding Transport Mechanisms for Improved CNS Drug Delivery?* AAPS J, 2017. **19**(4): p. 931-939.
100. Gil-Martins, E., et al., *Dysfunction of ABC transporters at the blood-brain barrier: Role in neurological disorders.* Pharmacol Ther, 2020. **213**: p. 107554.
101. Kim, B.J., et al., *Streptococcus agalactiae disrupts P-glycoprotein function in brain endothelial cells.* Fluids Barriers CNS, 2019. **16**(1): p. 26.
102. Kusuhara, H. and Y. Sugiyama, *Active efflux across the blood-brain barrier: role of the solute carrier family.* NeuroRx, 2005. **2**(1): p. 73-85.
103. Pragallapati, S. and R. Manyam, *Glucose transporter 1 in health and disease.* J Oral Maxillofac Pathol, 2019. **23**(3): p. 443-449.
104. Fishman, J.B., et al., *Receptor-mediated transcytosis of transferrin across the blood-brain barrier.* J Neurosci Res, 1987. **18**(2): p. 299-304.
105. King, G.L. and S.M. Johnson, *Receptor-mediated transport of insulin across endothelial cells.* Science, 1985. **227**(4694): p. 1583-6.
106. Pardridge, W.M., *Drug transport across the blood-brain barrier.* J Cereb Blood Flow Metab, 2012. **32**(11): p. 1959-72.
107. Pron, B., et al., *Interaction of Neisseria maningitidis with the components of the blood-brain barrier correlates with an increased expression of PilC.* J Infect Dis, 1997. **176**(5): p. 1285-92.
108. Hardy, S.J., et al., *Interactions of Neisseria meningitidis with cells of the human meninges.* Mol Microbiol, 2000. **36**(4): p. 817-29.
109. Bernard, S.C., et al., *Pathogenic Neisseria meningitidis utilizes CD147 for vascular colonization.* Nat Med, 2014. **20**(7): p. 725-31.
110. Maissa, N., et al., *Strength of Neisseria meningitidis binding to endothelial cells requires highly-ordered CD147/beta2-adrenoceptor clusters assembled by alpha-actinin-4.* Nat Commun, 2017. **8**: p. 15764.
111. Schubert-Unkmeir, A., *Molecular mechanisms involved in the interaction of Neisseria meningitidis with cells of the human blood-cerebrospinal fluid barrier.* Pathog Dis, 2017. **75**(2).
112. Sa, E.C.C., N.J. Griffiths, and M. Virji, *Neisseria meningitidis Opc invasin binds to the sulphated tyrosines of activated vitronectin to attach to and invade human brain endothelial cells.* PLoS Pathog, 2010. **6**(5): p. e1000911.
113. Unkmeir, A., et al., *Fibronectin mediates Opc-dependent internalization of Neisseria meningitidis in human brain microvascular endothelial cells.* Mol Microbiol, 2002. **46**(4): p. 933-46.
114. Scietti, L., et al., *Exploring host-pathogen interactions through genome wide protein microarray analysis.* Sci Rep, 2016. **6**: p. 27996.
115. Alqahtani, F., et al., *Deciphering the complex three-way interaction between the non-integrin laminin receptor, galectin-3 and Neisseria meningitidis.* Open Biol, 2014. **4**(10).
116. Hung, M.C. and M. Christodoulides, *The biology of Neisseria adhesins.* Biology (Basel), 2013. **2**(3): p. 1054-109.
117. Tunio, S.A., et al., *The moonlighting protein fructose-1, 6-bisphosphate aldolase of Neisseria meningitidis: surface localization and role in host cell adhesion.* Mol Microbiol, 2010. **76**(3): p. 605-15.
118. Coureuil, M., et al., *Meningococcus Hijacks a beta2-adrenoceptor/beta-Arrestin pathway to cross brain microvasculature endothelium.* Cell, 2010. **143**(7): p. 1149-60.

119. Doulet, N., et al., *Neisseria meningitidis infection of human endothelial cells interferes with leukocyte transmigration by preventing the formation of endothelial docking structures.* J Cell Biol, 2006. **173**(4): p. 627-37.
120. Hoffmann, I., et al., *Activation of ErbB2 receptor tyrosine kinase supports invasion of endothelial cells by Neisseria meningitidis.* J Cell Biol, 2001. **155**(1): p. 133-43.
121. Simonis, A., et al., *Differential activation of acid sphingomyelinase and ceramide release determines invasiveness of Neisseria meningitidis into brain endothelial cells.* PLoS Pathog, 2014. **10**(6): p. e1004160.
122. Peters, S., et al., *Neisseria meningitidis Type IV Pili Trigger Ca(2+)-Dependent Lysosomal Trafficking of the Acid Sphingomyelinase To Enhance Surface Ceramide Levels.* Infect Immun, 2019. **87**(8).
123. Eugene, E., et al., *Microvilli-like structures are associated with the internalization of virulent capsulated Neisseria meningitidis into vascular endothelial cells.* J Cell Sci, 2002. **115**(Pt 6): p. 1231-41.
124. Lambotin, M., et al., *Invasion of endothelial cells by Neisseria meningitidis requires cortactin recruitment by a phosphoinositide-3-kinase/Rac1 signalling pathway triggered by the lipo-oligosaccharide.* J Cell Sci, 2005. **118**(Pt 16): p. 3805-16.
125. Charles-Orszag, A., et al., *Adhesion to nanofibers drives cell membrane remodeling through one-dimensional wetting.* Nat Commun, 2018. **9**(1): p. 4450.
126. Mikaty, G., et al., *Extracellular bacterial pathogen induces host cell surface reorganization to resist shear stress.* PLoS Pathog, 2009. **5**(2): p. e1000314.
127. Virji, M., et al., *Opc- and pilus-dependent interactions of meningococci with human endothelial cells: molecular mechanisms and modulation by surface polysaccharides.* Mol Microbiol, 1995. **18**(4): p. 741-54.
128. Slanina, H., et al., *Cell invasion by Neisseria meningitidis requires a functional interplay between the focal adhesion kinase, Src and cortactin.* PLoS One, 2012. **7**(6): p. e39613.
129. Sokolova, O., et al., *Interaction of Neisseria meningitidis with human brain microvascular endothelial cells: role of MAP- and tyrosine kinases in invasion and inflammatory cytokine release.* Cell Microbiol, 2004. **6**(12): p. 1153-66.
130. Nikulin, J., et al., *Intracellular survival and replication of Neisseria meningitidis in human brain microvascular endothelial cells.* Int J Med Microbiol, 2006. **296**(8): p. 553-8.
131. Coureuil, M., et al., *Meningococcal type IV pili recruit the polarity complex to cross the brain endothelium.* Science, 2009. **325**(5936): p. 83-7.
132. Schubert-Unkmeir, A., et al., *Neisseria meningitidis induces brain microvascular endothelial cell detachment from the matrix and cleavage of occludin: a role for MMP-8.* PLoS Pathog, 2010. **6**(4): p. e1000874.
133. Martins Gomes, S.F., et al., *Induced Pluripotent Stem Cell-Derived Brain Endothelial Cells as a Cellular Model to Study Neisseria meningitidis Infection.* Front Microbiol, 2019. **10**: p. 1181.
134. Asmat, T.M., et al., *Impact of calcium signaling during infection of Neisseria meningitidis to human brain microvascular endothelial cells.* PLoS One, 2014. **9**(12): p. e114474.
135. Dick, J., et al., *Comparison of the inflammatory response of brain microvascular and peripheral endothelial cells following infection with Neisseria meningitidis.* Pathog Dis, 2017. **75**(5).
136. Linhartova, I., et al., *Meningococcal adhesion suppresses proapoptotic gene expression and promotes expression of genes supporting early embryonic and cytoprotective signaling of human endothelial cells.* FEMS Microbiol Lett, 2006. **263**(1): p. 109-18.
137. Schubert-Unkmeir, A., et al., *Gene expression pattern in human brain endothelial cells in response to Neisseria meningitidis.* Infect Immun, 2007. **75**(2): p. 899-914.
138. Oldfield, N.J., et al., *T-cell stimulating protein A (TspA) of Neisseria meningitidis is required for optimal adhesion to human cells.* Cell Microbiol, 2007. **9**(2): p. 463-78.
139. Christodoulides, M., et al., *Interaction of Neisseria meningitidis with human meningeal cells induces the secretion of a distinct group of chemotactic, proinflammatory, and growth-factor cytokines.* Infect Immun, 2002. **70**(8): p. 4035-44.

140. Humphries, H.E., et al., *Activation of human meningeal cells is modulated by lipopolysaccharide (LPS) and non-LPS components of Neisseria meningitidis and is independent of Toll-like receptor (TLR)4 and TLR2 signalling.* Cell Microbiol, 2005. **7**(3): p. 415-30.
141. Fowler, M.I., et al., *Different meningitis-causing bacteria induce distinct inflammatory responses on interaction with cells of the human meninges.* Cell Microbiol, 2004. **6**(6): p. 555-67.
142. Helms, H.C., et al., *In vitro models of the blood-brain barrier: An overview of commonly used brain endothelial cell culture models and guidelines for their use.* J Cereb Blood Flow Metab, 2016. **36**(5): p. 862-90.
143. Bernas, M.J., et al., *Establishment of primary cultures of human brain microvascular endothelial cells to provide an in vitro cellular model of the blood-brain barrier.* Nat Protoc, 2010. **5**(7): p. 1265-72.
144. Schweitzer, K.M., et al., *Characterization of a newly established human bone marrow endothelial cell line: distinct adhesive properties for hematopoietic progenitors compared with human umbilical vein endothelial cells.* Lab Invest, 1997. **76**(1): p. 25-36.
145. Prudhomme, J.G., et al., *Studies of Plasmodium falciparum cytoadherence using immortalized human brain capillary endothelial cells.* Int J Parasitol, 1996. **26**(6): p. 647-55.
146. Stins, M.F., J. Badger, and K. Sik Kim, *Bacterial invasion and transcytosis in transfected human brain microvascular endothelial cells.* Microb Pathog, 2001. **30**(1): p. 19-28.
147. Stins, M.F., F. Gilles, and K.S. Kim, *Selective expression of adhesion molecules on human brain microvascular endothelial cells.* J Neuroimmunol, 1997. **76**(1-2): p. 81-90.
148. Weksler, B.B., et al., *Blood-brain barrier-specific properties of a human adult brain endothelial cell line.* FASEB J, 2005. **19**(13): p. 1872-4.
149. Weksler, B., I.A. Romero, and P.O. Couraud, *The hCMEC/D3 cell line as a model of the human blood brain barrier.* Fluids Barriers CNS, 2013. **10**(1): p. 16.
150. Aaron, P.A., et al., *The blood-brain barrier internalises Cryptococcus neoformans via the EphA2-tyrosine kinase receptor.* Cell Microbiol, 2018. **20**(3).
151. Deng, L., et al., *Characterization of a Two-Component System Transcriptional Regulator, LtdR, That Impacts Group B Streptococcal Colonization and Disease.* Infect Immun, 2018. **86**(7).
152. Jimenez-Munguia, I., et al., *Proteomic and bioinformatic pipeline to screen the ligands of S. pneumoniae interacting with human brain microvascular endothelial cells.* Sci Rep, 2018. **8**(1): p. 5231.
153. N'Dilimabaka, N., et al., *P. falciparum isolate-specific distinct patterns of induced apoptosis in pulmonary and brain endothelial cells.* PLoS One, 2014. **9**(3): p. e90692.
154. Volle, R., et al., *Differential permissivity of human cerebrovascular endothelial cells to enterovirus infection and specificities of serotype EV-A71 in crossing an in vitro model of the human blood-brain barrier.* J Gen Virol, 2015. **96**(Pt 7): p. 1682-95.
155. Wang, J., et al., *Interaction of fibrinogen and muramidase-released protein promotes the development of Streptococcus suis meningitis.* Front Microbiol, 2015. **6**: p. 1001.
156. Eigenmann, D.E., et al., *Comparative study of four immortalized human brain capillary endothelial cell lines, hCMEC/D3, hBMEC, TY10, and BB19, and optimization of culture conditions, for an in vitro blood-brain barrier model for drug permeability studies.* Fluids Barriers CNS, 2013. **10**(1): p. 33.
157. Lippmann, E.S., et al., *A retinoic acid-enhanced, multicellular human blood-brain barrier model derived from stem cell sources.* Sci Rep, 2014. **4**: p. 4160.
158. Lippmann, E.S., et al., *Derivation of blood-brain barrier endothelial cells from human pluripotent stem cells.* Nat Biotechnol, 2012. **30**(8): p. 783-91.
159. Lim, R.G., et al., *Huntington's Disease iPSC-Derived Brain Microvascular Endothelial Cells Reveal WNT-Mediated Angiogenic and Blood-Brain Barrier Deficits.* Cell Rep, 2017. **19**(7): p. 1365-1377.
160. Vatine, G.D., et al., *Modeling Psychomotor Retardation using iPSCs from MCT8-Deficient Patients Indicates a Prominent Role for the Blood-Brain Barrier.* Cell Stem Cell, 2017. **20**(6): p. 831-843 e5.

161. Clark, P.A., et al., *Analysis of Cancer-Targeting Alkylphosphocholine Analogue Permeability Characteristics Using a Human Induced Pluripotent Stem Cell Blood-Brain Barrier Model.* Mol Pharm, 2016. **13**(9): p. 3341-9.
162. Espinal, E.R., et al., *Group B Streptococcus-Induced Macropinocytosis Contributes to Bacterial Invasion of Brain Endothelial Cells.* Pathogens, 2022. **11**(4).
163. Kim, B.J., et al., *Modeling Group B Streptococcus and Blood-Brain Barrier Interaction by Using Induced Pluripotent Stem Cell-Derived Brain Endothelial Cells.* mSphere, 2017. **2**(6).
164. Alimonti, J.B., et al., *Zika virus crosses an in vitro human blood brain barrier model.* Fluids Barriers CNS, 2018. **15**(1): p. 15.
165. Krasemann, S., et al., *The blood-brain barrier is dysregulated in COVID-19 and serves as a CNS entry route for SARS-CoV-2.* Stem Cell Reports, 2022. **17**(2): p. 307-320.
166. DeStefano, J.G., et al., *Real-time quantification of endothelial response to shear stress and vascular modulators.* Integr Biol (Camb), 2017. **9**(4): p. 362-374.
167. DeStefano, J.G., et al., *Effect of shear stress on iPSC-derived human brain microvascular endothelial cells (dhBMECs).* Fluids Barriers CNS, 2017. **14**(1): p. 20.
168. Reinitz, A., et al., *Human brain microvascular endothelial cells resist elongation due to shear stress.* Microvasc Res, 2015. **99**: p. 8-18.
169. Vatine, G.D., et al., *Human iPSC-Derived Blood-Brain Barrier Chips Enable Disease Modeling and Personalized Medicine Applications.* Cell Stem Cell, 2019. **24**(6): p. 995-1005 e6.
170. DeStefano, J.G., et al., *Benchmarking in vitro tissue-engineered blood-brain barrier models.* Fluids Barriers CNS, 2018. **15**(1): p. 32.
171. Appelt-Menzel, A., et al., *Establishment of a Human Blood-Brain Barrier Co-culture Model Mimicking the Neurovascular Unit Using Induced Pluri- and Multipotent Stem Cells.* Stem Cell Reports, 2017. **8**(4): p. 894-906.
172. Hollmann, E.K., et al., *Accelerated differentiation of human induced pluripotent stem cells to blood-brain barrier endothelial cells.* Fluids Barriers CNS, 2017. **14**(1): p. 9.
173. Jamieson, J.J., et al., *Role of iPSC-derived pericytes on barrier function of iPSC-derived brain microvascular endothelial cells in 2D and 3D.* Fluids Barriers CNS, 2019. **16**(1): p. 15.
174. Canfield, S.G., et al., *An isogenic neurovascular unit model comprised of human induced pluripotent stem cell-derived brain microvascular endothelial cells, pericytes, astrocytes, and neurons.* Fluids Barriers CNS, 2019. **16**(1): p. 25.
175. Canfield, S.G., et al., *An isogenic blood-brain barrier model comprising brain endothelial cells, astrocytes, and neurons derived from human induced pluripotent stem cells.* J Neurochem, 2017. **140**(6): p. 874-888.
176. Johswich, K.O., et al., *In vivo adaptation and persistence of Neisseria meningitidis within the nasopharyngeal mucosa.* PLoS Pathog, 2013. **9**(7): p. e1003509.
177. Johswich, K.O., et al., *Sterilizing immunity elicited by Neisseria meningitidis carriage shows broader protection than predicted by serum antibody cross-reactivity in CEACAM1-humanized mice.* Infect Immun, 2015. **83**(1): p. 354-63.
178. Zariri, A., et al., *Expression of human CEACAM1 in transgenic mice limits the Opa-specific immune response against meningococcal outer membrane vesicles.* Vaccine, 2013. **31**(47): p. 5585-93.
179. Denis, K., et al., *Targeting Type IV pili as an antivirulence strategy against invasive meningococcal disease.* Nat Microbiol, 2019. **4**(6): p. 972-984.
180. Melican, K., F. Aubey, and G. Dumenil, *Humanized mouse model to study bacterial infections targeting the microvasculature.* J Vis Exp, 2014(86).
181. Melican, K., et al., *Adhesion of Neisseria meningitidis to dermal vessels leads to local vascular damage and purpura in a humanized mouse model.* PLoS Pathog, 2013. **9**(1): p. e1003139.
182. Stebbins, M.J., et al., *Differentiation and characterization of human pluripotent stem cell-derived brain microvascular endothelial cells.* Methods, 2016. **101**: p. 93-102.
183. Rho, H.W., et al., *Identification of valid reference genes for gene expression studies of human stomach cancer by reverse transcription-qPCR.* BMC Cancer, 2010. **10**: p. 240.

184. Han, S.P., et al., *SNAI1 is involved in the proliferation and migration of glioblastoma cells.* Cell Mol Neurobiol, 2011. **31**(3): p. 489-96.
185. van Sorge, N.M., et al., *Anthrax toxins inhibit neutrophil signaling pathways in brain endothelium and contribute to the pathogenesis of meningitis.* PLoS One, 2008. **3**(8): p. e2964.
186. Yu, J., et al., *Induced pluripotent stem cell lines derived from human somatic cells.* Science, 2007. **318**(5858): p. 1917-20.
187. McGuinness, B.T., et al., *Point mutation in meningococcal por A gene associated with increased endemic disease.* Lancet, 1991. **337**(8740): p. 514-7.
188. Endres, L.M., A. Schubert-Unkmeir, and B.J. Kim, *Neisseria meningitidis Infection of Induced Pluripotent Stem-Cell Derived Brain Endothelial Cells.* J Vis Exp, 2020(161).
189. Kurosawa, H., *Application of Rho-associated protein kinase (ROCK) inhibitor to human pluripotent stem cells.* J Biosci Bioeng, 2012. **114**(6): p. 577-81.
190. Gray, K.M., et al., *Quantitative Phenotyping of Cell-Cell Junctions to Evaluate ZO-1 Presentation in Brain Endothelial Cells.* Ann Biomed Eng, 2019. **47**(7): p. 1675-1687.
191. Prufert, K., A. Vogel, and G. Krohne, *The lamin CxxM motif promotes nuclear membrane growth.* J Cell Sci, 2004. **117**(Pt 25): p. 6105-16.
192. Livak, K.J. and T.D. Schmittgen, *Analysis of relative gene expression data using real-time quantitative PCR and the 2(-Delta Delta C(T)) Method.* Methods, 2001. **25**(4): p. 402-8.
193. Carrozzino, F., et al., *Inducible expression of Snail selectively increases paracellular ion permeability and differentially modulates tight junction proteins.* Am J Physiol Cell Physiol, 2005. **289**(4): p. C1002-14.
194. Ikenouchi, J., et al., *Regulation of tight junctions during the epithelium-mesenchyme transition: direct repression of the gene expression of claudins/occludin by Snail.* J Cell Sci, 2003. **116**(Pt 10): p. 1959-67.
195. Kim, B.J., et al., *Bacterial induction of Snail1 contributes to blood-brain barrier disruption.* J Clin Invest, 2015. **125**(6): p. 2473-83.
196. Martinez-Estrada, O.M., et al., *The transcription factors Slug and Snail act as repressors of Claudin-1 expression in epithelial cells.* Biochem J, 2006. **394**(Pt 2): p. 449-57.
197. Ohkubo, T. and M. Ozawa, *The transcription factor Snail downregulates the tight junction components independently of E-cadherin downregulation.* J Cell Sci, 2004. **117**(Pt 9): p. 1675-85.
198. Kaufhold, S. and B. Bonavida, *Central role of Snail1 in the regulation of EMT and resistance in cancer: a target for therapeutic intervention.* J Exp Clin Cancer Res, 2014. **33**: p. 62.
199. Tunkel, A.R. and W.M. Scheld, *Pathogenesis and pathophysiology of bacterial meningitis.* Clin Microbiol Rev, 1993. **6**(2): p. 118-36.
200. Doran, K.S., et al., *Host-pathogen interactions in bacterial meningitis.* Acta Neuropathol, 2016. **131**(2): p. 185-209.
201. Kim, B.J., E.V. Shusta, and K.S. Doran, *Past and Current Perspectives in Modeling Bacteria and Blood-Brain Barrier Interactions.* Front Microbiol, 2019. **10**: p. 1336.
202. Daneman, R., et al., *Wnt/beta-catenin signaling is required for CNS, but not non-CNS, angiogenesis.* Proc Natl Acad Sci U S A, 2009. **106**(2): p. 641-6.
203. Stenman, J.M., et al., *Canonical Wnt signaling regulates organ-specific assembly and differentiation of CNS vasculature.* Science, 2008. **322**(5905): p. 1247-50.
204. Kawaguchi, R., et al., *A membrane receptor for retinol binding protein mediates cellular uptake of vitamin A.* Science, 2007. **315**(5813): p. 820-5.
205. Hatherell, K., et al., *Development of a three-dimensional, all-human in vitro model of the blood-brain barrier using mono-, co-, and tri-cultivation Transwell models.* J Neurosci Methods, 2011. **199**(2): p. 223-9.
206. Lippmann, E.S., et al., *Commentary on human pluripotent stem cell-based blood-brain barrier models.* Fluids Barriers CNS, 2020. **17**(1): p. 64.
207. Delsing, L., et al., *Barrier Properties and Transcriptome Expression in Human iPSC-Derived Models of the Blood-Brain Barrier.* Stem Cells, 2018. **36**(12): p. 1816-1827.

208. Lu, T.M., et al., *Pluripotent stem cell-derived epithelium misidentified as brain microvascular endothelium requires ETS factors to acquire vascular fate.* Proc Natl Acad Sci U S A, 2021. **118**(8).
209. Lu, T.M., et al., *Human induced pluripotent stem cell-derived neuroectodermal epithelial cells mistaken for blood-brain barrier-forming endothelial cells.* bioRxiv, 2019: p. 699173.
210. Qian, T., et al., *Directed differentiation of human pluripotent stem cells to blood-brain barrier endothelial cells.* Sci Adv, 2017. **3**(11): p. e1701679.
211. Wilson, H.K., et al., *Exploring the effects of cell seeding density on the differentiation of human pluripotent stem cells to brain microvascular endothelial cells.* Fluids Barriers CNS, 2015. **12**: p. 13.
212. Workman, M.J. and C.N. Svendsen, *Recent advances in human iPSC-derived models of the blood-brain barrier.* Fluids Barriers CNS, 2020. **17**(1): p. 30.
213. Brochner, C.B., C.B. Holst, and K. Mollgard, *Outer brain barriers in rat and human development.* Front Neurosci, 2015. **9**: p. 75.
214. Whish, S., et al., *The inner CSF-brain barrier: developmentally controlled access to the brain via intercellular junctions.* Front Neurosci, 2015. **9**: p. 16.
215. Derk, J., et al., *Living on the Edge of the CNS: Meninges Cell Diversity in Health and Disease.* Front Cell Neurosci, 2021. **15**: p. 703944.
216. Gericke, B., et al., *A face-to-face comparison of claudin-5 transduced human brain endothelial (hCMEC/D3) cells with porcine brain endothelial cells as blood-brain barrier models for drug transport studies.* Fluids Barriers CNS, 2020. **17**(1): p. 53.
217. Hinkel, S., et al., *Parametric investigation of static and dynamic cell culture conditions and their impact on hCMEC/D3 barrier properties.* Int J Pharm, 2019. **566**: p. 434-444.
218. Gaillard, P.J. and A.G. de Boer, *Relationship between permeability status of the blood-brain barrier and in vitro permeability coefficient of a drug.* Eur J Pharm Sci, 2000. **12**(2): p. 95-102.
219. Mantle, J.L., L. Min, and K.H. Lee, *Minimum Transendothelial Electrical Resistance Thresholds for the Study of Small and Large Molecule Drug Transport in a Human in Vitro Blood-Brain Barrier Model.* Mol Pharm, 2016. **13**(12): p. 4191-4198.
220. Butt, A.M. and H.C. Jones, *Effect of histamine and antagonists on electrical resistance across the blood-brain barrier in rat brain-surface microvessels.* Brain Res, 1992. **569**(1): p. 100-5.
221. Crone, C. and S.P. Olesen, *Electrical resistance of brain microvascular endothelium.* Brain Res, 1982. **241**(1): p. 49-55.
222. Vigh, J.P., et al., *Transendothelial Electrical Resistance Measurement across the Blood-Brain Barrier: A Critical Review of Methods.* Micromachines (Basel), 2021. **12**(6).
223. Neal, E.H., et al., *A Simplified, Fully Defined Differentiation Scheme for Producing Blood-Brain Barrier Endothelial Cells from Human iPSCs.* Stem Cell Reports, 2019. **12**(6): p. 1380-1388.
224. Neuhaus, J., W. Risau, and H. Wolburg, *Induction of blood-brain barrier characteristics in bovine brain endothelial cells by rat astroglial cells in transfilter coculture.* Ann N Y Acad Sci, 1991. **633**: p. 578-80.
225. Abbott, N.J., *Astrocyte-endothelial interactions and blood-brain barrier permeability.* J Anat, 2002. **200**(6): p. 629-38.
226. Sobue, K., et al., *Induction of blood-brain barrier properties in immortalized bovine brain endothelial cells by astrocytic factors.* Neurosci Res, 1999. **35**(2): p. 155-64.
227. Igarashi, Y., et al., *Glial cell line-derived neurotrophic factor induces barrier function of endothelial cells forming the blood-brain barrier.* Biochem Biophys Res Commun, 1999. **261**(1): p. 108-12.
228. Utsumi, H., et al., *Expression of GFRalpha-1, receptor for GDNF, in rat brain capillary during postnatal development of the BBB.* Am J Physiol Cell Physiol, 2000. **279**(2): p. C361-8.
229. Hoheisel, D., et al., *Hydrocortisone reinforces the blood-brain properties in a serum free cell culture system.* Biochem Biophys Res Commun, 1998. **247**(2): p. 312-5.
230. Shen, J., et al., *PDGFR-beta restores blood-brain barrier functions in a mouse model of focal cerebral ischemia.* J Cereb Blood Flow Metab, 2019. **39**(8): p. 1501-1515.

231. Laksitorini, M.D., et al., *Modulation of Wnt/beta-catenin signaling promotes blood-brain barrier phenotype in cultured brain endothelial cells.* Sci Rep, 2019. **9**(1): p. 19718.
232. Veszelka, S., et al., *Comparison of a Rat Primary Cell-Based Blood-Brain Barrier Model With Epithelial and Brain Endothelial Cell Lines: Gene Expression and Drug Transport.* Front Mol Neurosci, 2018. **11**: p. 166.
233. Forster, C., et al., *Differential effects of hydrocortisone and TNFalpha on tight junction proteins in an in vitro model of the human blood-brain barrier.* J Physiol, 2008. **586**(7): p. 1937-49.
234. Cucullo, L., et al., *Immortalized human brain endothelial cells and flow-based vascular modeling: a marriage of convenience for rational neurovascular studies.* J Cereb Blood Flow Metab, 2008. **28**(2): p. 312-28.
235. Dos Santos Souza, I., et al., *Meningococcal disease: A paradigm of type-IV pilus dependent pathogenesis.* Cell Microbiol, 2020. **22**(4): p. e13185.
236. Liu, Y., A. Beyer, and R. Aebersold, *On the Dependency of Cellular Protein Levels on mRNA Abundance.* Cell, 2016. **165**(3): p. 535-50.
237. Jovanovic, M., et al., *Immunogenetics. Dynamic profiling of the protein life cycle in response to pathogens.* Science, 2015. **347**(6226): p. 1259038.
238. Kaufhold, S. and B. Bonavida, *Central role of Snail1 in the regulation of EMT and resistance in cancer: a target for therapeutic intervention.* J Exp Clin Cancer Res, 2014. **33**(1): p. 62.
239. Cano, A., et al., *The transcription factor snail controls epithelial-mesenchymal transitions by repressing E-cadherin expression.* Nat Cell Biol, 2000. **2**(2): p. 76-83.
240. Gratz, N., et al., *Pneumococcal neuraminidase activates TGF-beta signalling.* Microbiology (Reading), 2017. **163**(8): p. 1198-1207.
241. Yang, R., et al., *Induction of VEGFA and Snail-1 by meningitic Escherichia coli mediates disruption of the blood-brain barrier.* Oncotarget, 2016. **7**(39): p. 63839-63855.
242. Beard, R.S., Jr., et al., *Non-muscle Mlck is required for beta-catenin- and FoxO1-dependent downregulation of Cldn5 in IL-1beta-mediated barrier dysfunction in brain endothelial cells.* J Cell Sci, 2014. **127**(Pt 8): p. 1840-53.
243. Taddei, A., et al., *Endothelial adherens junctions control tight junctions by VE-cadherin-mediated upregulation of claudin-5.* Nat Cell Biol, 2008. **10**(8): p. 923-34.
244. Hwang, W.L., et al., *SNAIL regulates interleukin-8 expression, stem cell-like activity, and tumorigenicity of human colorectal carcinoma cells.* Gastroenterology, 2011. **141**(1): p. 279-91, 291 e1-5.
245. Stanisavljevic, J., et al., *The p65 subunit of NF-kappaB and PARP1 assist Snail1 in activating fibronectin transcription.* J Cell Sci, 2011. **124**(Pt 24): p. 4161-71.
246. Wu, W.S., et al., *Snail collaborates with EGR-1 and SP-1 to directly activate transcription of MMP 9 and ZEB1.* Sci Rep, 2017. **7**(1): p. 17753.
247. Le Guennec, L., et al., *Strategies used by bacterial pathogens to cross the blood-brain barrier.* Cell Microbiol, 2020. **22**(1): p. e13132.
248. Tegtmeyer, N., et al., *Helicobacter pylori Employs a Unique Basolateral Type IV Secretion Mechanism for CagA Delivery.* Cell Host Microbe, 2017. **22**(4): p. 552-560 e5.
249. Wessler, S. and S. Backert, *A novel basolateral type IV secretion model for the CagA oncoprotein of Helicobacter pylori.* Microb Cell, 2017. **5**(1): p. 60-62.
250. Cloutier, G., A. Sallenbach-Morrissette, and J.F. Beaulieu, *Non-integrin laminin receptors in epithelia.* Tissue Cell, 2019. **56**: p. 71-78.
251. Peterson, R.J. and M. Koval, *Above the Matrix: Functional Roles for Apically Localized Integrins.* Front Cell Dev Biol, 2021. **9**: p. 699407.
252. Deora, A.A., et al., *The basolateral targeting signal of CD147 (EMMPRIN) consists of a single leucine and is not recognized by retinal pigment epithelium.* Mol Biol Cell, 2004. **15**(9): p. 4148-65.
253. Deora, A.A., et al., *Mechanisms regulating tissue-specific polarity of monocarboxylate transporters and their chaperone CD147 in kidney and retinal epithelia.* Proc Natl Acad Sci U S A, 2005. **102**(45): p. 16245-50.

254. Jin, R., et al., *Inhibition of CD147 (Cluster of Differentiation 147) Ameliorates Acute Ischemic Stroke in Mice by Reducing Thromboinflammation.* Stroke, 2017. **48**(12): p. 3356-3365.
255. Lu, M., et al., *Basolateral CD147 induces hepatocyte polarity loss by E-cadherin ubiquitination and degradation in hepatocellular carcinoma progress.* Hepatology, 2018. **68**(1): p. 317-332.
256. Pan, P., et al., *Cyclophilin a signaling induces pericyte-associated blood-brain barrier disruption after subarachnoid hemorrhage.* J Neuroinflammation, 2020. **17**(1): p. 16.
257. Dixon, G.L., et al., *Endothelial adhesion molecule expression and its inhibition by recombinant bactericidal/permeability-increasing protein are influenced by the capsulation and lipooligosaccharide structure of Neisseria meningitidis.* Infect Immun, 1999. **67**(11): p. 5626-33.
258. Nishihara, H., et al., *Advancing human induced pluripotent stem cell-derived blood-brain barrier models for studying immune cell interactions.* FASEB J, 2020. **34**(12): p. 16693-16715.
259. Hurst, L.A., et al., *Expression of ADAM-17, TIMP-3 and fractalkine in the human adult brain endothelial cell line, hCMEC/D3, following pro-inflammatory cytokine treatment.* J Neuroimmunol, 2009. **210**(1-2): p. 108-12.
260. Subileau, E.A., et al., *Expression of chemokines and their receptors by human brain endothelium: implications for multiple sclerosis.* J Neuropathol Exp Neurol, 2009. **68**(3): p. 227-40.
261. Agerer, F., S. Waeckerle, and C.R. Hauck, *Microscopic quantification of bacterial invasion by a novel antibody-independent staining method.* J Microbiol Methods, 2004. **59**(1): p. 23-32.
262. Solger, F., et al., *A Role of Sphingosine in the Intracellular Survival of Neisseria gonorrhoeae.* Front Cell Infect Microbiol, 2020. **10**: p. 215.
263. Moroni, L., et al., *Biofabrication: A Guide to Technology and Terminology.* Trends Biotechnol, 2018. **36**(4): p. 384-402.
264. Heydarian, M., et al., *Triple co-culture and perfusion bioreactor for studying the interaction between Neisseria gonorrhoeae and neutrophils: A novel 3D tissue model for bacterial infection and immunity.* J Tissue Eng, 2021. **12**: p. 2041731420988802.
265. Jagau, H., et al., *Von Willebrand Factor Mediates Pneumococcal Aggregation and Adhesion in Blood Flow.* Front Microbiol, 2019. **10**: p. 511.
266. Kopenhagen, A., et al., *Streptococcus pneumoniae Affects Endothelial Cell Migration in Microfluidic Circulation.* Front Microbiol, 2022. **13**: p. 852036.
267. Jagau, H., et al., *Pneumococcus Infection of Primary Human Endothelial Cells in Constant Flow.* J Vis Exp, 2019(152).
268. Sosa-Hernandez, J.E., et al., *Organs-on-a-Chip Module: A Review from the Development and Applications Perspective.* Micromachines (Basel), 2018. **9**(10).

AFFIDAVIT

I hereby confirm that my thesis entitled 'Development of multicellular in vitro models of the meningeal blood-CSF barrier to study Neisseria meningitidis infection' is the result of my own work. I did not receive any help or support from commercial consultants. All sources and / or materials applied are listed and specified in the thesis.

Furthermore, I confirm that this thesis has not yet been submitted as part of another examination process neither in identical nor in similar form.

Place, Date Signature

EIDESSTATTLICHE ERKLÄRUNG

Hiermit erkläre ich an Eides statt, die Dissertation ‚Entwicklung multizellulärer in vitro Modelle der meningealen Blut-Liquor Schranke zur Untersuchung der Neisseria meningitidis Infektion' eigenständig, d.h. insbesondere selbständig und ohne Hilfe eines kommerziellen Promotionsberaters, angefertigt und keine anderen als die von mir angegebenen Quellen und Hilfsmittel verwendet zu haben.

Ich erkläre außerdem, dass die Dissertation weder in gleicher noch in ähnlicher Form bereits in einem anderen Prüfungsverfahren vorgelegen hat.

Ort, Datum Unterschrift

APPENDIX

List of Figures

Figure 1. Stages of *Neisseria meningitidis* pathogenesis. 11
Figure 2. The meningeal blood-CSF barrier. . 15
Figure 3. *N. meningitidis* interaction with brain endothelial cells. . 18
Figure 4. Set-up and application of the iBEC-LMC co-culture model. . 42
Figure 5. Characterization of the iBEC-LMC co-culture model. 43
Figure 6. Characterization of the hCMEC/D3-LMC co-culture model. 44
Figure 7. Barrier properties of iBEC-LMC co-culture models. 45
Figure 8. Barrier properties of hCMEC/D3-LMC co-culture models. 46
Figure 9. *N. meningitidis* interaction with BECs from the BEC-LMC co-culture models. 47
Figure 10. *N. meningitidis* traversal of BEC and BEC-LMC barrier models. 48
Figure 11. Microscopic analysis of *N. meningitidis* interaction with the iBEC-LMC direct co-culture model. 49
Figure 12. Effects of *N. meningitidis* infection on barrier integrity of BEC-LMC co-culture models. 50
Figure 13. Effects of *N. meningitidis* infection on cell-junction expression in iBECs. 51
Figure 14. Effects of *N. meningitidis* infection on cell-junction expression in hCMEC/D3s. 52
Figure 15. Effects of SNAI1 knockdown downregulation of cell-junction expression in hCMEC/D3s. 53
Figure 16. Effects of *N. meningitidis* infection on cell-junction protein expression in iBECs. 54
Figure 17. Effects of *N. meningitidis* infection on expression of proinflammatory cytokines in iBECs. 55
Figure 18. Effects of *N. meningitidis* infection on the expression of cytokines in hCMEC/D3s. 56
Figure 19. Effects of *N. meningitidis* infection on IL-8 secretion in the mBCSFB models. 57

List of Tables

Table 1. Devices. 24
Table 2. Consumables. 24
Table 3. Chemicals and reagents. 25
Table 4. Cell culture media. Media were filter-sterilized and **stored at 4 °C**. 27
Table 5. Media and solutions for bacterial culture. 28
Table 6. Buffers and other solutions. 28
Table 7. Antibodies used for immunofluorescence staining. 29
Table 8. qPCR primers. 29
Table 9. Cells. 27
Table 10. Bacterial strains. 27
Table 11. PCR cycling protocol for cDNA synthesis. 38
Table 12. qPCR reaction mix [1x; 25 µl]. 38
Table 13. qPCR thermocycler protocol. 39

Abbreviation Index

BBB	Blood-brain-barrier
BEC	Brain endothelial cell
bFGF	basic fibroblast growth factor
cDNA	Complementary DNA
cfu	Colony forming units
CNS	Central nervous system
CSF	Cerebrospinal fluid
DAPI	4',6-diamidino-2-phenylindole
DMEM	Dulbecco's Modified Eagle's Medium
EC	Endothelial cell
ELISA	Enzyme-linked immunosorbent assay
GBS	Group B *Streptococcus*
GFP	Green fluorescent protein
Group B *Streptococcus*	*Streptococcus agalactiae*
HBMEC	Human brain microvascular endothelial cells
hCMEC	Human cerebral microvascular endothelial cell
hESFM	Human endothelial serum-free medium
iBEC	iPSC-derived brain endothelial-like cell
IMD	Invasive meningococcal disease
iPSC	Induced pluripotent stem cell
LMC	Leptomeningeal cell
LOS	Lipooligosaccharide
mBCSFB	Meningeal blood-cerebrospinal fluid barrier
MOI	Multiplicity of infection
mRNA	Messenger ribonucleic acid
N. meningitidis	*Neisseria meningitidis*
NaF	Sodium fluorescein
Nm	*Neisseria meningitidis*
p.i.	Post-infection
PBS	Phosphate buffered saline
PCR	Polymerase chain reaction
PPM	Proteose peptone medium
qPCR	quantitative RT-PCR
RA	Retinoic acid
RT	Room temperature
RT-PCR	Reverse transcription-PCR
SAS	Subarachnoid space
SIM	Structured illumination microscopy
siRNA	Short interfering RNA
TC	Tissue culture
TEER	Transendothelial electrical resistance
TEM	Transmission electron microscopy
Tfp	Type IV pilus
UM	Unconditioned medium

List of Publications

- Endres LM, Jungblut M, Divyapicigil M, et al. Development of a multicellular in vitro model of the meningeal blood-CSF barrier to study Neisseria meningitidis infection. *Fluids Barriers CNS*. 2022;19(1):81. Published 2022 Oct 26. doi:10.1186/s12987-022-00379-z

- Endres LM, Schubert-Unkmeir A, Kim BJ. Neisseria meningitidis Infection of Induced Pluripotent Stem-Cell Derived Brain Endothelial Cells. *J Vis Exp*. 2020;(161):10.3791/61400. Published 2020 Jul 14. doi:10.3791/61400

Acknowledgments

First and foremost, I want to thank Prof. Alexandra Schubert-Unkmeir for giving me the opportunity to be part of her research group and to work on this project. I am grateful for her encouragement and trust, and gently pushing me in the right direction, when it was needed. I really appreciated the level of honest communication between us and cherished the discussion in our meetings, which often tended to be on the lengthier side.

Another big thank you goes to my second mentor, Asst. Prof. Brandon J Kim, whom I heavily leaned on during the first year of my PhD, when he was a Postdoc in our lab, and who still supports me until today. I will always be grateful for his guidance in and out of the lab and cherish times such as our GRC attendance in New Hampshire in 2022. Thanks for not letting my English get too rusty.

I would also like to thank my thesis committee members Prof. Roy Gross and Jun. Prof. Alexander Westermann for their support and reliability, and the fruitful discussions during our meetings. Special thanks to Roy Gross for agreeing to function as second examiner of this thesis, even after retirement.

Next, I want to express my appreciation for the many great local and international colleagues that I have had the pleasure of collaborating with. Thanks go to Prof. Myron Christodoulides, who provided the meningioma cells along with much appreciated advice, Prof. Christian Stigloher and his team, especially Claudia Gehrig-Höhn and Daniela Bunsen, for their expertise and help electron microscopy, and to Mustafa Divyapicigil for his work on the tight junction analysis using the JanAP software. Lastly, I want to thank Marvin Jungblut and Prof. Markus Sauer for the great collaboration on the SIM analysis.

Furthermore, I am very grateful for my colleagues at the Institute for Hygiene and Microbiology and especially my lab mates from the AG Schubert-Unkmeir. Special thanks go to Lena Wolter and Hannah Franke for their technical assistance and my brothers in the lab, Ingo Fohmann and Simon Peters, for the fruitful discussions and being generally great colleagues and friends.

I was also very lucky to be a part of the DFG funded research training group GRK2157 “3D Tissue Models for Studying Microbial Infections by Human Pathogens” lead by Prof. Thomas Rudel, which provided not only funding for the project, but also a network of wonderful colleagues. I really enjoyed our meetings, retreats, symposium, and overall time together.

Finally, I want to thank my friends and family, who played a big part in making this a pleasant journey. I am so glad to have had my brother and his wife as well as my cousins around me during this time, and words cannot express how much I value my parents’ support through it all. Thank you for always being there for me!